SYNTHESIS AND ELECTROCHEMISTRY OF 1,2,4,6-THIATRIAZINE RADICALS

TRACEY LYNNE ROEMMELE
B.Sc., University of Lethbridge, 2000

A Thesis
Submitted to the School of Graduate Studies
of the University of Lethbridge
in Partial Fulfillment of the
Requirements for the Degree

MASTER OF SCIENCE

Chemistry and Biochemistry
University of Lethbridge
LETHBRIDGE, ALBERTA, CANADA

To Matthew and Noel

ABSTRACT

1,2,4,6-thiatriazine radicals can be neutral radical conductors in the context of molecular metal design. After initial investigations they were ignored in favor of other prospective ring systems. A more general route to 1,2,4,6-thiatriazine radicals herein is reported. Two crystal structures were obtained for the radicals 5-phenyl-3-trichloromethyl-1,2,4,6-thiatriazine **7c** and 5-phenyl-3-trifluoromethyl-1,2,4,6-thiatriazine **8c**. **7c** displays a unique head-to-tail packing arrangement not seen in previous thiatriazine structures. Two crystal structures of the precursor phenyl/trichloro imidoylamidine **1c** and phenyl/trifluoromethyl imidoylamidine **2c** show strong intramolecular hydrogen bonding and relatively weak intermolecular hydrogen bonding. EPR of the radicals are highly diagnostic and display coupling to three unique nitrogen atoms, of which a small but very distinct influence on the hyperfine coupling constants from the remote aryl-substituents is seen. Solution electrochemistry assessed the redox tunability of the radicals to these substituents. DFT calculations of the hyperfine coupling constants and oxidation and reduction potentials corroborated well with experimental data.

ACKNOWLEDGEMENTS

I cannot give enough thanks to my supervisor, Dr. René Boeré, who has been such a capable instructor and mentor both inside and outside of the lab. His insight, encouragement, and patience have given positive direction to my undergraduate and graduate time here. I especially want to thank him for the numerous hours spent on the analysis of my data, along with getting this thesis through its final stages.

Thanks also go to my MSc. companion Jason Masuda, who was a wonderful co-worker and so easy to get along with. Sharing lab space (and crackers) with you was never a problem! The adjoining Dibble lab also added much to the atmosphere. Thanks to Dr. Peter Dibble for his insight and creative choice in music! As well, my sincere thanks to Luis Delgado for all his help with glass blowing. It was essential to the completion of this thesis.

To my fellow graduate students Mandy Bondaruk, Taunia Clossom, and Michelle Thibault, thanks for your friendship and advice. Going through graduate school together was more fun because of you.

My husband Matthew has supported me in so many ways during both my undergraduate and graduate work here, and I am so grateful to him. The family support I have received subsequent to having my son Noel has been crucial to the finishing of this work, and for this I especially thank Matthew, my mothers Maureen and Rosalind, and my sister Stephanie. I also thank Noel for giving up time with me so that I could complete my graduate work.

Table of Contents

Approval..... ii
Dedication..... iii
Abstract..... iv
Acknowledgements..... v
Table of Contents..... vi
List of Tables..... ix
List of Figures..... xi
List of Abbreviations..... xiii
Compound Numbering Scheme..... xiv

Chapter 1: Summary of the work..... 1
1.1 Introduction..... 1
1.2 Background: Molecular conducting materials..... 2
1.2.1 Neutral Radical Conductors vs. Radical Ion Conductors..... 6
1.3 Known Redox-Active Heterocycles..... 7
1.3.1 Five-membered rings..... 9
1.3.2 Six-membered rings..... 10
1.4 1,2,4,6-thiatriazines..... 11
1.5 Conclusions..... 14
References..... 15

Chapter 2: Preparation of the 1,2,4,6-thiatriazines..... 18
2.1 Introduction..... 18
2.1.1 Previous synthetic routes to 1-chloro-1,2,4,6-thiatriazines..... 18
2.1.2 A more versatile synthetic method..... 19
2.2 Synthesis of amidines..... 20
2.3 Synthesis of the aryl N-imidoylamidines..... 21
2.3.1 Trichloromethyl imidoylamidines..... 22
2.3.2 Trifluoromethyl imidoylamidines..... 23
2.3.3 Discussion..... 25
2.4 Preparation of the aryl N-imidoylamidine hydrochlorides..... 34
2.4.1 Trichloromethyl imidoylamidine hydrochlorides..... 34
2.4.2 Trifluoromethyl imidoylamidine hydrochlorides..... 35
2.5 Preparation of the 1-chloro-1,2,4,6-thiatriazines..... 36
2.5.1 1-chloro-5-aryl-3-trichloromethyl thiatriazines..... 36
2.5.2 1-chloro-5-aryl-3-trifluoromethyl thiatriazines..... 40
2.6 Preparation of the 1,2,4,6-thiatriazine radicals..... 40
2.6.1 5-aryl-3-trichloromethyl thiatriazine radicals..... 41
2.6.2 5-aryl-3-trifluoromethyl thiatriazine radicals..... 43
2.7 Conclusions..... 46
References..... 47

Chapter 3: Crystal structures of the imidoylamidines **1c** and **2c**, and the 1,2,4,6-thiatriazine radicals **7c** and **8c**..... 48

3.1 Introduction..... 48
3.2 Phenyl/trichloromethyl imidoylamidine **1c**..... 50
3.2.1 Experimental..... 50
3.2.2 Space group determination..... 50
3.2.3 Data collection and refinement..... 51
3.2.4 Discussion..... 52
3.3 Phenyl/trifluoromethyl imidoylamidine **2c**..... 56
3.3.1 Experimental..... 56
3.3.2 Space group determination..... 57
3.3.3 Data collection and refinement..... 57
3.3.4 Discussion..... 58
3.4 5-phenyl-3-trichloromethyl-1,2,4,6-thiatriazine radical **7c**..... 63
3.4.1 Experimental..... 63
3.4.2 Space group determination..... 63
3.4.3 Data collection and refinement..... 64
3.4.4 Discussion..... 64
3.5 5-phenyl-3-trifluoromethyl-1,2,4,6-thiatriazine radical **8c**..... 67
3.5.1 Experimental..... 67
3.5.2 Space group determination..... 67
3.5.3 Data collection and refinement..... 67
3.5.4 Discussion..... 68
3.6 Conclusion..... 74
References..... 75

Chapter 4: Electron paramagnetic resonance (EPR) analysis and density functional theory (DFT) calculations of the 1,2,4,6-thiatriazine radicals..... 76
4.1 Introduction..... 76
4.2 Electron paramagnetic resonance (EPR)..... 76
4.3 Experimental..... 78
4.4 Results..... 78
4.5 Density Functional Theory (DFT) calculations..... 82
4.6 Discussion..... 84
4.5 Conclusion..... 86
References..... 88

Chapter 5: Redox electrochemistry of the 1,2,4,6-thiatriazine radicals..... 89
5.1 Introduction..... 89
5.2 Electroanalytical techniques..... 90
5.2.1 Cyclic voltammetry (CV)..... 91
5.2.2 Osteryoung square wave voltammetry (OSWV)..... 94
5.2.3 Solvents..... 96
5.2.4 Specialized electrochemical cell..... 98
5.3 Experimental..... 99
5.4 Results and discussion..... 100
5.4.1 5-aryl-3-trichloromethyl-1,2,4,6-thiatriazine radicals **7a-e**..... 105
5.4.2 5-aryl-3-trifluoromethyl-1,2,4,6-thiatriazine radicals **8a-e**..... 109

5.4.3 Correlation of redox potentials with gas phase calculations..... 116
5.4.4 Error limits for the voltammetric data..... 123
5.5 Conclusions..... 123
5.6 Thesis conclusions and future prospects..... 124
References..... 126

Chapter 6: Experimental..... 127
6.1 Introduction..... 127
6.2 Synthesis of the trichloromethyl imidoylamidines **1a-e**..... 128
6.3 Synthesis of the trifluoromethyl imidoylamidines **2a-e**..... 131
6.4 Synthesis of the trichloromethyl imidoylamidine hydrochlorides **3a-e**.. 134
6.5 Synthesis of the trifluoromethyl imidoylamidine hydrochlorides **4a-e**.. 135
6.6 Synthesis of the 1-chloro-5-aryl-3-trichloromethyl-1,2,4,6-thiatriazines **5a-e**..... 137
6.7 Synthesis of the 1-chloro-5-aryl-3-trifluoromethyl-1,2,4,6-thiatriazines **6a-e**..... 139
6.8 Synthesis of the 3-trichloromethyl-5-aryl-1,2,4,6-thiatriazine free radicals **7a-e**..... 140
6.9 Synthesis of the 3-trifluoromethyl-5-aryl-1,2,4,6-thiatriazine free radicals **8a-e**..... 142
6.10 Crystallography data tables..... 144
References..... 176

List of Tables

Table 2.1 ^{1}H NMR of the aryl imidoylamidines **1a-e**, **2a-e**..... 28
Table 2.2 ^{13}C NMR of the aryl imidoylamdines **1a-e**, **2a-e**..... 29
Table 2.3 IR data for the imidoylamidines **1a-e**, **2a-e**..... 31
Table 2.4 Mass spectra of the aryl imidoylamidines **1a-e**, **2a-e**..... 32
Table 2.5 Analytical and melting point data for the aryl imidoylamidines **1a-e**, **2a-e**..... 33
Table 2.6 ^{1}H NMR of the thiatriazine chlorides..... 38
Table 2.7 Mass spectra of the 1,2,4,6-thiatriazine free radicals **7a-e**, **8a-e**..... 44
Table 2.8 Analytical and melting point data for the thiatriazine radicals **7a-e**, **8a-e**..... 45
Table 3.1 Comparison of C–N bond lengths[1] and averages of **1c** and **2c** with other imidoylamidines..... 62
Table 3.2 Comparison of bond lengths[1] in 1,2,4,6-thiatriazine radicals with oxidation state 0..... 72
Table 3.3 Comparison of bond angles(°) in 1,2,4,6-thiatriazine radicals with oxidation state 0..... 73
Table 4.1 Experimental and calculated EPR data of **7a-e**, **8a-e**..... 83
Table 4.2 All EPR data for 1,2,4,6-thiatriazines..... 85
Table 5.1 Electrochemical data for X-$C_6H_4C_2N_3SCCl_3$ thiatriazines..... 102
Table 5.2 Electrochemical data for X-$C_6H_4C_2N_3SCF_3$ thiatriazines at the full indicated concentrations..... 103
Table 5.3 Electrochemical data for X-$C_6H_4C_2N_3SCF_3$ thiatriazines at below the indicated concentrations..... 104
Table 5.4. Voltammetric data for compounds **7a-e**..... 108
Table 5.5 Voltammetric data for compounds **8a-e** at low concentration..... 112
Table 5.6 Voltammetric data for compounds **8a-e** at high concentration..... 113
Table 5.7 Calculated and experimental redox potentials of **7a-e**..... 117
Table 5.8 Calculated and experimental redox potentials of **8a-e** for the monomeric radical..... 120
Table 6.1 Crystal data and structure refinement for **1c**..... 144
Table 6.2 Atomic coordinates ($x\ 10^4$) and equivalent isotropic displacement parameters ($Å^2 x\ 10^3$) for **1c**. U(eq) is defined as one third of the trace of the orthogonalized U^{ij} tensor..... 145
Table 6.3 Bond lengths [Å], angles [°] and H-bonds [Å and °] for **1c**..... 147
Table 6.4 Anisotropic displacement parameters ($Å^2 x\ 10^3$) for **1c**. The anisotropic displacement factor exponent takes the form: $-2\pi^2[h^2 a^{*2} U^{11} + ... + 2 h k a^* b^* U^{12}]$..... 151
Table 6.5 Hydrogen coordinates ($x\ 10^4$) and isotropic displacement parameters ($Å^2 x\ 10^3$) for **1c**..... 153
Table 6.6 Torsion angles [°] for **1c**..... 154
Table 6.7 Crystal data and structure refinement for **2c**..... 156

Table 6.8 Atomic coordinates (x 10^4) and equivalent isotropic displacement parameters ($Å^2$ x 10^3) for **2c**. U(eq) is defined as one third of the trace of the orthogonalized U^{ij} tensor..... 157
Table 6.9 Bond lengths [Å] and angles [°] for **2c**..... 158
Table 6.10 Anisotropic displacement parameters ($Å^2$ x 10^3) for **2c**. The anisotropic displacement factor exponent takes the form: $-2\pi^2[h^2 a^{*2}U^{11} + ... + 2 h k a^* b^* U^{12}]$..... 161
Table 6.11 Hydrogen coordinates (x 10^4) and isotropic displacement parameters ($Å^2$ x 10^3) for **2c**..... 162
Table 6.12 Crystal data and structure refinement for **7c**..... 163
Table 6.13 Atomic coordinates (x 10^4) and equivalent isotropic displacement parameters ($Å^2$ x 10^3) for **7c**. U(eq) is defined as one third of the trace of the orthogonalized U^{ij} tensor..... 164
Table 6.14 Bond lengths [Å] and angles [°] for **7c**..... 165
Table 6.15 Anisotropic displacement parameters ($Å^2$ x 10^3) for **7c**. The anisotropic displacement factor exponent takes the form: $-2\pi^2[h^2 a^{*2}U^{11} + ... + 2 h k a^* b^* U^{12}]$..... 167
Table 6.16 Hydrogen coordinates (x 10^4) and isotropic displacement parameters ($Å^2$ x 10^3) for **7c**..... 168
Table 6.17 Crystal data and structure refinement for **8c**..... 169
Table 6.18 Atomic coordinates (x 10^4) and equivalent isotropic displacement parameters ($Å^2$ x 10^3) for **8c**. U(eq) is defined as one third of the trace of the orthogonalized U^{ij} tensor..... 170
Table 6.19 Bond lengths [Å] and angles [°] for **8c**..... 171
Table 6.20 Anisotropic displacement parameters ($Å^2$ x 10^3) for **8c**. The anisotropic displacement factor exponent takes the form: $-2\pi^2[h^2 a^{*2}U^{11} + ... + 2 h k a^* b^* U^{12}]$..... 174
Table 6.21 Hydrogen coordinates (x 10^4) and isotropic displacement parameters ($Å^2$ x 10^3) for **8c**..... 175

List of Figures

Figure 1.1 Target 1,2,4,6-thiatriazine radicals **7a-e**, **8a-e**..... 1
Figure 1.2 Proper vs. improper splitting of the conduction band..... 4
Figure 1.3 Some five-membered thiazyl heterocycles..... 9
Figure 1.4 Some six-membered thiazyl heterocycles..... 10
Figure 1.5 Substituent variation of the 1,2,4,6-thiatriazines..... 12
Figure 2.1 Synthetic route to the 1,2,4,6-thiatriazine radicals **7a-e**, **8a-e**..... 20
Figure 2.2 Trifluoroacetonitrile glass transfer apparatus..... 24
Figure 2.3 Pear-shaped solids addition funnel..... 41
Figure 2.4 Recrystallization H-vessel for compounds **7a-e**..... 42
Figure 3.1 Thermal ellipsoid plot and atom numbering scheme for **1c**. Dotted lines represent both inter- and intramolecular hydrogen bonding that is occurring in the solid-state lattice..... 53
Figure 3.2 Unit cell diagram of **1c**..... 54
Figure 3.3 Solid-state packing diagram of **1c**..... 54
Figure 3.4 Diagram of **1c**. Dashed lines represent intermolecular contacts that are less than the sum of van der Waals radii..... 56
Figure 3.5 Thermal ellipsoid plot and atom numbering scheme for **2c**. Dotted lines represent both inter- and intramolecular hydrogen bonding that is occurring in the solid state lattice..... 58
Figure 3.6 Packing diagram of **2c** showing 2/m symmetry in the unit cell. The screw axis is indicated by the jagged line in the middle of the picture..... 59
Figure 3.7 Diagram of **2c**. Dashed lines represent intermolecular contacts that are less than the sum of van der Waals radii..... 61
Figure 3.8 Thermal ellipsoid plot and atom numbering scheme of the asymmetric unit of **7c**..... 65
Figure 3.9 Unit cell diagram of **7c**..... 65
Figure 3.10 Solid-state packing diagram of **7c**..... 66
Figure 3.11 Thermal ellipsoid plot and atom numbering scheme for **8c**. Dashed line indicates the close contact between sulfur atoms..... 69
Figure 3.12 Unit cell diagram of **8c**..... 69
Figure 3.13 Crystal packing diagram of **8c** viewed perpendicular to the [1,1,1] axis, along the body diagonal..... 71
Figure 3.14 Simplified packing diagram for **8c**..... 71
Figure 4.1. Energy gap between the +1/2 and –1/2 spin orientations..... 77
Figure 4.2 EPR spectrum of **7d** in CH_2Cl_2..... 80
Figure 4.3 EPR spectrum of **8d** in CH_2Cl_2..... 81
Figure 4.4 Shaded surface plot of the π-SOMO of **8c**..... 82
Figure 5.1 Waveform for cyclic voltammetry..... 91
Figure 5.2 Idealized cyclic voltammogram trace for an oxidation reaction followed by return to the initial conditions. I_{pa} is the peak anodic current and I_{pc} is the peak cathodic current. E_{pa} and E_{pc} are the potentials at which these currents are observed. $E_{1/2}$ is the half wave potential, and $t_0 - t_2$ are defined previously in Figure 5.1..... 92
Figure 5.3 Waveform for osteryoung square wave voltammetry (OSWV).

ΔE_s is the step height or potential increase over each cycle, ΔE_p is the pulse amplitude, and 1 & 2 are points at which the current is sampled. Diagram is not drawn to scale..... 95
Figure 5.4 Forward (i_1) and reverse (i_2) current for an idealized square wave voltammogram (Δi) in a reversible reaction..... 96
Figure 5.5 Specialized electrochemical cell design. Break-seals can be loaded in a glove box and are fused to the cell prior to rigorous vacuum drying and loading of electrolyte and solvent..... 99
Figure 5.6 CV of a saturated solution of **7c** in CH_3CN solution (0.1 M $N^nBu_4PF_6$)..... 105
Figure 5.7 CV of a saturated solution of **7e** in CH_2Cl_2 (0.5 M $N^nBu_4PF_6$) at a scan rate of 5120mVs^{-1}..... 106
Figure 5.8 OSWV diagram of **7c**..... 107
Figure 5.9 Overlapping CV's of the oxidation and reduction potentials of **8e** in CH_3CN solution (0.5M $N^nBu_4PF_6$) at A) dilute concentration, B) moderate concentration, and C) high concentration..... 110
Figure 5.10 OSWV of **8e** in CH_3CN solution (0.5M $N^nBu_4PF_6$) at dilute concentration, corresponding to trace A) in Figure 5.9..... 111
Figure 5.11 OSWV of **8e** in CH_3CN solution (0.5M $N^nBu_4PF_6$) at higher concentration (6.7 x 10^{-3} M), corresponding to trace C) in Figure 5.9..... 111
Figure 5.12 Schematic MO diagram for dimer formation..... 116
Figure 5.13 Plot of the calculated vs. experimental oxidation potential of **7a-e** as measured by cyclic voltammetry in (a) CH_3CN and (b) CH_2Cl_2 solution..... 118
Figure 5.14 Plot of the calculated vs. experimental reduction potential of **7a-e** as measured by cyclic voltammetry in (a) CH_3CN and (b) CH_2Cl_2 solution..... 119
Figure 5.15 Plot of the calculated vs. experimental oxidation potential of **8a-e** as measured by cyclic voltammetry in (a) CH_3CN and (b) CH_2Cl_2 solution..... 121
Figure 5.16 Plot of the calculated vs. experimental reduction potential of **8a-e** as measured by cyclic voltammetry in (a) CH_3CN and (b) CH_2Cl_2 solution..... 121
Figure 5.17 Plot of the calculated vs. experimental oxidation potential of **8a-e** as measured by Osteryoung squarewave voltammetry in (a) CH_3CN and (b) CH_2Cl_2 solution..... 122

List of Abbreviations

B3LYP	Becke's Three Parameter Hybrid Functional Using the Lee, Yang, and Parr Correlation Functional
DFT	Density Functional Theory
EPR	electron paramagnetic resonance
ET	[bis(ethylenedithio)tetrathiafulvalene]
eV	electron Volt
Fc	ferrocene
g	gram
G	Gauss
hfc	hyperfine coupling
HOMO	highest occupied molecular orbital
Hz	Hertz
IR	infrared
LUMO	lowest unoccupied molecular orbital
mL	milliliter
mmol	millimole
MNDO	modified neglect of diatomic overlap
MO	molecular orbital
mp	melting point
MS	mass spectroscopy
NMR	nuclear magnetic resonance
NRC	neutral radical conductor
ORTEP	Oakridge thermal ellipsoid plot
Ph	phenyl
ppm	parts per million
RHF	restricted hartree fock
RIC	radical ion conductor
SOMO	singly occupied molecular orbital
TBAFP	tetrabutylammonium hexafluorophosphate
TCNQ	7,7,8,8-tetracyano-p-quinodimethane
TTF	tetrathiafulvalene
$w_{1/2}$	width of peak at half height

Compound Numbering Scheme

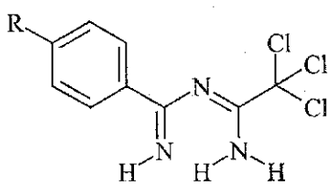

	R
1a	OCH_3
1b	CH_3
1c	H
1d	Cl
1e	CF_3

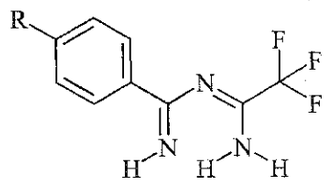

	R
2a	OCH_3
2b	CH_3
2c	H
2d	Cl
2e	CF_3

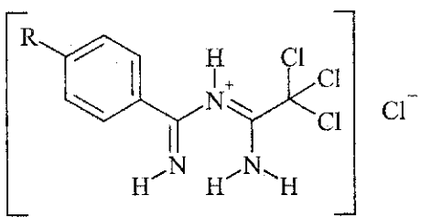

	R
3a	OCH_3
3b	CH_3
3c	H
3d	Cl
3e	CF_3

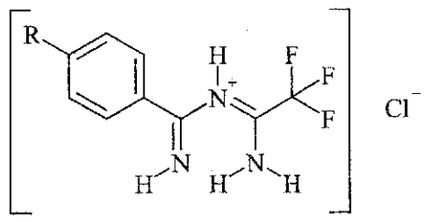

	R
4a	OCH_3
4b	CH_3
4c	H
4d	Cl
4e	CF_3

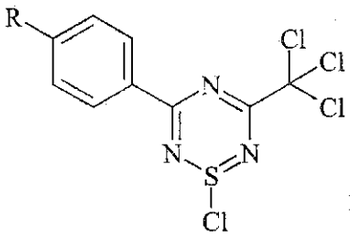

	R
5a	OCH_3
5b	CH_3
5c	H
5d	Cl
5e	CF_3

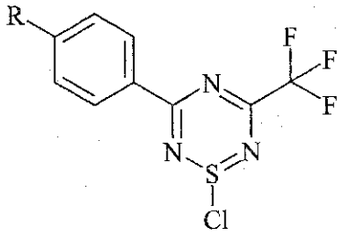

	R
6a	OCH_3
6b	CH_3
6c	H
6d	Cl
6e	CF_3

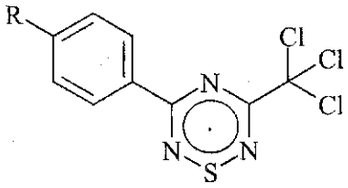

	R
7a	OCH_3
7b	CH_3
7c	H
7d	Cl
7e	CF_3

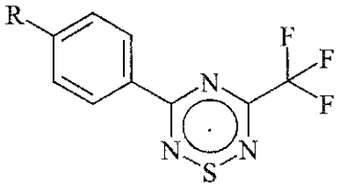

	R
8a	OCH_3
8b	CH_3
8c	H
8d	Cl
8e	CF_3

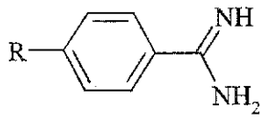

	R
9a	OCH_3
9b	CH_3
9c	H
9d	Cl
9e	CF_3

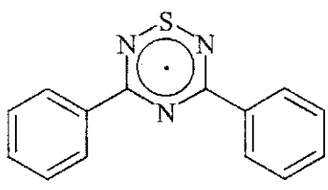

10

Chapter 1

Summary of the work

1.1 Introduction

One of the main objectives of this thesis was to develop and present a general synthetic route to the 1-chloro-1,2,4,6-thiatriazines, as well as to their corresponding 7π radicals (Figure 1.1).

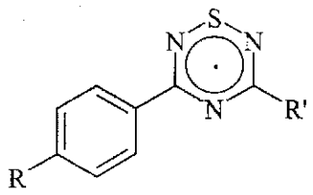

R'	R
7 = CCl_3	**a** = OCH_3
8 = CF_3	**b** = CH_3
	c = H
	d = Cl
	e = CF_3

Figure 1.1 Target 1,2,4,6-thiatriazine radicals **7a-e**, **8a-e**.

This objective has been successfully accomplished, with full and complete characterization of the radicals and their precursers (through solid-state X-ray crystallography, solution electrochemistry, and electron paramagnetic resonance) along with discussion of the results. Solution electrochemistry was performed on all ten radicals identified in Figure 1.1 in two different solvents, allowing for a measure of their redox potentials as a function of 'push' and 'pull' substituents. Hybrid *ab initio*/density functional theory (DFT) calculations were used to interpret the experimental results.

This thesis is divided into several sections. Chapter 2 is a review of background synthetic work of the 1-chloro-1,2,4,6-thiatriazine derivatives, along with a discussion of the synthetic work leading to the series of 1,2,4,6-thiatriazine radicals, and the results of

those investigations. Chapter 3 is a discussion of the crystal structures of two thiatriazine radicals (**7c**, **8c**) and two of their precursor imidoylamidines (**1c**, **2c**). The extended 3-dimensional structure of the solid radicals is discussed in connection with their potential as electrically conducting materials. Chapter 4 reviews the electron paramagnetic resonance (EPR) data and DFT calculations for the thiatriazine. Chapter 5 is an extensive study of the electrochemical data obtained for all ten thiatriazine radicals. Finally, Chapter 6 presents the details of the experimental procedures used to synthesize the thiatriazine radicals and their precursors, along with crystallographic data tables.

1.2 Background: Molecular conducting materials

The majority of known organic materials do not possess any electrical conductivity and are considered to be electrical insulators. However, a few have been found with enough conductivity to be considered semi-conductors, while even fewer still have conductivities approaching those of metals. These have been classified as 'organic metals' and have electrical conductivities, σ, that increase with decreasing temperature ($\sigma \approx 10\text{-}10^4\ \Omega^{-1}\ cm^{-1}$). Conductivity arises in these systems from the formation of a partially filled energy band that can arise from π-orbital overlap between one-dimensional stacks of molecules. These organic conductors usually consist of radical ion pairs or charge transfer salts which allow for the migration of electrical charge though the solid state lattice. The majority of charge transfer salts are modeled on the donor tetrathiafulvalene (TTF)[1] and acceptor 7,7,8,8-tetracyano-p-quinodimethane (TCNQ).[2] This was the first conducting system of its type and it resulted in the synthesis of thousands of variants.

Routes to molecular superconductivity using organic compounds began with the combination of TTF and TCNQ in a 1:1 ratio.

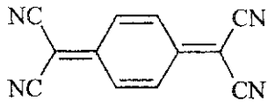

TCNQ

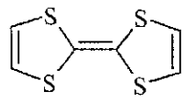

TTF

Other organic metals have now been found to become superconducting (i.e., complete loss of electrical resistance) at low temperature. These materials can be traced back to 1842, when Knop unknowingly prepared the first 'Molecular Inorganic Conductor'.[3] 'Kupferglänzenden', or copper-shining crystals were created by partial oxidation of $K_2[Pt(CN)_4]$ with chlorine or bromine, and were not fully characterized at the time. Later Bechgaard *et al.* discovered and used tetramethyltetraselenafulvalene (TMTSF, a derivative of TTF) to prepare the radical salts $(TMTSF)_2PF_6$ and $(TMTSF)_2ClO_4$. The former was the first molecular compound to become superconducting under pressure[4], whilst the latter was the first molecular superconductor at ambient pressure.[5] Superconducting radical cation salts that are TTF derivatives such as [bis(ethylenedithio)tetrathiafulvalene] (ET) are now commonly known as Bechgaard salts.

The critical criteria[3,6] allowing for a molecular material to achieve metallic conductivity are:

(i) The existence of one or more unpaired electrons, which leads to a partially filled orbital which is capable of forming a conduction band.

(ii) A uniform crystal structure. The singly occupied molecular orbital (SOMO) of each molecule should combine to give a conduction band from π-electron

overlap between adjacent molecules. Improper stacking results in the splitting of the conduction band (a Peierls-like distortion[7]), which then results in a change from metallic conductivity to either semi-conducting or insulating behavior (Figure 1.2).

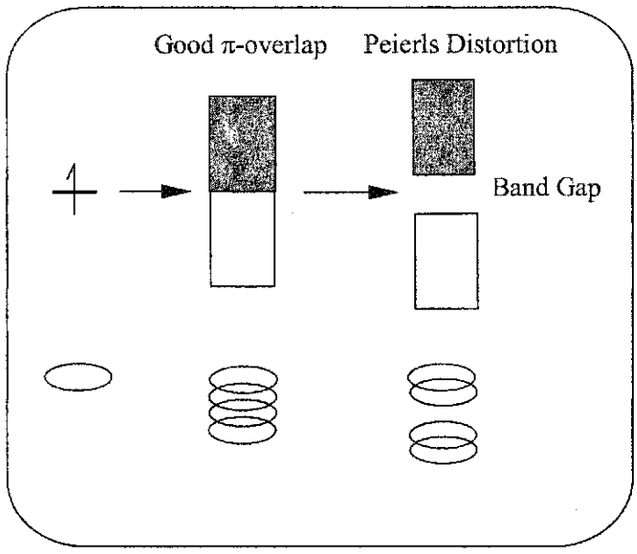

Figure 1.2. Proper vs. improper splitting of the conduction band.

(iii) It is necessary to maximize the overlap ("bonding") between molecules by having an unfilled orbital with a large extension perpendicular to the plane of the molecule, and by minimizing the separation between molecules in the stack.

(iv) The ionic fluctuation energy (U_{eff}) must be minimized, so that the electron-electron repulsion is weakened. This can be done by either (1) using a larger delocalized π-system, or (2) incorporating heteroatoms (i.e., S, N) into the molecules.

An ongoing goal of research in this area is the design of a compound that can attain the optimal π-overlap in a 1-dimensional stack; possess an unpaired electron as the charge carrier through the π-stack; with minimum electron repulsion. The ideal 'molecular metal' may have several advantages: (i) lower weight than conventional metals; (ii) unique ability to process materials allowing for the design of novel devices; (iii) conduct in an anisotropic fashion, for example in the design of unique types of circuits.

The most likely candidates for applications to conducting systems are those species which have at least three redox states that are easily attainable and, preferably, reversibly interconvertible. Group 15/16 heterocycles are among the most prolific types of compounds where these special properties are observable (outside this area are primarily transition metals with multiple redox states (such as vanadium) or the recently identified redox isomers of the fullerenes[8]).

As mentioned above, one of the chief design factors sought in molecular metals is weak electron-electron (coulombic) repulsion, because this can be correlated with a minimization of ionic fluctuation (U_{eff}) during current flow through the solid. A chemical expression of weak coulombic repulsion is a low disproportionation energy, i.e. for the reaction:

$$2 \text{ radical} \leftrightarrow \text{oxidized form} + \text{reduced form} \qquad [1.1]$$

the (unfavorable) free energy should be minimized. It is experimentally difficult to determine the solid–state disproportionation energy. However, it has long been recognized that measurement of the solution phase disproportionation energy using electrochemistry (electrochemical cell potentials, E_{cell}, see below) provides a useful first

estimate of the solid-state disproportionation energy. E_{cell} values have been obtained for classical charge-transfer type radical ion conductors such as TTF[9] and TCNQ[10] as well as for many neutral radical candidates including the 1,2,3,5-dithiadiazoles.[11] The use of solution electrochemistry on this series of 1,2,4,6-thiatriazine radicals gives insight into the width of its redox window, as well as the tunability of the redox states by ring substituents.

1.2.1 Neutral Radical Conductors vs. Radical Ion Conductors

Molecular metal design can be broadly classified into (1) radical ion conductors (RICs) and (2) neutral radical conductors (NRCs). The vast majority of synthetic organic conductors are RIC's: that is they contain charged radicals, either in the form of charge transfer salts (TTF TCNQ) or radical ion salts (Bechgaard). RIC's are two component conductors (cations and anions), and usually only one of the components are active in conduction. NRCs are a new approach that involve the use of neutral rather than charged π-radicals, and hence eliminate the need for counterions. Designing a molecular metal that would meet this criteria using odd alternant hydrocarbons was first suggested by Haddon.[6,12] Odd alternant hydrocarbons are radicals with a non-bonding SOMO and zero π-charge density at all atoms. They should have extensive delocalization of charge density and be capable of forming stable cations and anions. Haddon's proposed phenalenyl (ply) radical was found to have a comparable disproportionation energy to that of the TTF^{+} $TCNQ^{-}$ charge transfer salt through MNDO/3 calculations. However, in practice their utility has been dramatically limited by their tendency to form strongly C–C bonded molecular dimers rather than infinite stacks of solid-state materials. Recent advances in the field have allowed for the solid-state characterization of a spiro-

biphenalenyl that uses a borate structural core and no additional heterocyclic substituents. The spiro-biphenalenyl system is not subject to some of the previous downfalls of the ply radical.[13]

Heterocyclic thiazyl radicals have been proposed as alternatives to hydrocarbon-based radicals.[14-19] A wide variety of both charged and neutral radical species can be made by the incorporation of SN and SeN units into heterocyclic frameworks, along with carbon (and/or phosphorous). These radicals offer both advantages and disadvantages as building blocks for molecular metals. Thiazyl rings have a smaller tendency for σ-bond formation than their carbon-based counterparts because of the lower bond energies associated with sulfur and nitrogen. As well, heterocycles built from a series of –S=N– units provide strong π interactions due to a comparable overlap between the sulfur $3p_\pi$ and nitrogen $2p_\pi$ orbitals to that of adjacent carbon $2p_\pi$ orbitals. Their ability to delocalize charge throughout the π-system means that there is less of a tendency for dimerization. On the other hand, a disadvantage of using sulfur or nitrogen is their higher effective electronegativity. This tends to localize charge at these elements and hence can be a detriment to conductivity. This tendency can be countermanded to some extent by the judicious use of substituents on the heterocyclic ring. This thesis describes one such attempt.

1.3 Known Redox-active Heterocycles

The term 'redox-active' applies to any compound that can be easily oxidized or reduced. It is an arbitrary definition, but we apply here a more restricted version by (1) requiring both the oxidation and reduction processes to be accessible, and (2) restricting

the interval between the oxidation and reduction to 2 Volts or less. We use the term 'redox window' to mean the voltage range within which the central oxidation state is stable. Generally, the smaller the redox window attainable, the lower the disproportionation energy and hence the greater potential the compound has as an NRC.

It is well known that polycyclic aromatic compounds can be chemically or electrochemically reduced, often forming stable radical anions. Under some circumstances, they can also be reversibly oxidized. Benzene has a very large redox stability window that stretches from approximately – 3 to + 3 Volts. It is thus decidedly redox-inactive. However, with increasing ring conjugation the redox stability window decreases. This behavior has been correlated to both the raising of the HOMO and the lowering of the LUMO. Thus the redox stability window of naphthalene is 4.04 Volts in acetonitrile[20], while that of anthracene is only 2.87 Volts in the similar solvent DMF.[21]

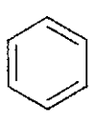

benzene

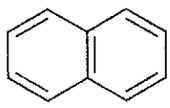

naphthalene

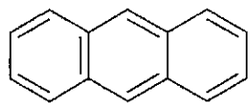

anthracene

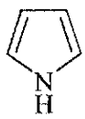

pyrrole

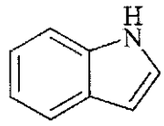

indole

thiophene

Compared to these carbacycles, heterocycles such as pyrrole, indole, and thiophene have decidedly smaller redox windows. The 1,2,3,5-dithiadiazoles have a redox window of approximately 1.5 Volts and extensive research has gone into their potential as candidates for NRCs. The large amount of heterocyclic ring systems studied thus far for

their potential as NRC candidates vary in many ways including ring size, heteroatom substituents, and tunability. A brief general description of each class by ring size follows.

1.3.1 Five-membered rings

Five-membered thiazyl heterocycles have been by far the most studied ring size. They can be split up into the following categories (Figure 1.3.1):

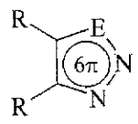

1,2,3-thiadiazoles (E = S)
1,2,3-selenadiazoles (E = Se)

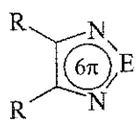

2,1,3-thiadiazoles (E = S)
2,1,3-selenadiazoles (E = Se)

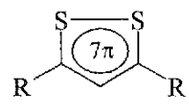

1,2-Dithioles

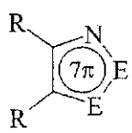

1,2,3-dithiazoles (E = S)
1,2,3-diselenazoles (E = Se)

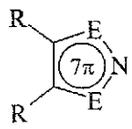

1,3,2-dithiazoles (E = S)
1,3,2-diselenazoles (E = Se)

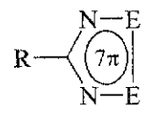

1,2,3,5-dithiadiazoles (E = S)
1,2,3,5-diselenadiazoles (E = Se)

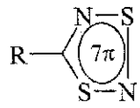

1,3,2,4-dithiadiazoles (S)

Figure 1.3 Some five-membered thiazyl heterocycles.

The thiadiazoles are ineligible as NRC candidates because they have 6π-electrons, and therefore do not have an unpaired electron. The 1,2-dithioles have 7π electrons and have been studied for their ability to make NRCs. 1,2,3,5-dithiadiazoles have been the most extensively studied systems to date with regard to their potential as NRCs[11,15,19,22-

[27], although their disproportionation energies are higher in comparison to TTF^{+} $TCNQ^{-}$, and they have a strong tendency to dimerize through the sulfur atoms in the solid state. Overcoming Peierls distortion by creating derivatives with suitable intra- and interstack interactions has been pursued and some have been found to be intrinsic semi-conductors.[16]

1.3.2 Six-membered rings

Known six-membered thiazyl heterocycles belong to two categories, the thiatriazines and the dithiatriazines (Figure 1.4), each of which have numerous isomeric forms.

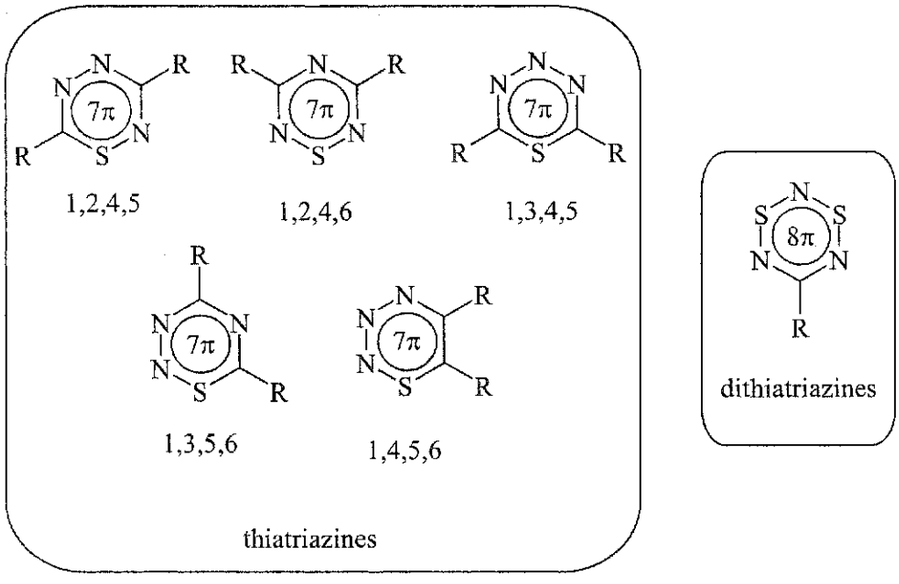

Figure 1.4 Some six-membered thiazyl heterocycles

Very little is known about these six-membered heterocycles. Such ring systems are often less stable and harder to synthesize than the numerous kinds of five-membered ring compounds. The dithiatriazines have an 8π-electron count and as such are not

suitable candidates for making NRCs. Thiatriazines, in the neutral form, are seven π-electron systems (making them candidates for NRCs). Recently the 3,6-diphenyl-4*H*-1,2,4,5-thiatriazine was synthesized as a precursor to a 1,2,4,5-thiatriazine radical.[28] Attempts at obtaining the radical via conversion to the sulfiminyl chloride followed by reduction with triphenylantimony yielded a weak EPR signal with ambiguous interpretation. A cumulative comparison of all known isomers of thiatriazine rings using *ab initio* calculations predicted the 1,2,4,6-thiatriazine to form the most stable neutral radical.[28-30] The 3,6-diphenyl-1,2,4,6-thiatriazine and its selenium analogue[31], are the only neutral thiatriazine radicals that have been structurally characterized.[32] Both radicals were shown to contain strongly dimerized units that have no long range stacking in the solid state. Oxidation of the 3,6-diphenyl-1,2,4,6-thiatriazine radical with nitrosonium salts yielded the thiatriazine cation, while reduction by sodium in liquid ammonia yielded the $Ph_2C_2N_3SH$ anion. Both ions were structurally characterized. MNDO calculations on the triad of oxidation states were performed to determine the structural stability of this radical to redox changes. After these initial investigations, the thiatriazine ring system was largely ignored in favor of the various five-membered heterocycles mentioned above.

1.4 1,2,4,6-thiatriazines

Because thiatriazines possess an unpaired electron and little information is known on these ring systems, it was felt that more research was warranted on their behavior in solution, their packing in the solid state, and the degree to which their redox properties could be 'tuned' by variation of the 'R' substituents. My approach was to try to prepare a

homologous series of compounds, which both allows for an investigation of 'tunability' and provides an internal check on the reliability of measurements taken on potentially reactive materials.

1,2,4,6-thiatriazines possess three positions for substituents. The parent heterocycle (all H's) is unknown. The nature of these substituents has profound influence on the properties of the rings. Figure 1.4 emphasizes the possible pattern of substitution. Carbon substitution is distinguished from heteroelement substitution, since only the latter can be further derivatized.

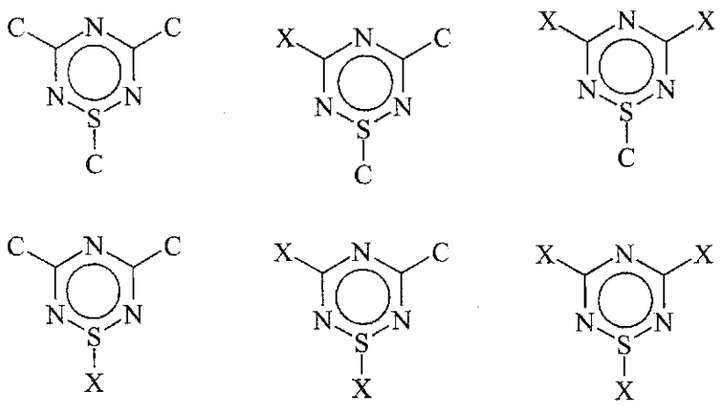

X = amine, halogen
C = alkyl or aryl group

Figure 1.4. Substituent variation of the 1,2,4,6-thiatriazines

The majority of known thiatriazine derivatives are cyclic sulfonamides (an amide group attached to sulfur) or are part of fused ring systems.[33-37] As well, derivatives with alkyl or aryl groups in the 1, 3, and 5 positions have been prepared by the reaction of N-haloamidines with thiolates or N-sulfenylamidines.[38,39] My interest lies with S-X

derivatives, and more specifically the S-Cl compounds because reductive elimination of chloride can lead to delocalized π-radicals which are stored as weakly dimerized species in the solid state. Such radicals are known so far for:

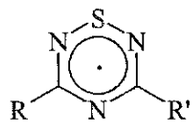

11 R = R' = Cl
12 R = R' = NEt_2
10 R = R' = Ph
13 R = R' = 4-NO_2-C_6H_4
14 R = R' = 4-CH_3O-C_6H_4
15 R = R' = CF_3

For compounds **11** and **15**, only EPR and PES data was reported.[40] Compound **12** has been fully characterized[41], as has compound **10**.[32,42] Only EPR data is available for compounds **13** and **14**.[40] All have been made from the S-Cl starting materials by either (a)Ph_3Sb or (b)Zn/SO_2 reduction.

In view of the unusual electronic structure of thiatriazines, it is worth briefly considering the basic structure of these compounds. I start with the parent S-Cl compounds. The S-Cl bond is strongly polarized, and if we imagine these rings to be fully ionized we get the following structure:

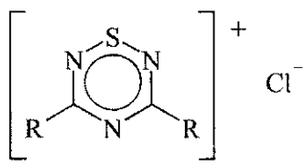

Oakley[32] has structurally characterized such a cation (R = Ph), and it was shown to be planar. Hence we can ascribe sp^2 hybridization to each ring atom. If we count the valence electrons, we find enough electrons to occupy an in-plane lone electron pair on each hetero element.

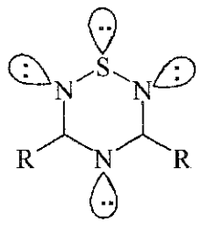

In addition, each ring atom contributes one additional electron, which must reside in the π-electronic system. Hence we get the classical 6π benzene–like description:

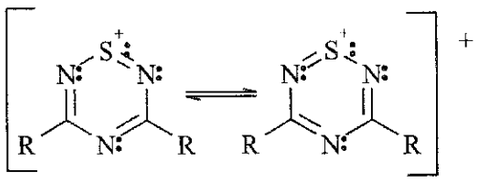

The high electronegativity of both sulfur and nitrogen is expected to polarize the π-electron density substantially. The same factor also explains the affinity of the ring to accept an additional electron. Hence neutral 1,2,4,6-thiatriazines are considered to be 7π radicals, and are thought to be planar ring compounds.

1.5 Conclusions

Heterocyclic thiazene ring systems have been aggressively studied as possible candidates for molecular metal design. The 1,2,4,6-thiatriazine radicals can be thought of as neutral radical conductors within the scope of this research. However, they have been largely ignored in favor of other five-membered ring systems. The limited knowledge base of these compounds warrants a more thorough investigation through the use of x-ray structure determination, EPR, and solution electrochemistry. This will give much needed insight to the radicals' behavior both in solution and in the solid state.

References

1. Wudl, F.; Smith, G. M.; Hufnagel, E. J. *J. Chem. Soc., Chem. Commun.* **1970**, 1453.

2. Acker, D. S.; Harder, R. J.; Hertler, W. R.; Mahler, W.; Melby, L. R.; Benson, R. E.; Mochel, W. E. *J. Am. Chem. Soc.* **1960**, *82*, 6408.

3. Bruce, D. W.; O'Hare, D. *Inorganic Materials*; John Wiley & Sons Ltd.: West Sussex, England, 1996.

4. Jerome, D.; Mazaud, A.; Ribault, M.; Bechgaard, K. *J. Phys. Lett. (Orsay, France)* **1980**, *41*, 95.

5. Bechgaard, K.; Carneiro, K.; Rasmussen, F. B.; Olsen, H.; Rindorf, G.; Jacobsen, C. S.; Pedersen, H.; Scott, J. E. *J. Am. Chem. Soc.* **1981**, *103*, 2440.

6. Haddon, R. C. *Aust. J. Chem.* **1975**, *28*, 2343.

7. Peierls, R. E. *Quantum Theory of Solids*; Oxford University Press: London, 1955.

8. Xie, Q.; Pérez-Cordero, E.; Echegoyen, L. *J. Am. Chem. Soc.* **1992**, *114*, 3978.

9. Sandman, D. J.; Zoski, G. D.; Burke, W. A.; Hamill, G. P.; Ceasar, G. P.; Baker, A. D. *J. Chem. Soc., Chem. Commun.* **1981**, 829.

10. Kaplan, M. L.; Haddon, R. C.; Bramwell, F. B.; Wudl, F.; Marshall, J. H.; Cowan, D. O.; Gronowitz, S. *J. Phys. Chem.* **1980**, *84*, 427.

11. Boeré, R. T.; Moock, K. H. *J. Am. Chem. Soc.* **1995**, *117*, 4755.

12. Haddon, R. C. *Aust. J. Chem.* **1975**, *28*, 2333.

13. Chi, X.; Itkis, M. E.; Patrick, B. O.; Barclay, T. M.; Reed, R. W.; Oakley, R. T.; Cordes, A. W.; Haddon, R. C. *J. Am. Chem. Soc.* **1999**, *121*, 10395.

14. Oakley, R. T. *Progress in Inorganic Chemistry* **1988**, *36*, 299.

15. Beer, L.; Cordes, A. W.; Myles, D. J. T.; Oakley, R. T.; Taylor, N. J. *Cryst. Eng. Comm.* **2000**, *20*, 109.

16. Beer, L.; Oakley, R. T.; Mingie, J. R.; Preuss, K. E.; Taylor, N. J. *J. Am. Chem. Soc.* **2000**, *122*, 7602.

17. Chi, X.; Itkis, M. E.; Kirschbaum, K.; Pinkerton, A. A.; Oakley, R. T.; Cordes, A. W.; Haddon, R. C. *J. Am. Chem. Soc.* **2001**, *123*, 4041.

18. Beer, L.; Britten, J. F.; Cordes, A. W.; Clements, O. P.; Oakley, R. T.; Pink, M.; Reed, R. W. *Inorg. Chem.* **2001**, *40*, 4705.

19. Britten, J. F.; Clements, O. P.; Cordes, A. W.; Haddon, R. C.; Oakley, R. T.; Richardson, J. F. *Inorg. Chem.* **2001**, *40*, 6820.

20. Zweig, A.; Hoffman, K. *J. Org. Chem.* **1965**, *30*, 3997.

21. *CRC Handbook of Chemistry and Physics*; Weast, R. C.; CRC Press: Boca Raton, FL, **1989**, p D-159.

22. Cordes, A. W.; Haddon, R. C.; Hicks, R. G.; Oakley, R. T.; Palstra, T. T. M. *Inorg. Chem.* **1992**, *31*, 1802.

23. Aherne, C. M.; Banister, A. J.; Gorrell, I. B.; Hansford, M. I.; Hauptman, Z. V.; Luke, A. W.; Rawson, J. M. *J. Chem. Soc., Dalton Trans.* **1993**, 967.

24. Beekman, R.; Boeré, R. T.; Moock, K. H.; Parvez, M. *Can. J. Chem.* **1998**, *76*, 85.

25. Feeder, N.; Less, R. J.; Rawson, J. M.; Oliete, P.; Palacio, F. *Chem. Commun.* **2000**, 2449.

26. Brownridge, S.; Du, H.; Fairhurst, S. A.; Haddon, R. C.; Oberhammer, H.; Parsons, S.; Passmore, J.; Schriver, M. J.; Sutcliffe, L. H.; Westwood, N. P. C. *J. Chem. Soc., Dalton Trans.* **2000**, *19*, 3365.

27. Boeré, R. T.; Moock, K. H.; Parvez, M. *Z. Anorg. Allg. Chem.* **1994**, *620*, 1589.

28. Farrar, J. M.; Patel, M. K.; Kaszynski, P.; Young Jr., V. G. *J. Org. Chem.* **2000**, *65*(4), 931.

29. Kaszynski, P. *J. Phys. Chem. A* **2001**, *105*, 7615.

30. Kaszynski, P. *J. Phys. Chem. A* **2001**, *105*, 7626.

31. Oakley, R. T.; Reed, R. W.; Cordes, A. W.; Craig, S. L.; Graham, J. B. *J. Am. Chem. Soc.* **1987**,*109* , 7745.

32. Boeré, R. T.; Cordes, A. W.; Hayes, P. J.; Oakley, R. T.; Reed, R. W.; Pennington, W. T. *Inorg. Chem.* **1986**, *25*, 2445.

33. Schramm, W.; Voss, G.; Rembarz, G. *Z. Chem.* **1974**, *12*, 471.

34. Leonhardt, G.; Scheibe, R.; Schramm, W.; Voss, G.; Fischer, E.; Rembarz, G. *Z. Chem.* **1975**, *15*, 193.

35. Storek, W.; Schramm, W.; Voss, G.; Rembarz, G.; Fischer, E. *Z. Chem.* **1975**, *15* , 104.

36. Jeroschewski, P.; Voss, G.; Fischer, E. *Z. Chem.* **1977**, *17*, 145.

37. Kornuta, P. P.; Derii, L. I.; Romanenko, E. A. *Chemistry of Heterocyclic Compounds* **1978**, *273*, 226.

38. Goerdeler, J.; Loevenich, D. *Chem. Ber.* **1954**, *87*, 1079.

39. Goerdeler, J.; Wedekind, B. *Chem. Ber.* **1962**, *95*, 147.

40. Boeré, R. T.; Oakley, R. T.; Reed, R. W.; Westwood, N. P. C. *J. Am. Chem. Soc.* **1989**, *111*, 1180.

41. Boeré, R. T. *Unpublished Data* .

42. Hayes, P. J.; Oakley, R. T.; Cordes, A. W.; Pennington, W. T. *J. Am. Chem. Soc.* **1985**, *107*, 1346.

Chapter 2

Preparation of the 1,2,4,6-thiatriazines

2.1 Introduction

2.1.1 Previous synthetic routes to 1-chloro-1,2,4,6-thiatriazines

The earliest work involving 1,2,4,6-thiatriazines dates back to 1970 when Geevers reacted sodium dicyanamide with thionyl chloride to give the 1,3,5-trichloro-1,2,4,6-thiatriazine (but incorrectly identified it).[1] Reduction of this compound to the radical was reported much later[2], while other workers corrected the structural assignment.[3] Kornuta and co-workers reported the formation of several 1-chloro-1,2,4,6-thiatriazine rings by substitution of the chlorine atoms in the above compound, and reported their reduction to radicals.[4,5] More recently the 1-chloro-3,5,-diphenyl-1,2,4,6-thiatriazine was made by Oakley and co-workers[6], from the reaction of benzamidine with $S_3N_3Cl_3$ to give the 1-chloro thiatriazine precursor in low yields, together with S_4N_4 and the dithiadiazolium chloride $PhCN_2S_2^+ Cl^-$.

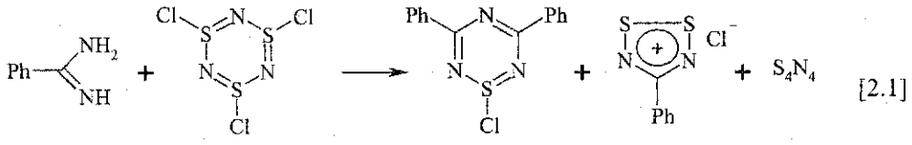

[2.1]

Reduction to the thiatriazine radical has been reported[7] and an EPR spectrum has been reported. The spectrum indicates that the unpaired electron's spin distribution is divided equally over the three nitrogen atoms (with a substantial sulfur contribution as well), with no additional coupling to the phenyl protons. Spin delocalization onto the external rings does not occur to any measurable extent due to the electronegative potential exerted by the thiatriazine ring. Molecular orbital energies calculated at the Restricted Hartree Fock (RHF) modified neglect of diatomic overlap (MNDO) level correlated well with the

observed coupling constants.[6] They indicated an antibonding distribution localized over the N=S=N region. In the dimer, a net bonding interaction occurs between the two sulfur atoms which arises from overlap of the π*-SOMOs of the radical partners. An overall diamagnetic ground state for the dimer was predicted. Solid state characterization by X-ray crystallography revealed discrete pairs of thiatriazine rings linked cofacially in a totally eclipsed conformation, with a core that exhibited a shallow boat, or open book, conformation. In addition, salts of the cation and a derivative of the anion were also isolated and structurally characterized.[8]

2.1.2 A more versatile synthetic method

Oakley's method works well enough for the diphenyl thiatriazine chloride, despite the complex product distribution. However, it is not generalizable, as other aryl amidines produce only trace quantities of thiatriazine among even more complex side products.[9] The focus of my synthetic work has been on the development of a more flexible and general route to the 1,2,4,6-thiatriazine radical that will allow for modification of the exocyclic substituents. My method is based on the postulate that benzamidine, shown in Equation 2.1, undergoes a condensation reaction with the elimination of ammonia or ammonium chloride. The resulting imidoylamidine can react with thiazyl chloride to form the 1-chloro-1,2,4,6-thiatriazine. This suggests that if one can prepare an imidoylamidine, it should react with a source of "SCl" to form the 1-chloro-1,2,4,6-thiatriazines directly. Hence simple sulfur chlorides should accomplish this reaction rather than $S_3N_3Cl_3$. A scheme outlining the synthetic route which I developed is shown below (Figure 2.1):

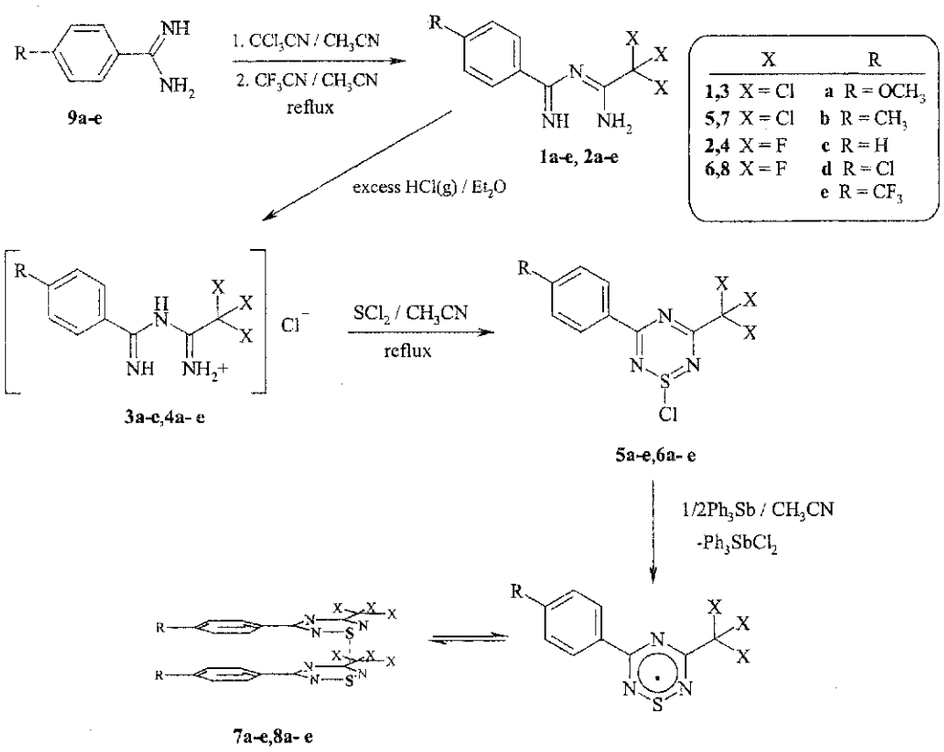

Figure 2.1 Synthetic route to the 1,2,4,6-thiatriazine radicals **7a-e**, **8a-e**.

2.2 Synthesis of amidines

Primary amidines are not particularly stable, and only a few are commercially available as hydrochloride salts (i.e., $RC(NH_2)NH_2Cl$ (R = Ph, Me)). All the substituted free amidines **I** required (except Ph) were made from the corresponding nitriles as the hydrochloride salts.[10] Free amidines were obtained by dissolving the hydrochloride salt in water and adding 5M sodium hydroxide. Addition of the base caused the amidine to precipitate out of solution. The amidines were purified by sublimation under vacuum at ~130°C. Benzamidine was made by treatment of the commercial hydrochloride salt with potassium hydroxide followed by extraction with dichloromethane. The dichloromethane

extract was dried with magnesium sulfate, filtered and evaporated to yield quantitative amounts of crude benzamidine. A final purification by sublimation *in vacuo* was performed at ~45°C to yield a white powder.

2.3 Synthesis of the aryl N-imidoylamidines

Aryl N-imidoylamidines have been implicated as intermediates in many reactions, but few have actually been isolated and characterized. Some previous routes to aryl imidoylamidines include combining benzamidine and N-thiobenzoylbenzamidine to produce N-benzimidoylbenzamidine (Equation 2.2).[11]

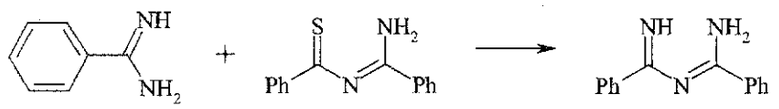

[2.2]

Another route involves reacting primary amidine hydrochlorides with primary imidates (R'C(NH)OEt) in the presence of NaOEt (Equation 2.3).[12]

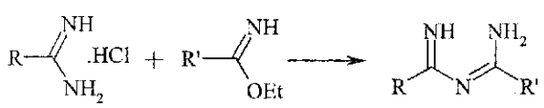

R	R'
Ph	Ph
Me	Me
4-$NO_2C_6H_4$	Ph
4-ClC_6H_4	4-ClC_6H_4
4-ClC_6H_4	Ph
3-pyridinyl	Ph

[2.3]

Adding two equivalents of trifluoroacetonitrile or trichloroacetonitrile with one equivalent of ammonia produces N-(trifluoroacetimidoyl)-trifluoroacetamidine or N-(trichloroacetimidoyl)-trichloroacetamidine in quantitive yields (Equation 2.4).[13]

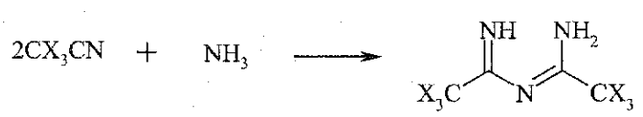

[2.4]

X = Cl, F

My initial attempts to prepare an imidoylamidine involved the dropwise addition of trichloroacetonitrile to a mixture of benzamidine hydrochloride and sodium hydroxide in methanol (Equation 2.5).[14]

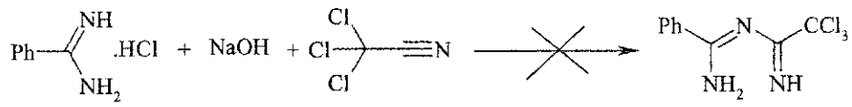

[2.5]

The condensation reaction that should occur here is not unlike the acidic conditions that occur in Oakley's reaction shown in Equation 2.1. Unfortunately, even after several attempts this reaction proved unsuccessful, as the product obtained was always a dark oil that could not be purified or characterized. However, by using the free amidine, which should be a much stronger nucleophile, I found that the condensation reaction with tri-halogen substituted acetonitriles gave the desired imidoylamidine products in high yields.

2.3.1 Trichloromethyl imidoylamidines

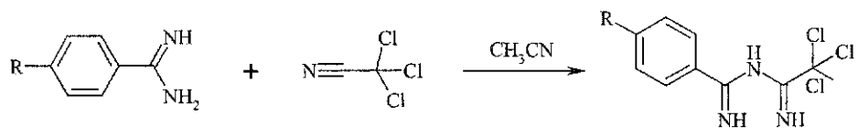

[2.6]

para-substituted benzamidines **9a-e**

trichloroacetonitrile

para-substituted trichloromethyl imidoylamidines **1a-e**

R = OCH_3, CH_3, H, Cl, CF_3

Once the free amidines were obtained the next step was to add them to trichloroacetonitrile in dried acetonitrile. This is a nucleophilic addition reaction, with the electronegative chlorine atoms drawing negative charge away from the nitrile carbon and enhancing its electrophilicity. The reaction took place in solution under nitrogen and was allowed to reflux for 2-3 hours. Once cooled, all solutions were rotary evaporated to give relatively high yields of crude solid product (between 70-99%), and colors varied from off-white to pink or purple. The NMR data did not show significant quantities of

impurities in the crude product, hence this was used in subsequent steps without any further purification. The scale was kept to between one and five grams. The imidoylamidines were characterized by ^{1}H and ^{13}C NMR as well as MS and elemental analysis. For MS and elemental analysis data, the crude material was placed in a three zone tube furnace and sublimed to give colorless solids in all cases. Although it was expected that the imidoylamidines would be thermally labile species, the sublimed materials had very similar ^{1}H NMR spectra to the crude products.

2.3.2 Trifluoromethyl imidoylamidines

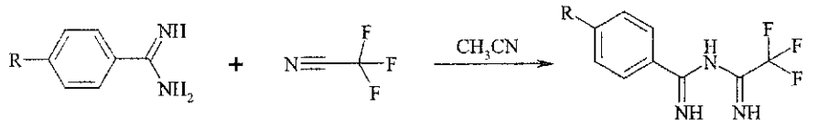

[2.7]

para-substituted benzamidines **9a-e** | trifluoroacetonitrile | *para*-substituted trifluoromethyl imidoylamidines **2a-e**

R = OCH_3, CH_3, H, Cl, CF_3

A different approach was used in making the substituted trifluoromethyl imidoylamidines, because trifluoroacetonitrile is a gas at room temperature. It was necessary to add trifluoroacetonitrile to the substituted amidines in dried acetonitrile by a vacuum line transfer. In early experiments the trifluoroacetonitrile was loaded into the Pyrex tube fitted with a rotaflow stopcock on a vacuum line. This tube was then attached to the reaction vessel using an all-glass transfer line (Figure 2.2). The frozen trifluoroacetonitrile was removed from the $N_2(l)$ and allowed to warm slowly, while a

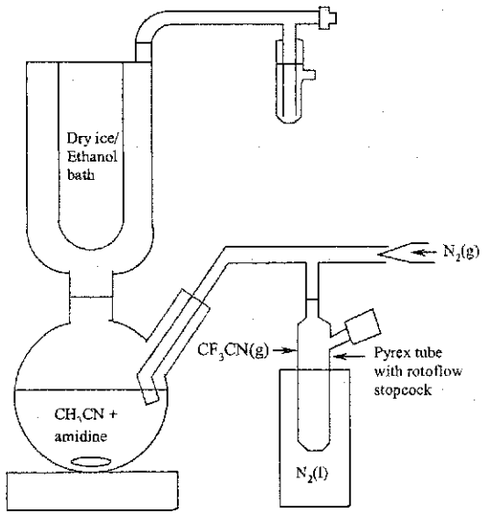

Figure 2.2 Trifluoroacetonitrile glass transfer apparatus.

stream of N_2(g) directed it into the acetonitrile solution containing the aryl amidine. A cold finger with an ethanolic/dry ice bath was attached to the round bottom flask to try and keep the trifluoroacetonitrile from escaping while the reaction was taking place. Once all of the trifluoroacetonitrile was added, the glass apparatus was removed from the round bottom flask and the hole stopped to ensure that none of the gas could escape. The mixture was refluxed for approximately 1 to 2 hours.

This method of preparing the imidoylamidine was only moderately successful as some of the trifluoroacetonitrile always appeared to escape from the experimental apparatus. Usually a 1:1 mixture of product and unreacted amidine would be obtained, which meant further purification to isolate the imidoylamidine. Adding an excess of trifluoroacetonitrile did not improve yields. Efforts to improve techniques for transferring the trifluoroacetonitrile were equally unsuccessful. At this stage an alternate route to making the imidoylamidine was attempted.

The second approach taken to making **2a-e** involved adding a quantified amount of the *para*-substituted aryl amidine and solvent to a heavy-wall Pyrex tube fitted with a rotaflow stopcock. The Pyrex tube was then attached to a vacuum line and the contents were freeze-thaw-degassed once. The aryl amidine and solvent were refrozen and the trifluoroacetonitrile was transferred into the vacuum line quantitatively in 1:1 stoichiometry. The trifluoroacetonitrile was then added into the vessel, which was warmed to room temperature, or slightly warmer, with stirring to ensure reaction completion. The solution was then transferred to a round bottom flask and rotary evaporated to dryness. In some cases an oil remained (i.e., **2c**), but these would solidify if left in the refrigerator overnight. All products were placed on the vacuum line to remove any remaining solvent. The results of synthesizing the trifluoromethyl imidoylamidines in this manner were much more successful than the previous method. All five compounds were created without any mixtures or unreacted amidines appearing, and yields were generally very high. The crude products were sublimed in a three zone tube furnace for further purification, which left colorless solids in all cases. The sublimed products were found to be pure according to ^{1}H and ^{13}C NMR spectroscopy, MS and elemental analysis.

2.3.3 Discussion

A proposed mechanism for the formation of the imidoylamidine is:

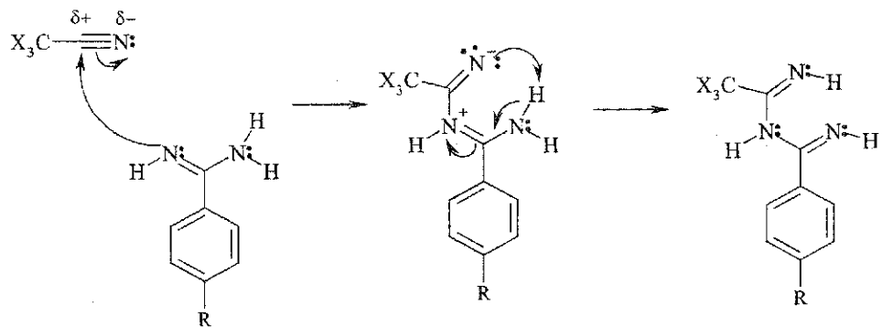

R = OCH_3, CH_3, H, Cl, CF_3
X = Cl, F

Hydrogen bonding is most likely occuring on the two terminal nitrogens, allowing for a stable 'pseudo' ring complex to occur with a greater delocalization of charge.

The imidoylamidine has several tautomeric forms, two of which are shown below.

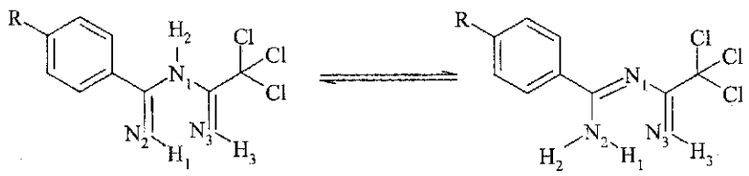

^{1}H NMR data showed three separate NH peaks (Table 2.1), indicating non-equivalency of the hydrogen atom environments. One possible suggestion is that the hydrogen atoms are each bonded to a separate nitrogen atom (as shown on the left hand tautomer). Another possibility is that the two hydrogen atoms attached to N_2 in the right hand tautomer are not equivalent due to hydrogen bonding of H_1 to N_3. The situation in the solid state is discussed in Chapter 3 for compounds **1c** and **2c**, for which X-ray structures have been determined. Each NH peak was also distinctly different in height and line width, indicating dynamic exchange of hydrogen atoms.

In all cases except the phenyl derivative **1c**, two doublets occured in the 6–8 ppm range, consistent with the hydrogen atoms in the *meta* and *ortho* positions on the phenyl

ring. **1c** gave a multiplet in the same range (6-8 ppm). The only other peaks that occurred were singlets due to the *para* substituted CH_3 (2.40 ppm) and OCH_3 (3.86 ppm) groups on the phenyl ring. No additional peaks occurred in the spectra, indicating a high purity in the crude material. However, further purification of the crude by sublimation produced colorless crystals, which indicated that the variation in color of the crude was most likely due to the presence of trace impurities. ^{1}H NMR spectra of **2a-e** were directly comparable with those of **1a-e** (Table 2.1). Three NH peaks (very similar to **1a-e**) appeared in all spectra, along with two doublets (for compounds **2a**, **2b**, **2d**, and **2e**) in the 6-8 ppm range and a multiplet for **2c**. Singlets appeared in **2b** (CH_3, 2.84 ppm) and **2a** (OCH_3, 3.85 ppm).

^{13}C NMR showed seven distinct carbon peaks (Table 2.2), which are attributable to the seven different carbon atoms in **1a-e** and **2a-e**. A consistent set of assignments could be made using a combination of standard data compilation[15] and ^{19}F coupling in the **2a-e** analysis.

The precursor amidines are known to be very strong bases (high pKa values) due to the delocalization of charge in the amidinium cation, which creates a more stabilized structure.[16] Based on this premise the imidoylamidines should be even stronger bases due to more extensive delocalization of charge. This delocalization, along with the known tautomerism and hydrogen bonding, give a very stable pseudo ring structure. The delocalization of charge in the imidoylamidinium cation is shown below:

Table 2.1 ^{1}H NMR of the aryl imidoylamidines **1a-e**, **2a-e**.

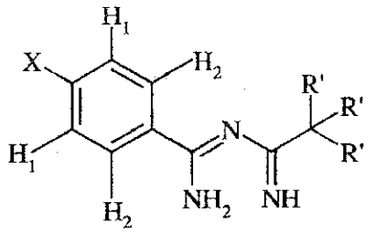

Compound	R'	X	H_1 [1]	H_2 [1]	J_{AB} (Hz)	X [1]	NH [1]	NH	NH
1a	Cl	OCH_3	6.96	7.94	9.0	3.86	10.7	9.3	6.5
1b		CH_3	7.25	7.84	8.4	2.40	10.7	9.3	6.6
1c		H	m 7.45 – 7.48	m 7.93 – 7.96	------	m 7.42 – 7.56	10.7	9.4	6.6
1d		Cl	7.42	7.88	8.9	-------	10.7	9.4	6.7
1e		CF_3	7.73	8.06	8.1	------	10.8	9.5	6.6
2a	F	OCH_3	6.93	7.87	9.0	3.85	11.0	9.0	6.7
2b		CH_3	7.26	7.81	8.1	2.41	11.0	9.1	6.7
2c		H	m 7.38 – 7.54	m 7.83 – 7.88	------	m 7.38 – 7.54	11.0	9.1	6.8
2d		Cl	7.42	7.84	8.8	-------	11.0	9.2	6.7
2e		CF_3	7.73	8.02	8.1	------	11.1	9.3	6.8

1. All values are in ppm, with reference to TMS

Table 2.2 ^{13}C NMR of the aryl imidoylamidines **1a-e**, **2a-e**.

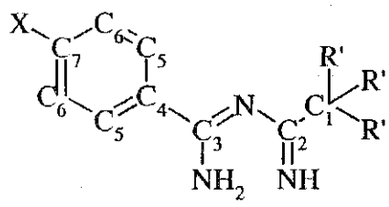

Compound	R'	X	C_1 [1]	C_2 [1]	C_3 [1]	C_4 [1]	C_5 [1]	C_6 [1]	C_7 [1]	X [1]
1a	Cl	OCH_3	98.18	163.02	168.15	127.75	129.36	114.33	164.23	55.71
1b		CH_3	98.11	164.66	168.17	132.64	127.52	129.62	142.60	21.65
1c		H	97.99	164.72	168.17	135.48	127.56	128.97	132.07	----
1d		Cl	97.78	163.59	167.94	133.83	128.90	129.17	138.39	----
1e		CF_3	97.62	163.39	168.03	138.90	128.03	126.00[2]	133.83[3]	123.97[4]
2a	F	OCH_3	117.86[5]	163.41[3]	165.33	127.33	129.25	114.32	163.09	55.66
2b		CH_3	117.84[5]	163.55[3]	165.83	132.37	127.64	129.70	142.84	21.65
2c		H	117.80[5]	163.51[3]	165.92	135.22	127.44	129.02	132.20	----
2d		Cl	117.70[5]	163.31[3]	164.76	133.60	128.83	129.28	138.62	----
2e		CF_3	117.67[5]	163.23[3]	164.65	138.55	127.91	125.98[2]	133.91[3]	123.91[4]

1. All values are in ppm, with reference to TMS
2. q, $^3J_{(F,C)} = 3.9$ Hz
3. q, $^3J_{(F,C)} = 33$ Hz
4. q, $^3J_{(F,C)} = 273$ Hz
5. q, $^3J_{(F,C)} = 281$ Hz

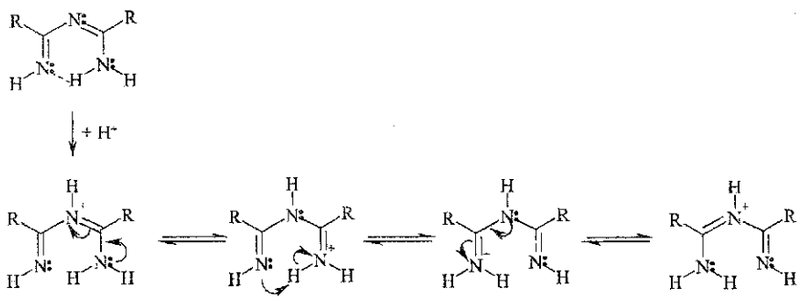

Important stretching frequencies in the IR data have been listed below in Table 2.3. Whilst the energies are not consistent enough to predict patterns, what can be noted is that three stretching frequencies appear that can be correlated with their solid state arrangement. For example, I found that in the crystal structure of **1c** (Section 3.2.4), there were three very distinct environments for the hydrogen atoms attached to nitrogen. One hydrogen atom is isolated from hydrogen bonding, and could correspond to the sharp band at 3320 cm^{-1}. Another hydrogen is involved in typical intermolecular hydrogen bonding. This could be the broadened band at 3281 cm^{-1} (i.e., shifted to lower energy). The third hydrogen atom is involved in very strong intramolecular hydrogen bonding, which could correspond to the very broad band at 3128 cm^{-1} (i.e., shifted to even lower energy). Variations in the IR data may reflect different crystallographic arrangements among these ten compounds.

CN stretches occurred in the 1625 ± 25 cm^{-1} range, and are clearly complex due to the presence of several C–N bonds with partial double bond character. These values do not differ greatly from the CN valence vibrations reported for various substituted amidines[16]. All other vibrations occurred in the fingerprint region.

Table 2.3 IR data for the imidoylamidines **1a-e**, **2a-e**[1]

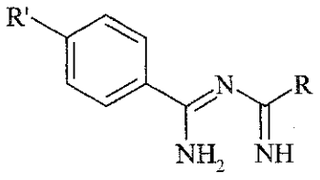

CMPD	R	R'	NH	NH	NH	CN[2]
1a	CCl_3	OCH_3	3387 (br)	3320 (sh)	3129 (br)	1604
1b	CCl_3	CH_3	3451 (br)	3324 (sh)	3121 (br)	1624
1c	CCl_3	H	3320 (sh)	3281 (br)	3128 (br)	1630
1d	CCl_3	Cl	3441 (br)	3314 (sh)	3111 (br)	1628
1e	CCl_3	CF_3	3469 (br)	3322 (sh)	3100 (br)	1619
2a	CF_3	OCH_3	3383 (br)	3325 (sh)	3178 (br)	1601
2b	CF_3	CH_3	3456 (sh)	3330 (br)	3100 (br)	1612
2c	CF_3	H	3322 (sh)	3299 (br)	3119 (br)	1628
2d	CF_3	Cl	3333 (sh)	3257 (br)	3102 (br)	1644
2e	CF_3	CF_3	3331 (sh)	3249 (br)	3083 (br)	1636

1. Frequencies listed are in cm^{-1}.
2. The most intense peak is recorded, shoulders appear in all cases.

The mass spectra of compounds **1a-e** and **2a-e** showed remarkably consistent fragmentation patterns. The major fragment peaks are listed in Table 2.4. Although the imidoylamidines are expected to be thermally labile compounds, I was able to purify most of them by fractional sublimation. In most cases, satisfactory elemental analyses (Table 2.5) were obtained on sublimed samples. However, **1b** and **1c** consistently have lower than expected nitrogen content. This is most likely due to the admixture of some of the aryl nitrile as a result of partial thermal decomposition.

Table 2.4 Mass Spectra of the aryl imidoylamidines **1a-e**, **2a-e**.

$R'C_6H_4C_2(NH)_3CR''_3$, R' = R''=	OCH_3 Cl[1]	CH_3 Cl[1]	H Cl[1]	Cl Cl[1]	CF_3 Cl[1]	OCH_3 F	CH_3 F	H F	Cl F[1]	CF_3 F
(M – H)	292	276	262	298	330	244	228	214	248	282
Loss HR", CN	---	215	201	---	---	199	183	169	---	237
Loss CR''_3	176	160	146	180	214	176	160	146	180	214
Loss NH_3, CR''_3	159	143	129	163	197	159	143	129	163	197
Loss CN, CR''_3, NH_2	134	118	104	138	172	134	118	104	138	172

1. Peaks containing one or more Cl atom had the correct isotopic pattern, but are reported on the basis of ^{35}Cl-containing isotopomers.

Table 2.5 Analytical and melting point data for the aryl imidoylamidines **1a-e**, **2a-e**.

Complex	Formula	%C		%H		%N		Colour	mp, °C
		calc.	found	calc.	found	calc.	found		uncorrected
1c $PhC(NH)_2C(NH)CCl_3$	$C_9H_8N_3Cl_3$	40.86	40.78	3.05	3.10	15.88	15.69	clear	68-9
1b $4\text{-}CH_3PhC(NH)_2C(NH)CCl_3$	$C_{10}H_{10}N_3Cl_3$	43.12	41.79*	3.62	3.70	15.08	13.13*	white	42-4
1a $4\text{-}OCH_3PhC(NH)_2C(NH)CCl_3$	$C_{10}H_{10}N_3OCl_3$	40.78	40.69	3.42	3.42	14.26	13.02*	clear	104-6
1d $4\text{-}ClPhC(NH)_2C(NH)CCl_3$	$C_9H_7N_3Cl_4$	36.16	36.20	2.36	2.47	14.05	14.27	white	110-2
1e $4\text{-}CF_3PhC(NH)_2C(NH)CCl_3$	$C_{10}H_7N_3F_3Cl_3$	36.12	36.03	2.12	2.19	12.64	12.48	clear	96-7
2c $PhC(NH)_2C(NH)CF_3$	$C_9H_8N_3F_3$	50.24	50.35	3.75	4.01	19.53	19.37	clear	42-5
2b $4\text{-}CH_3PhC(NH)_2C(NH)CF_3$	$C_{10}H_{10}N_3F_3$	52.40	52.34	4.40	4.60	18.33	18.50	clear	54-7
2a $4\text{-}OCH_3PhC(NH)_2C(NH)CF_3$	$C_{10}H_{10}N_3OF_3$	48.98	48.85	4.11	4.22	17.14	17.32	clear	41-5
2d $4\text{-}ClPhC(NH)_2C(NH)CF_3$	$C_9H_7N_3F_3Cl$	43.31	43.50	2.83	3.00	16.83	17.06	clear	45-8
2e $4\text{-}CF_3PhC(NH)_2C(NH)CF_3$	$C_{10}H_7N_3F_6$	42.42	42.32	2.49	2.39	14.84	14.88	clear	80-3

*Satisfactory EA could not be obtained from samples subjected to fractional sublimation in a three zone tube furnace.

2.4 Preparation of the aryl N-imidoylamidine hydrochlorides

In previous attempts to synthesize the radical **7c**, conversion of the imidoylamidine to its hydrochloride salt was omitted. The imidoylamidine was converted directly to the 1-chloro thiatriazine using SCl_2, and although this method was successful in producing product, an oil remained and was difficult to purify. It was felt that converting the imidoylamidine into a salt would allow for greater stability, better reactions, higher yields and purer products in subsequent steps.

2.4.1 Trichloromethyl imidoylamidine hydrochlorides

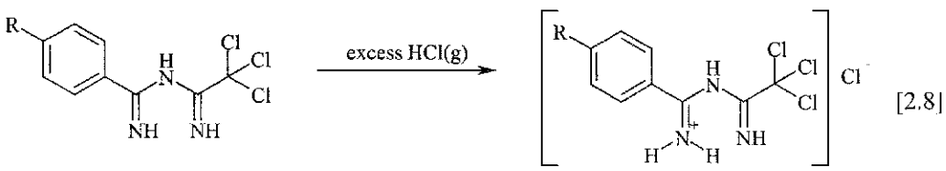

para-substituted trichloromethyl imidoylamidines
1a-e

para-substituted trichloromethyl imidoylamidine hydrochloride salts
3a-e

$R = OCH_3, CH_3, H, Cl, CF_3$

[2.8]

Converting the imidoylamidine into the hydrochloride salt was relatively straightforward. Dried ether was added to a two-necked round bottom flask along with a quantified amount of the imidoylamidine and a stir bar. The flask was then placed in an ice bath, and an excess of HCl(g) was blown through the flask with stirring. A white precipitate (product) formed instantaneously, and was filtered in air on a glass frit funnel with suction to dryness. The ice bath was introduced because in early reaction attempts it was found that heat may have caused some of the imidoylamidine to revert back to amidine. The mixture of both amidine and imidoylamidine hydrochloride were then reacted *in-situ* with the SCl_2, which created a mixture of both thiatriazine and the unfavorable dithiadiazoyl ring products.

A mechanism for the formation of the hydrochloride salt is:

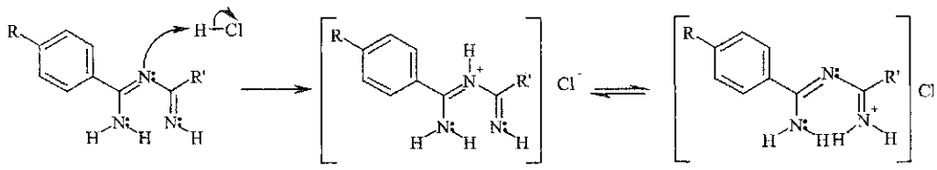

Because the imidoylamidine is a very strong base and has the ability to delocalize charge over a greater area, this makes it very stable to the addition of a proton. The creation of a salt therefore allows for even more stability in the amidine core.

Attempts to characterize the hydrochloride salt by ^{1}H or ^{13}C NMR were unsuccessful as the salt was not soluble in chloroform or any other non polar solvent. In addition, the salt was found to decompose in polar solvents such as methanol. IR data indicated a distinct spectrum compared to that of the imidoylamidine, offering support to the premise (by this and by the success in obtaining the 1-chloro precursor) that the correct product had been formed. This product was used in subsequent steps without attempting further purification.

2.4.2 Trifluoromethyl imidoylamidine hydrochlorides

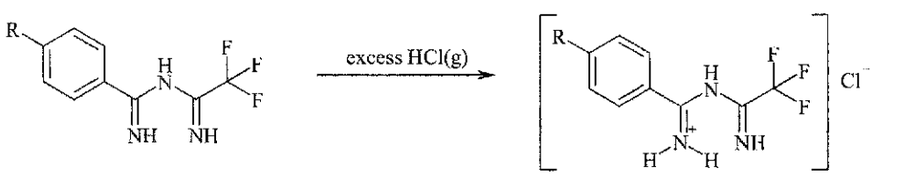

para-substituted trifluoromethyl imidoylamidines

2a-e

para-substituted trifluoromethyl imidoylamidine hydrochloride salts

4a-e

[2.9]

$R = OCH_3, CH_3, H, Cl, CF_3$

This reaction is completely analogous to the previous reactions with **1a-e**. In all cases a white precipitate formed which proved too insoluble for NMR. The yields of these reactions were also very high and no product mixtures were noted. Further

purification was not attempted. IR data indicated a unique fingerprint region compared to that of the imidoylamidine, but similar broad bands in the 3300 cm^{-1} range characteristic of the NH stretches and hydrogen bonding.

2.5 Preparation of the 1-chloro-1,2,4,6-thiatriazines

Previous synthetic work pertaining to the 1,2,4,6-thiatriazine involved a ring closure of the imidoylamidine using an excess of sulfur dichloride.[4] This method was slightly modified to utilize the hydrochloride salt of the imidoylamidine, as the products obtained were easier to purify.

2.5.1 1-chloro-5-Aryl-3-trichloromethyl-1,2,4,6-thiatriazines

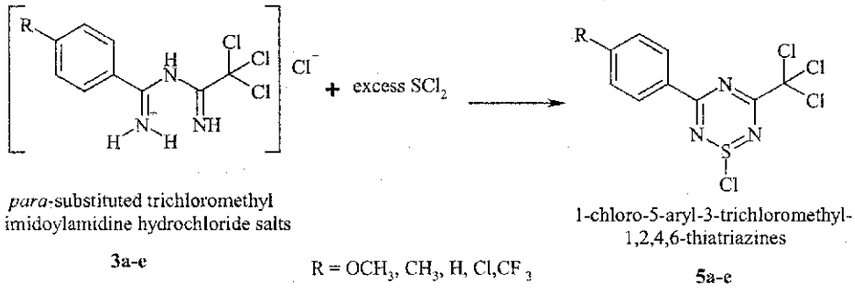

para-substituted trichloromethyl imidoylamidine hydrochloride salts

3a-e

$R = OCH_3, CH_3, H, Cl, CF_3$

1-chloro-5-aryl-3-trichloromethyl-1,2,4,6-thiatriazines

5a-e

[2.10]

In this reaction step the imidoylamidine salt was added to a side arm flask along with dried acetonitrile and a stir bar. SCl_2 was distilled and used within an hour of preparation to prevent decomposition to S_2Cl_2. A five-fold excess of SCl_2 was added to a dropping funnel, along with 10mL of dried acetonitrile. This was attached to the side arm flask and added dropwise. After addition of the SCl_2 the precipitate would turn a cloudy yellow and then eventually to a clear yellow. A condenser was attached to the flask and $N_2(g)$ was blown through while the solution was refluxed for 2 – 3 hours. The solution was observed to turn from a yellow to a deep orange/red color. HCl(g) was

given off during the reaction and could be seen as a yellow color in the bubbler. Initially the solution was refluxed overnight, but it was discovered that running the reaction for any extra time over a few hours did not increase yield or purity of the product.

After refluxing, the flasks were then cooled, sealed, and placed in a refrigerator overnight to allow for possible crystallization. No crystals were obtained in this manner, so the solvent was pumped off on the vacuum line and the product was recrystallized using either heptane or acetonitrile. In all cases, microcrystalline material of sufficient purity for NMR and mass spectral analysis was obtained. Several attempts were made at recrystallization using a variety of solvents, but crystals of X-ray quality were never created. In some cases, crystals of decomposition product were obtained. Sublimation of the crude material using both a tube furnace and a cold finger sublimer also failed to produce crystals.

Yields of the crude ring were typically high (80-99%). Reaction conditions were altered in several ways. One equivalent of SCl_2 and one equivalent of SO_2Cl_2 were added to the hydrochloride salt, one equivalent of only SCl_2 was added to the salt, and an excess of SCl_2 was added to the imidoylamidine. All of these attempts failed to give a product purer by NMR for use in subsequent steps.

Table 2.6 ^{1}H NMR of the thiatriazine chlorides

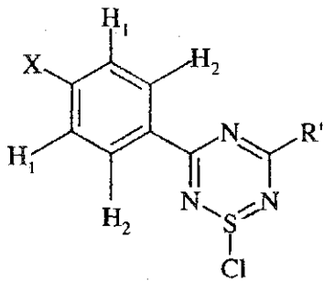

Compound	R'	X	H_1 [1]	H_2 [1]	X [1]	J_{AB} (Hz)
5a	CCl_3	OCH_3	7.03	8.49	3.94	9.2
5b		CH_3	7.35	8.40	2.48	8.4
5c		H	m 7.53 – 7.60	m 8.49 – 8.53	m 7.68 – 7.74	----
5d		Cl	7.53	8.45	-----	8.9
5e		CF_3	7.84	8.62	-----	8.9
6a	CF_3	OCH_3	7.02	8.45	3.94	9.0
6b		CH_3	7.35	8.37	2.49	8.2
6c		H	m 7.52 – 7.58	m 8.45 – 8.48	m 7.67 – 7.74	----
6d		Cl	7.53	8.41	-----	8.9
6e		CF_3	7.82	8.59	-----	8.5

1. All values are in ppm, with reference to TMS.

^{1}H NMR data (Table 2.6) confirmed ring formation in all five cases, with the absence of NH bands from the imidoylamidine and only the phenyl and *para*-substituted hydrogen atoms appearing in the spectra. The location of the two doublets was similar to that of the imidoylamidines **1a-e**, **2a-e**, and appeared in the 6-8ppm range. H_1, which is *meta* to the thiatriazine core (and hence further away), seems to have been less affected from the conversion to ring from imidoylamidine and appears only ~0.10 ppm further downfield in all cases. H_2, which is *ortho* to the heterocyclic core has had a much more noticeable effect, which shifted the doublets further downfield in all cases by ~0.60 ppm. Such dramatic deshielding of aromatic protons *ortho* to an aromatic thiazyl ring is diagnostic. For example, the chemical shifts of the *ortho* hydrogen atoms in comparably substituted 1,5-dithia-2,4,6,8-tetrazocine heterocycles have very similar chemical shifts to those of **5a-e** and **6a-e**.[17,18] This has been ascribed to the ring current of the thiazyl ring. ^{13}C NMR were not obtained due to instability of the compounds in solution (they hydrolyzed before spectra could be obtained).

An excess of SCl_2 was used to ensure the completion of the reaction of the imidoylamidine hydrochloride salt to the thiatriazine ring. The removal of all of the hydrogen atoms by chloride requires at least two equivalents of SCl_2. This is a redox reaction with S^{II} converting to S^{IV}, and it could be postulated that SCl_2 disproportionates into S_2Cl_2 and Cl_2, with chlorine serving as the oxidizing agent.

2.5.2 1-chloro-5-Aryl-3-trifluoromethyl-1,2,4,6-thiatriazines

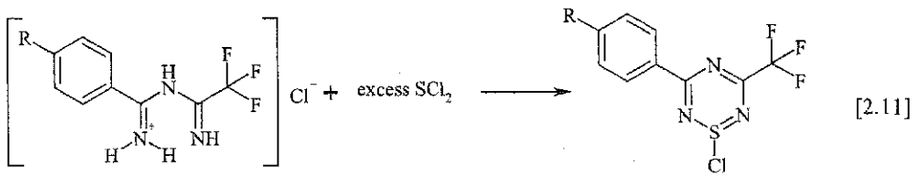

[2.11]

para-substituted trifluoromethyl imidoylamidine hydrochloride salts

4a-e

1-chloro-5-aryl-3-trifluoromethyl-1,2,4,6-thiatriazines

6a-e

R = OCH_3, CH_3, H, Cl, CF_3

This method was also performed in a manner analogous to that for the trichloromethyl compounds. However, unlike compounds **5a-e**, these compounds could only be obtained as oils. Crude yields were typically high (>80%), and these were used directly to make the radicals. Characterization through the use of ^{1}H NMR yielded spectra very similar to that for **5a-e** and hence are diagnostic. IR spectroscopy was not attempted due to the oxygen and moisture sensitivity of these compounds.

2.6 Preparation of the 1,2,4,6-thiatriazine radicals

Several reducing agents have been used to effect the reductive elimination of chloride ion from 1-chloro-1,2,4,6-thiatriazines. I used triphenylantimony because of its general utility in the reduction of thiazyl halides.[6,7,9] In early work, sodium verdazyl was often used.[4,5,19] Zinc in sulfur dioxide is particularly useful for volatile radicals, where the product can be sublimed from the insoluble zinc and zinc halide residues.[9]

2.6.1 5-Aryl-3-trichloromethyl-1,2,4,6-thiatriazine radicals

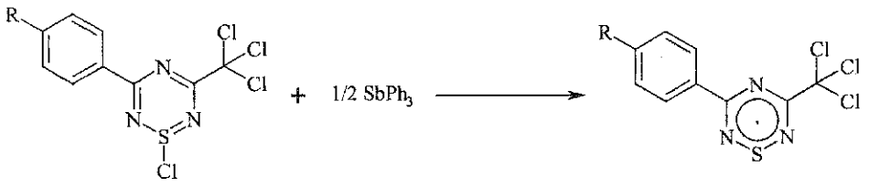

1-chloro-5-aryl-3-trichloromethyl-1,2,4,6-thiatriazines

5a-e

5-aryl-3-trichloromethyl-1,2,4,6-thiatriazine radicals

7a-e

[2.12]

R = OCH_3, CH_3, H, Cl, CF_3

For this reaction, to prevent exposure to the atmosphere a pear-shaped solids addition funnel was used (Figure 2.3).

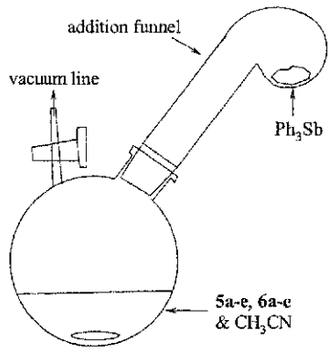

Figure 2.3 Pear-shaped solids addition funnel.

A side arm flask was filled with compounds **5a-e**, **6a-e**, some acetonitrile solvent and a stir bar. The glass apparatus was then filled with a ½ molar ratio of the triphenylantimony and attached to the flask. It was necessary to remove all trace oxygen from the apparatus and so the flask was freeze-thaw-degassed at least three times. Once the contents had thawed and were at room temperature the triphenylantimony was added into the flask. Reduction to the radical was immediate in all cases, as the solution turned from a clear dark red to a dark purple (almost black) solution with precipitate evident. The reaction mixture was stirred to ensure reaction completion. The glass apparatus was

then removed and replaced by a glass frit filter stick and side arm flask to filter the crude radical and remove all trace solvent on the vacuum line.

Recrystallization of the crude solid was done using a glass H-vessel containing a central glass frit (Figure 2.4).

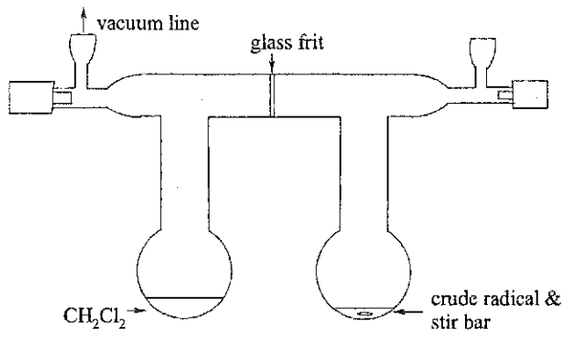

Figure 2.4 Recrystallization H-vessel for compounds **7a-e.**

Crude product was placed in one end of the apparatus and dried dichloromethane was placed in the other. The apparatus was attached to the vacuum line and the solvent was freeze thaw degassed three times. Then with the oxygen still removed the solvent was transferred through the frit over to the crude. The mixture was stirred and then filtered back to the other side (to remove trace impurities). It was placed in a cooling bath for several hours, after which shiny dark plate-like crystals of product would appear. These were filtered and the solvent pumped off on the vacuum line.

The recrystallized product was used for MS and elemental analysis. However, a three zone tube furnace was also used on the recrystallized material, which produced X-ray quality plates for the radical **7c**. All the radicals possessed a strong and persistent EPR signal, which is characteristic of the proposed structures (see Chapter 4). Mass spectral data is listed in Table 2.7 and elemental analysis data is listed in Table 2.8.

2.6.2 5-Aryl-3-trifluoromethyl-1,2,4,6-thiatriazine radicals

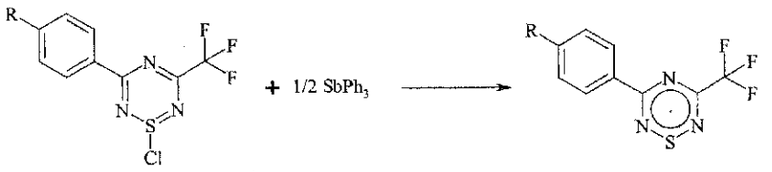

[2.13]

1-chloro-5-aryl-3-trifluoromethyl-1,2,4,6-thiatriazines

6a-e

5-aryl-3-trifluoromethyl-1,2,4,6-thiatriazine radicals

8a-e

$R = OCH_3$, CH_3, H, Cl, CF_3

Reduction of the trifluoromethyl substituted thiatriazines was analogous to the previously mentioned trichloromethyl derivatives. Radicals were produced in all cases, that were dark purple in color and in yields ranging from 60-80%. These radicals were further purified by sublimation in a three zone tube furnace over several days to produce MS, elemental analysis, and X-ray quality dark purple crystals. Recrystallization in the above mentioned H-vessel failed to produce crystals of higher quality. The sublimed products were characterized by m.p., EPR, MS, elemental analysis and IR spectroscopy. The EPR data for the trifluoromethyl thiatriazine radical showed further coupling onto the fluorine atoms, and are also fully characteristic of the proposed structures. Mass spectral data is listed in Table 2.7, and elemental analysis data is listed in Table 2.8.

Table 2.7 Mass Spectra of the 1,2,4,6-thiatriazine free radicals **7a-e**, **8a-e**.

$R'C_6H_4C_2N_3SCR''_3$, R' =	**OCH_3**	**CH_3**	**H**	**Cl**	**CF_3**	**OCH_3**	**CH_3**	**H**	**Cl**	**CF_3**
R'' =	**Cl[1]**	**Cl[1]**	**Cl[1]**	**Cl[1]**	**Cl[1]**	**F**	**F**	**F**	**F[1]**	**F**
Parent ion	324	308	292	328	362	274	258	245	278	312
Loss R''	---	---	---	---	---	255	239	227	259	---
Loss $NCCR''_3$	179	163	149	---	217	179	163	149	183	---
Loss $NSCCR''_3$	159	143	129	165	197	---	---	129	---	197
Loss $C_2N_2SCR''_3$	133	117	103	137	171	133	117	104	137	171

1. Peaks containing one or more Cl atom had the correct isotopic pattern, but are reported on the basis of ^{35}Cl-containing isotopomers.

Table 2.8 Analytical and melting point data for the thiatriazine radicals **7a-e**, **8a-e**.

Complex	Formula	%C		%H		%N		Colour	mp, °C
		calc.	found	calc.	found	calc.	found		uncorrected
7c $PhC_2N_3SCCl_3$	$C_9H_5N_3SCl_3$	36.82	36.88	1.72	1.69	14.31	14.07	dk. purple	98-101
7b 4-$CH_3PhC_2N_3SCCl_3$	$C_{10}H_7N_3SCl_3$	39.05	38.89	2.29	1.96	13.66	13.36	dk. purple	112-4
7a 4-$OCH_3PhC_2N_3SCCl_3$	$C_{10}H_7N_3OSCl_3$	37.12	36.89	2.18	2.35	12.98	12.89	dk. purple	98-101
7d 4-$ClPhC_2N_3SCCl_3$	$C_9H_4N_3SCl_4$	32.95	33.12	1.23	1.56	12.81	12.69	dk. purple	98-100
7e 4-$CF_3PhC_2N_3SCCl_3$	$C_{10}H_4N_3SF_3Cl_3$	50.24	50.35	3.75	4.01	19.53	19.37	dk. purple	100-3
8c $PhC_2N_3SCF_3$	$C_9H_5N_3SF_3$	44.26	44.12	2.06	2.24	17.21	17.13	dk. purple	110-3
8b 4-$CH_3PhC_2N_3SCF_3$	$C_{10}H_7N_3SF_3$	46.51	46.67	2.73	2.96	16.27	16.41	dk. purple	140-2
8a 4-$OCH_3PhC_2N_3SCF_3$	$C_{10}H_7N_3OSF_3$	43.80	43.90	2.57	2.71	15.32	15.18	dk. purple	135-140
8d 4-$ClPhC_2N_3SCF_3$	$C_9H_4N_3SF_3Cl$	38.79	38.72	1.45	1.41	15.08	15.08	dk. purple	131-4
8e 4-$CF_3PhC_2N_3SCF_3$	$C_{10}H_4N_3SF_6$	38.47	38.52	1.29	1.53	13.46	13.34	dk. purple	101-5

2.7 Conclusions

I have developed a general route to the 1,2,4,6-thiatriazine radical via the condensation of sulfur chlorides with imidoylamidines. All 40 compounds described in this work are either new or have not been fully characterized previously. The imidoylamidines themselves are highly interesting compounds which are expected to have extensive chemical utility. Full spectroscopic and analytical data have been presented to support the synthetic claims. Further confirmation of the structures of two imidoylamidines and two thiatriazine radicals has been obtained by X-ray crystallography, as described in the following chapter.

References

1. Geevers, J.; Hackmann, T.; Trompen, W. P. *J. Chem. Soc. (C)* **1970**, 875.

2. Boeré, R. T.; Oakley, R. T.; Reed, R. W.; Westwood, N. P. C. *J. Am. Chem. Soc.* **1989**, *111*, 1180.

3. Voss, G.; Fischer, E.; Rembarz, G.; Schramm, W. *Z. Chem.* **1976**, *16*, 358.

4. Kornuta, P. P.; Deril, L. I.; Markovski, L. N. *Zh. Org. Khim.* **1980**, *16*, 1308.

5. Markovskii, L. N.; Kornuta, P. P.; Katchkovskaya, L. S.; Polumbrik, P. M. *Sulfur Lett.* **1983**, *1*, 143.

6. Hayes, P. J.; Oakley, R. T.; Cordes, A. W.; Pennington, W. T. *J. Am. Chem. Soc.* **1985**, *107*, 1346.

7. Cordes, A. W.; Hayes, P. J.; Josephy, P. D.; Koenig, H.; Oakley, R. T.; Pennington, W. T. *J. Chem. Soc., Chem. Commun.* **1984**, 1021.

8. Boeré, R. T.; Cordes, A. W.; Hayes, P. J.; Oakley, R. T.; Reed, R. W.; Pennington, W. T. *Inorg. Chem.* **1986**, *25*, 2445.

9. Boeré, R. T. *Unpublished Data* .

10. Boeré, R. T.; Oakley, R. T.; Reed, R. W. *Journal of Organometallic Chemistry* **1987**, *331*, 161.

11. Peak, D. A. *J. Chem. Soc.* **1952**, 215.

12. Oto, K.; Ichikawa, E. *Chem. Abs.* **1975**, *79*, 428.

13. Brown, H. C.; Schuman, P. D. *J. Org. Chem.* **1963**, *28*, 1122.

14. Peters, G. A.; Schaefer, F. C. *Chem. Abs.* **1964**, 14694.

15. Silverstein, R. M.; Webster, F. X. *Spectrometric Identification of Organic Compounds.*; John Wiley & Sons, Inc.: New York, 1998.

16. Patai, S. *The Chemistry of Amidines and Imidates.*; John Wiley and Sons: New York, 1975.

17. Boeré, R. T.; Moock, K. H.; Derrick, S.; Hoogerdijk, W.; Preuss, K.; Yip, J. *Can. J. Chem.* **1993**, *71*, 473.

18. Boeré, R. T.; Fait, J.; Larsen, K.; Yip, J. *Inorg. Chem.* **1992**, *31*, 1417.

19. Kornuta, P. P.; Derii, L. I.; Romanenko, E. A. *Chemistry of Heterocyclic Compounds* **1978**, *273*, 226.

Chapter 3

Crystal structures of the imidoylamidines **1c** and **2c**, and the 1,2,4,6–thiatriazine radicals **7c** and **8c**

3.1 Introduction

This chapter will describe the X-ray structures of the radicals 5-phenyl-3-trichloromethyl-1,2,4,6-thiatriazine **7c**, and 5-phenyl-3-trifluoromethyl-1,2,4,6-thiatriazine **8c**, and of the precursor phenyl/trichloromethyl imidoylamidine **1c** and phenyl/trifluoromethyl imidoylamidine **2c**.

Single crystal X-ray diffraction is a technique used to measure both the position and intensity of the X-ray diffraction patterns of a crystal, to determine the space group as well as the precise atomic positions (and therefore the bond lengths and angles) of molecules within the crystal. These reflections are collected and measured by an automatic diffractometer, and the intensities of the indexed reflections are stored and then corrected for geometric and polarization effects.

The diffraction phenomenon is such that the coherence of the incident X-ray beam is lost. Thus, unlike optical microscopy, X-ray diffraction presents an image that has random phasing. The challenge of re-constructing the correct phase pattern is known as 'solving' the crystal structure. Crystal structures are usually solved using two main methods. The Patterson method relies on the presence of at least one heavy atom in the unit cell, while direct methods are used when all atoms in the molecule have a similar scattering power. The methodology used most commonly in crystallography is to compute the X-ray diffraction pattern that ought to be seen if atoms are located at the positions indicated by the structural model. These theoretical patterns are termed

'structure factors.' Once all atoms have been located, refinement of atomic positions is done until optimum agreement between calculated and observed structure factors is obtained. The R (residual) factor gives a measure of the difference between the two and therefore of how well the structure has been refined. X-ray diffraction is a powerful tool used for the characterization and analysis of many crystalline solids, and has been used more than all other structure determination techniques put together for the determination of molecular structures. Caution should always be used in the interpretation of structural data for X-ray diffraction. The results are only as good as the models that are used, and false structural models have been proposed from time to time.

The final objective of the synthetic work in this project was to obtain a series of thiatriazine compounds with varying subsituents on the attached phenyl ring. Crystal structures of similar thiatriazine rings are already known.[1-5] We have been able to isolate X-ray quality crystals from one compound of each series, **7c** and **8c** (both unsubstituted phenyl thiatriazine radicals), along with the precursor unsubstituted phenyl imidoylamidines **1c** and **2c**.

The 5-phenyl-3-trifluoromethyl-1,2,4,6-thiatriazine radical **8c** displayed dimerization similar to the known thiatriazine structures. However the 5-phenyl-3-trichloromethyl-1,2,4,6-thiatriazine radical **7c** forms a novel head-to-tail dimer (Section 3.4). The geometry of the core of both thiatriazine rings are directly comparable to previously known compounds. The long-range ordering of the dimer units (known as the 'packing') in each series is unique and unlike those of the previously determined structures.

X-ray structures of imidoylamidines are rare. In fact, no structures of free imidoylamidines have been reported, and only one structure of an imidoylamidine salt (with $[Se_2Cl_{10}]^{2-}$ as the counterion).[6] Imidoylamidinate anions coordinated to various metals are known.[7-9] Attempts were made at obtaining crystals of X-ray quality, and these attempts were successful in both series. Three-zone tube furnace sublimation produced clear plate like crystals of **1c** and **2c** that were pure by NMR, mass spectroscopy, and elemental analysis.

3.2 Phenyl/trichloromethyl imidoylamidine **1c**

3.2.1 Experimental

Clear crystalline plates of the imidoylamidine **1c** were grown by sublimation in a three zone tube furnace using Pyrex sublimation tubes under dynamic vacuum. Crystals were sent to Dr. Masood Parvez at the University of Calgary for collection of X–ray intensity data.

3.2.2 Space Group Determination

The Laue symmetry and systematic absences observed for this molecule gave two suitable options for possible space groups: $P1$ or $P\bar{1}$, both triclinic. A lack of chirality in the molecule suggested $P\bar{1}$ as the likely choice for the space group. The choice of $P\bar{1}$ as space group was substantiated by a successful refinement of the molecule with an R factor of less than 6%. **1c** is at the general positions and since the multiplicity for the general positions in this particular space group is two, and our Z value is six, this indicated that there are three molecules per motif, or six imidoylamidines in the unit cell.

3.2.3 Data Collection and Refinement

Intensity data were collected using a MoKα radiation source (0.71073 Å). Data were collected between $\theta = 1.3°$ and 27.7°. From the 14588 reflections collected, 7908 independent reflections were found, offering 17x oversampling of the 443 parameters to refine.

The structure was solved by direct methods (SIR92) and expanded using Fourier techniques (DIRDIF–94). The non-hydrogen atoms were refined anisotropically. Some hydrogen atoms were included at geometrically idealized positions and were not refined, while those bonded to nitrogen atoms were located from difference maps and were allowed to refine. The final cycle of full-matrix least-squares refinement using SHELXL97 converged with unweighted and weighted agreement factors of R = 0.055 and wR = 0.151 (all data) respectively, and goodness of fit, S = 0.97. The weighting scheme was based on counting statistics and the final difference map was essentially featureless.

F^2 is refined against all reflections. Goodness of fit (GooF) is based on F^2

$$GooF = \sqrt{\frac{\sum\left[w\left(F_o^2 - F_c^2\right)\right]}{(n-p)}} \qquad [3.1]$$

where n = number of reflections; p = number of refined parameters.

The weighted R–factor is also based on F^2

$$wR_2 = \sqrt{\frac{\sum\left[w\left(F_o^2 - F_c^2\right)^2\right]}{\sum\left[w\left(F_o^2\right)^2\right]}} \qquad [3.2]$$

and the conventional R_1 is based on the observed F values larger than $4\sigma(F_o)$.

$$R_1 = \frac{\sum \left| |F_o| - |F_c| \right|}{\sum |F_o|} \qquad [3.3]$$

R-factors based on F^2 are statistically about twice as large as those based on F, and R-factors based on ALL data will be even larger.

Data collection and refinement parameters are listed in Table 6.1. Atom coordinates as well as bond lengths and angles for **1c** are listed in Tables 6.2, 6.3 and 6.5. Table 6.4 contains the anisotropic thermal parameters for **1c**.

3.2.4 Discussion

Three independent imidoylamidines were determined to form the repeating motif in the crystal structure, which are labeled Molecules 1, 2, and 3 in Figure 3.1.

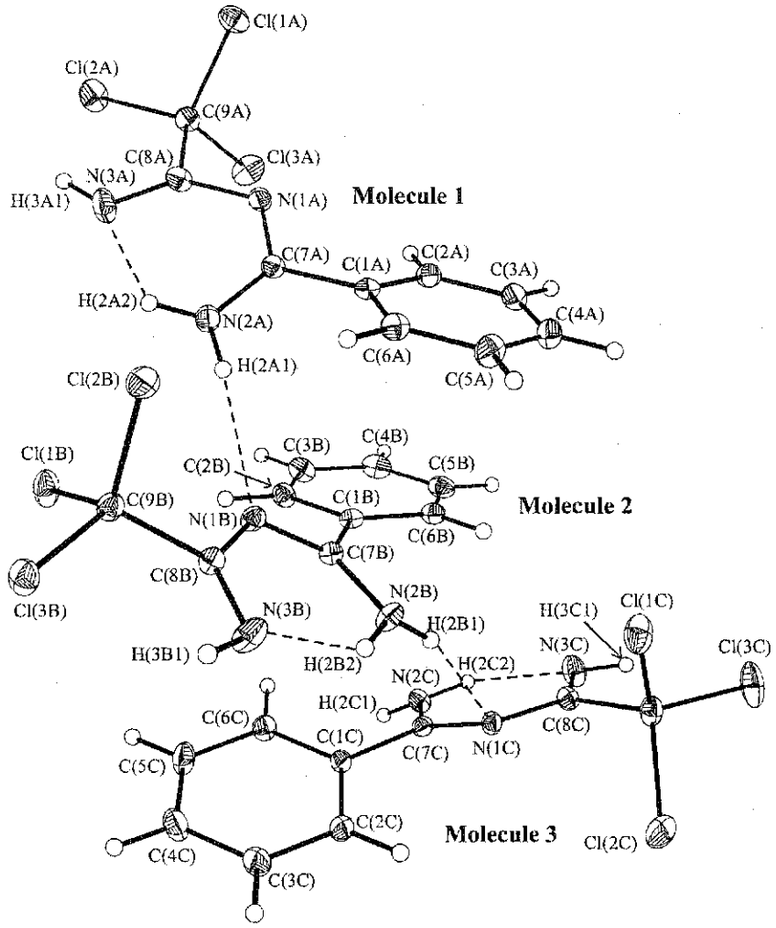

Figure 3.1 Thermal ellipsoid plot (25% probability) and atom numbering scheme for **1c**. Dotted lines represent both inter- and intramolecular hydrogen bonding that is occurring in the solid-state lattice.

The Z value of 6 indicates that there are 3 molecules per motif and 2 motifs in the general positions of the unit cell (Figure 3.2). A packing diagram is given in Figure 3.3.

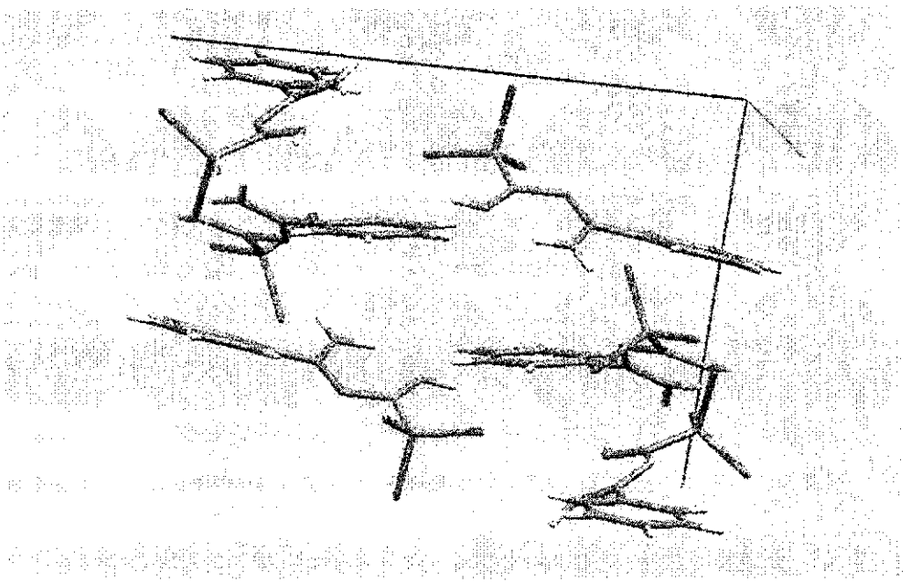

Figure 3.2 Unit cell diagram of **1c**.

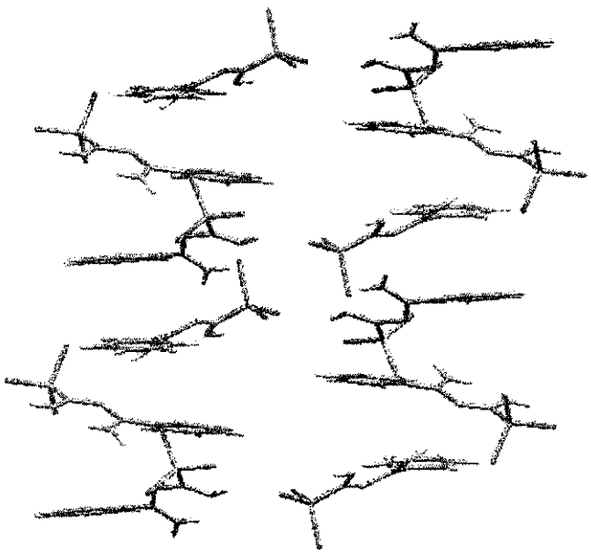

Figure 3.3 Solid-state packing diagram of **1c**.

Hydrogen bonding is predicted to occur in the solid state, and it does in fact appear throughout the crystal lattice. However, the extent of hydrogen bonding that

occurs is less than expected, as one might assume to see all three amino hydrogens involved in such bonding, which is not in fact the case. One hydrogen atom from each molecule [(H(3A1), H(3B1), and H(3C1)] does not participate in hydrogen bonding at all, and appears to be isolated from doing so. This may be related to the pseudo ring formation that occurs, which prohibits that particular hydrogen from any kind of close inter- or intramolecular contact. Packing of the independent molecules in the solid state may also play a role.

Intermolecular hydrogen bonding occurs between N(1B) and H(2A1), between N(1C) and H(2B1), and also between N(1A) and H(2C1). A typical N–H···N length for intermolecular bonding should be between 2.94 – 3.15 Å.[10] In Molecule 1 N(2A)–H(2A1)···N(1B) is 3.127 Å, in Molecule 2 N(2B)–H(2B1)···N(1C) is 3.074 Å, and in Molecule 3 N(2C)–H(2C1)···N(1A) is 3.139 Å which all fit this range nicely. Intramolecular hydrogen bonding is also occurring between N(3A) and H(2A2), between N(3B) and H(2B2), as well as between N(3C) and H(2C2) (indicated by dotted lines in Figure 3.). In Molecule 1 N(2A)–H(2A2)···N(3A) is 2.655 Å, in molecule 2 N(2B)–H(2B2)···N(3B) is 2.640 Å, and in molecule 3 N(2C)–H(2C2)···N(3C) is 2.642 Å. The N–H···N angles were 172.01°, 160.02°, 136.85°, 130.81°, 134.26°, and 171.20°, which are typical of H–bonding.[10] H(3A1), H(3B1), and H(3C1) appear to be well isolated and no hydrogen bonding involving these atoms is evident in the solid state structure. This pattern can be seen to repeat throughout the crystal lattice, so that there is a single intermolecular H–bond from one imidoylamidine molecule to the next, as well as the intramolecular H–bond which creates a pseudo ring structure.

There are notable H--Cl, Cl--Cl, C--Cl, C--C, N--N and C--N contacts between the three independent imidoylamidine molecules, which appear to be closer than the sum of van der Waals radii. These contacts are shown in Figure 3.4. A comparison of C--N bond lengths with **2c** and other metal ligand complexes is given in Section 3.3.4.

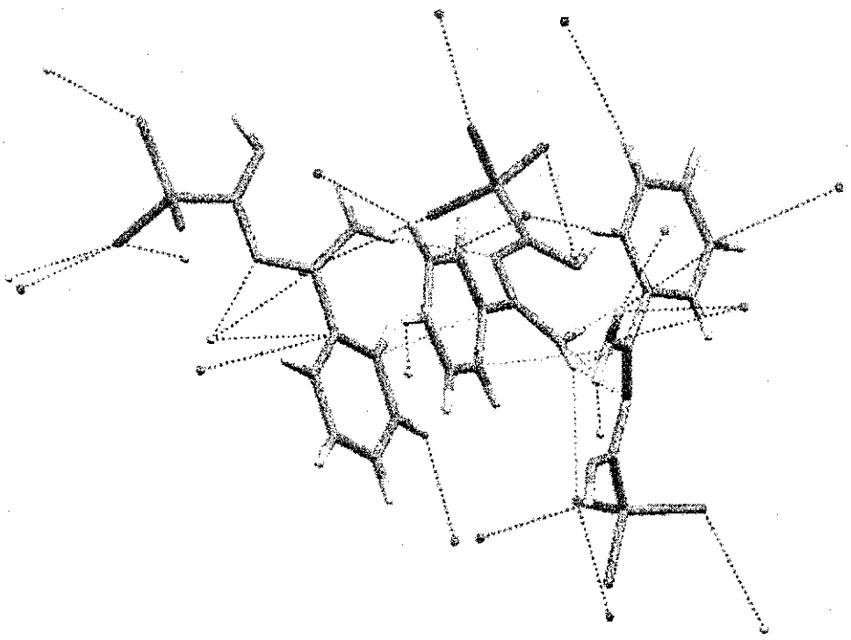

Figure 3.4 Diagram of **1c**. Dashed lines represent intermolecular contacts that are less than the sum of van der Waals radii.

3.3 Phenyl/trifluoromethyl imidoylamidine **2c**

3.3.1 Experimental

Crude white **2c** was initially sublimed under vacuum in a 45°C oil bath to produce white crystalline flakes that were pure by ^{1}H NMR. Clear crystalline plates of the imidoylamidine were then grown by sublimation in a three zone tube furnace using Pyrex sublimation tubes under dynamic vacuum. Crystals were sent to Dr. Gotthelf

Wolmershäuser of the Fachbereich Chemie at the Universität Kaiserslautern, Germany for collection of X-ray intensity data.

3.3.2 Space Group Determination

SHELXPREP in SHELXTL was used to determine the correct space group, as well as to establish if any corrections to data were warranted. $P2_1/n$ was given as the only possible space group, with a combined figure of merit of 93.93. In this particular space group each motif is related to the other by a 2_1 screw axis.

3.3.3 Data collection and refinement

Intensity data were collected using a MoKα radiation source (0.71073 Å). Data were collected between 2.47° and 25.94° θ. From the 28380 reflections collected, 3795 independent reflections were found, offering 12x oversampling of the 296 parameters to refine. Data processing and refinement was done with the SHELXTL set of programs. The structure was solved using SHELXS and direct methods. SHELXL was used for least squares refinement, and SHELXP was used to view the structure and modify atoms. Finally, SHELXCIF was used to make publication quality tables from the .cif files created by SHELXL. Following structure solution by SHELXS, the positions of all heavy atoms were easily found using difference Fourier-syntheses. Hydrogens were fixed on the aromatic ring so that the coordinates ride on the attached aromatic carbon's coordinates, whereas the amino hydrogens were refined along with all other atoms. Agreement factors of $R_1 = 0.0653$, $wR_2 = 0.1360$ were obtained.

Data collection and refinement parameters are listed in Table 6.1. Atom coordinates as well as bond lengths and angles for **2c** are listed in Tables 6.2, 6.3 and 6.5. Table 6.4 contains the anisotropic thermal parameters for **2c**.

3.3.4 Discussion

Two independent imidoylamidines were determined to form the repeating motif in the crystal structure, which are labeled Molecule 1 and 2 in Figure 3.5.

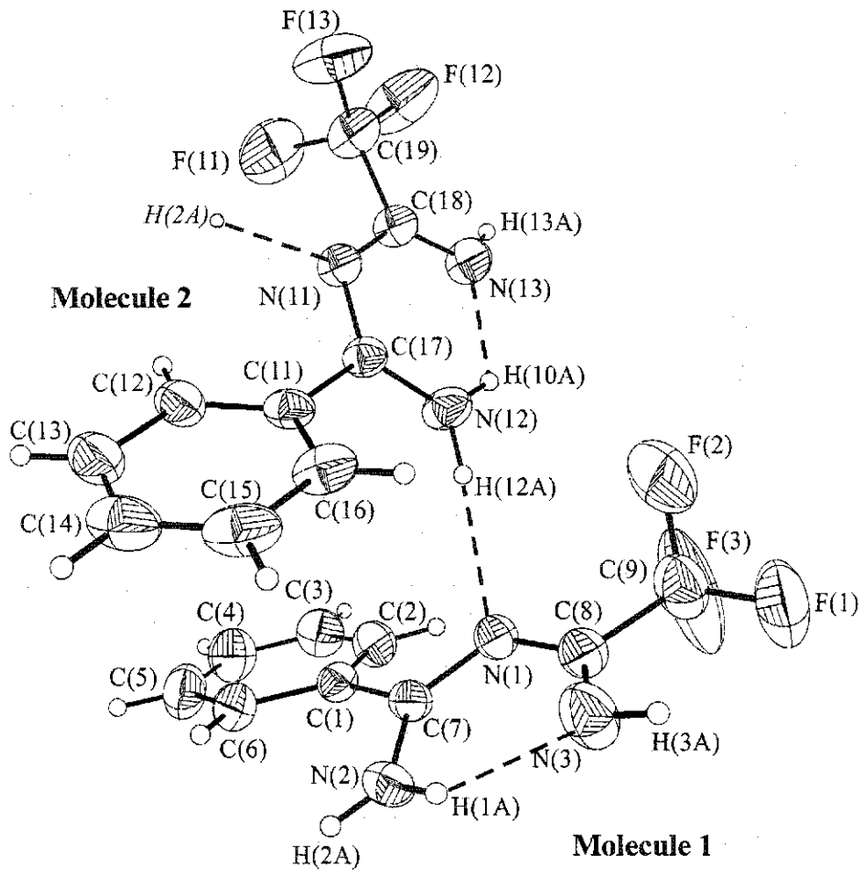

Figure 3.5 Thermal ellipsoid plot (25% probability) and atom numbering scheme for **2c**. Dotted lines represent both inter- and intramolecular hydrogen bonding that is occurring in the solid state lattice.

The Z value of 8 indicates that there are 2 molecules per motif because there are 4 motifs in the general positions of the unit cell in this space group. A packing diagram with screw axis shown is given below in Figure 3.6.

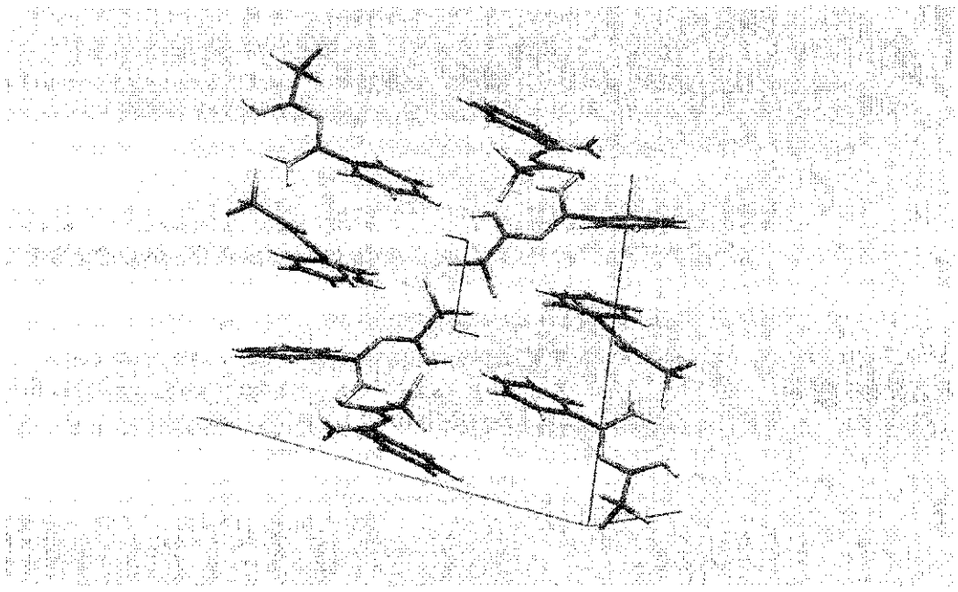

Figure 3.6 Packing diagram of **2c** showing 2/m symmetry in the unit cell. The screw axis is indicated by the jagged line in the middle of the picture.

The hydrogen bonding in this molecule is very similar to that of **1c**. One hydrogen atom from each molecule [(H(3A) and H(13A)] appears to be isolated from any type of hydrogen bonding. Both inter- and intramolecular hydrogen bonding are evident in the solid state crystal lattice. Intermolecular hydrogen bonding occurs between N(11) and H(2A) as well as between N(1) and H(12A). In molecule 1 N(2)–H(2A)···N(11) is 3.012 Å and in molecule 2 N(12)–H(12A)···N(1) is 3.120 Å, which fit well with typical N–H···N lengths. Intramolecular hydrogen bonding also occurs between N(3) and H(1A), as well as between N(13) and H(10A), which are also indicated by dotted lines in Figure 3. In Molecule 1 N(12)–H(10A)···N(13) is 2.654 Å and in Molecule 2 N(2)–H(1A)···N(3) is 2.626 Å, which correlate well with one another. The N–H···N angles were 131.09°, 125.69°, 142.66°, and 172.66°, which are typical of H-bonding.[10] Again H(3A) and H(13A) appear to be more isolated and no hydrogen bonding is evident in the

solid state. This pattern repeats in a manner analogous to **1c**, with both a single intermolecular bond occurring from one imidoylamidine molecule to the next, and an intramolecular bond.

The tautomeric equilibrium noted previously (Section 2.3.3) in both **1c** and **2c** can be compared to the one that exists in acetylacetone, where both the keto and enol forms of the molecule are seen to exist in equilibrium.[11] The enol form is stabilized by intramolecular hydrogen bonding so that both forms are evidenced in solution by NMR.

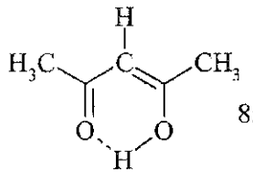

85% enol

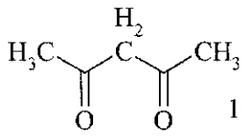

15% ketone

acetylacetone

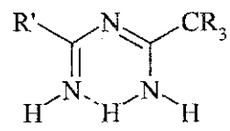

enamine

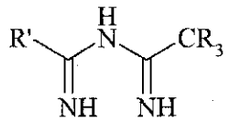

imine

imidoylamidine

In the case of our imidoylamidine only one tautomeric form seems to dominate the NMR spectrum, which may well be the enamine. The bond lengths indicate that the enamine is the preferred form in the solid state.

There are notable H–F, C–C, N–N and C–N contacts between the two independent imidoylamidine molecules, which appear to be closer than the sum of van der Waals radii (shown in Figure 3.7). These contacts are likely due to the tight packing induced by the large energy of hydrogen bonding, which can then overcome the electron-electron repulsion of these particular atoms.

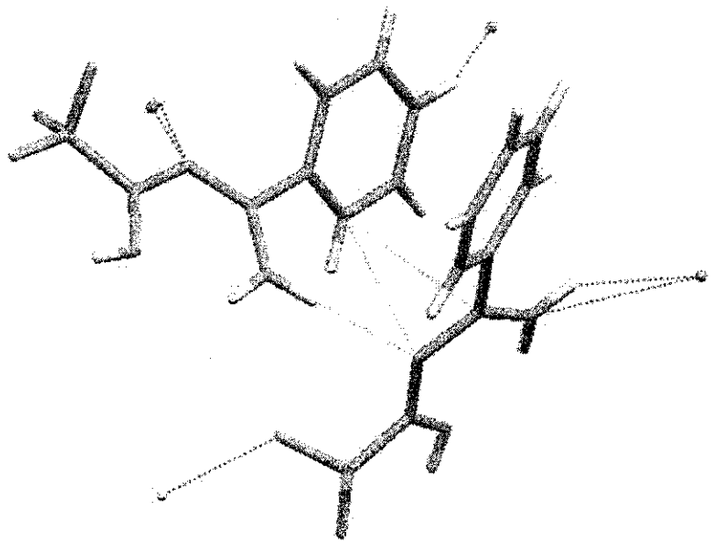

Figure 3.7 Diagram of **2c**. Dashed lines represent intermolecular contacts that are less than the sum of van der Waals radii.

Because no other solid state crystal structures of a free imidoylamidine have been reported previously, comparisons of bond lengths within the enamine core were made to metal complexes of the imidoylamidine that portrayed similar bonding in the solid state. The neutral imidoylamidine can be thought of as a Lewis base/Lewis acid adduct between IA^- and H^+, similar to that of a metal complexed imidoylamidinate $IA^- ML_x^+$ where IA = imidoylamidine and ML_x = metal plus ligand(s). The metal complexes are strongly stabilized by dative bonding of the imine to the Lewis acid, just as the free imidoylamidine is strongly stabilized by hydrogen bonding. Table 3.1 lists the C–N bond lengths for all comparable structures with averages.

Table 3.1 Comparison of C–N bond lengths[1] and averages of **1c** and **2c** with other imidoylamidines.

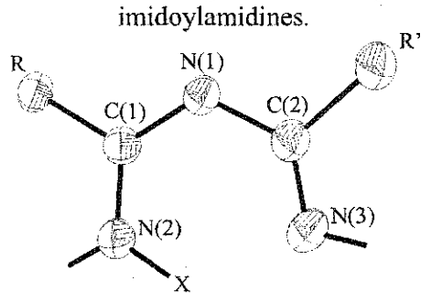

R	R'	X	N(2)-C(1)	C(1)-N(1)	N(1)-C(2)	C(2)-N(3)	Ref
Ph	CF_3	H	1.319(5)	1.318(4)	1.360(4)	1.263(5)	12
			1.320(4)	1.313(4)	1.364(5)	1.276(5)[2]	
Ph	CCl_3	H	1.323(4)	1.332(4)	1.366(4)	1.280(4)	12
			1.322(4)	1.327(4)	1.373(4)	1.280(4)	
			1.327(4)	1.328(4)	1.367(4)	1.282(4)[3]	
CF_3	CF_3	Ga	1.315(14)	1.294(14)	1.354(14)	1.274(13)	9
CF_3	CF_3	Ru	1.295(10)	1.309(10)	1.360(10)	1.299(9)	8
CF_3	CF_3	Ru	1.295(6)	1.331(7)	1.345(9)	1.276(7)	7
			1.294(8)	1.320(6)	1.362(8)	1.286(8)[2]	
Avg	Bond	Length	1.312(7)	1.319(7)	1.361(8)	1.280(7)	
		Δ_{CN}:	0.007		0.081		

1. Bond lengths are measured in angstroms (Å)
2. There are 2 independent molecules in the motif.
3. There are 3 independent molecules in the motif.

Statistical analysis performed on these data showed that bonds N(2)–C(1), C(1)–N(1), & C(2)–N(3) are considered the same to within 90% probability, while N(1)–C(2) bonds are the same to within 98% probability, and can therefore be considered equivalent and comparable with one another.

A typical C–N single bond is 1.472(5) Å in length, while C=N bond lengths in heterocycles are approximately 1.352(5) Å.[13] C=N double bonds in imines are found experimentally to be ~1.270(15)[14], so C(2)–N(3) is behaving similar to a double bond of an isolated imine. N(2)–C(1), C(1)–N(1), and N(1)–C(2) all seem to fall closer to the C=

N bond length than a single or double CN bond. However, N(1)–C(2) is longer than N(2)–C(1) and C(1)–N(1) by ~0.05 Å, displaying slightly more single bond character. Bonds N(2)–C(1) and C(1)–N(1) are very similar in length, and are directly involved in hydrogen bonding. N(1)–C(2) and C(2)–N(3), which have more single and double bond character are on the side of the imine core that has less involvement with hydrogen bonding. So the hydrogen bonding (or dative bonding in the metal complexes) seems to be evening-out the C–N bond lengths. These differences are not as prominent in the metal complexes, but the bonds in the imidoylamidine [N(2)–C(1) and C(1)–N(1)] are almost identical in length (0.001 Å and 0.005 Å in **2c**, and 0.005 Å and 0.005 Å in **1c**), which may mean that the hydrogen bonding has the greater effect on bond lengths. It should be noted that all of the C–N bonds are of intermediate length (not fully single and not fully double), but are still distinguishable from one another. There is remarkable consistency with widely different Lewis acids.

3.4 5-phenyl-3-trichloromethyl-1,2,4,6-thiatriazine radical **7c**

3.4.1 Experimental

Dark purple crystals of 5-phenyl-3-trichloromethyl-1,2,4,6-thiatriazine were grown by an initial recyrstallization from dry degassed dichloromethane. Following that, X-ray quality iridescent purple crystals were grown by sublimation in a three-zone tube furnace under dynamic vacuum using Pyrex sublimation tubes.

3.4.2 Space Group Determination

A determination of the space group for the **7c** molecule (5-phenyl-3-

trichloromethyl-1,2,4,6-thiatriazine) was performed using XPREP in the SHELXTL program. The Laue symmetry and systematic absences observed for this molecule gave two suitable options for possible space groups: $P1$ or $P\bar{1}$, both triclinic. A lack of chirality in the molecule and an overall Combined Figure of Merit of 0.50 led to the conclusion of $P\bar{1}$ as the likely choice for the space group. The preliminary cell contents gave two formula units per unit cell, which indicated that the radical was in the general position. Each radical possesses no crystallographic symmetry, but two such rings are related to each other by inversion. The choice of $P\bar{1}$ as space group was substantiated by a successful refinement of the molecule with a weighted R factor of less than 4%.

3.4.3 Data collection and refinement

Intensity data were collected using a MoKα radiation source (0.71073 Å). Data were collected between $\theta = 2.21°$ and 25.81°. From the 7683 reflections collected, 1986 independent reflections were found, offering 13x oversampling of the 145 parameters to refine. Data processing and refinement were done using the SHELXTL set of programs, analogous to that used for **2c**. Following structure solution by SHELXS, the positions of all heavy atoms were easily found using direct methods. Hydrogens were fixed on the aromatic ring so that the coordinates ride on the attached aromatic carbon's coordinates. Agreement factors of $R_1 = 0.0353$, $wR_2 = 0.0476$ were found.

Data collection and refinement parameters are listed in Table 6.12. Atom coordinates as well as bond lengths and angles for **7c** are listed in Tables 6.13, 6.14, and 6.16. Table 6.15 contains the anisotropic thermal parameters for **7c**.

3.4.4 Discussion

Figure 3.8 is an ORTEP diagram showing the motif in this crystal structure.

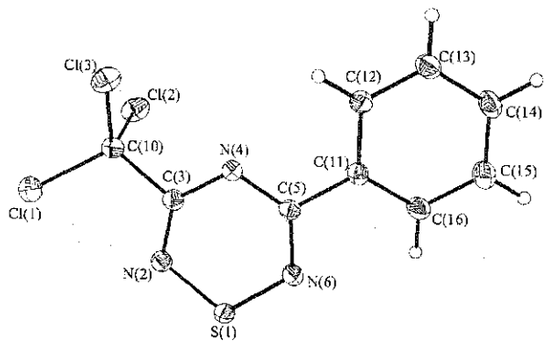

Figure 3.8 Thermal ellipsoid plot (25% probability) and atom numbering scheme of the asymmetric unit of **7c**.

The unique feature of the structure of this particular thiatriazine (compared with other known thiatriazine radicals) is its head-to-tail dimerization, as clearly shown in Figure 3.9. In the solid state, the C_2N_3S ring is still over top of another ring but S(1) lies overtop of N(4) instead of another S(1) atom. The two rings are related to one another by a center of symmetry (or inversion).

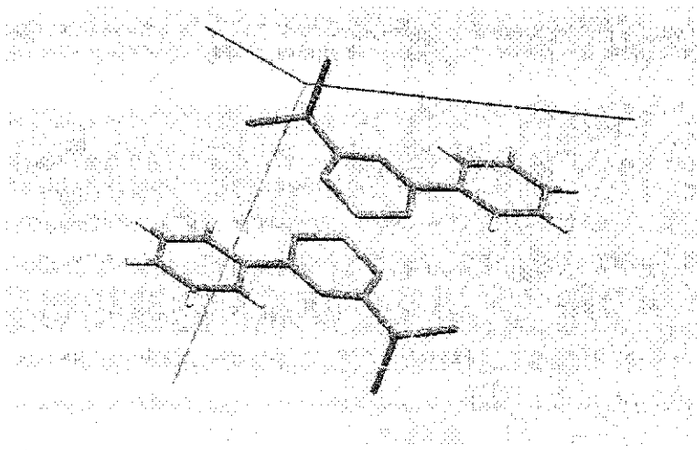

Figure 3.9 Unit cell diagram of **7c**.

As with bis(3,5-diphenyl-1,2,4,6-thiatriazine) **10**, the two C_2N_3S rings exhibit shallow boat conformations. S(1) is displaced 0.0217 (31) Å, while N(4) is displaced 0.0495 (35) Å from the mean plane of the central four atoms (N(2), C(3), C(5), and N(6)), which are coplanar to within 0.003 Å. The mean planes of the two thiatriazine rings are parallel to one another by virtue of crystallographically imposed inversion symmetry. The closest inter-ring contacts are between S(1) and N(4), at 2.957 Å.

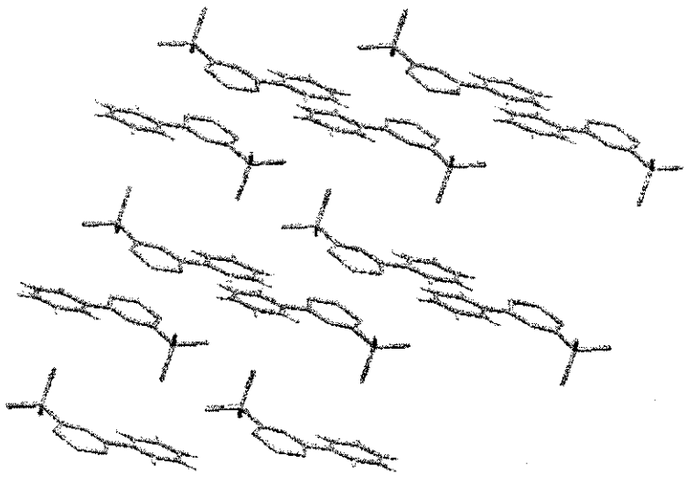

Figure 3.10 Solid-state packing diagram of **7c**.

Even though the arrangement of two independent molecules is not cofacial, they are still discrete units, or dimers, with no long distance communication along any given dimension (they still suffer from Peierls distortion). The dimeric units can be seen with phenyl and CCl_3 groups attached to the C_2N_3S ring alternating through the one dimension in Figure 3.10. This alternating pattern could be due to the larger size of the chlorine atoms sterically hindering a close alignment with the chlorine atoms of another ring.

3.5 5-phenyl-3-trifluoromethyl-1,2,4,6-thiatriazine radical **8c**.

3.5.1 Experimental

X-ray quality dark purple crystals of 5-phenyl-3-trifluoromethyl-1,2,4,6-thiatriazine **8c** were acquired from crude dark purple powder by sublimation with Pyrex sublimation tubes using a three-zone tube furnace under dynamic vacuum.

3.5.2 Space group determination

Space group determination was performed using XPREP in SHELXTL, which indicated that the molecule packs itself in three dimensional space into a triclinic unit cell, which has no minimum symmetry requirements (there were no glide planes, screw axis, mirror planes, etc.). Searches for higher metric symmetry only retained the original unit cell. There are therefore only two options for possible space groups: $P1$ or $P\bar{1}$. $P1$ allows for chirality in the molecule (which our molecule does not have), and also gave a significantly higher combined figure of merit (CFOM was 0.36 for $P\bar{1}$ and 6.38 for $P1$). This led to the conclusion of $P\bar{1}$ as the suitable space group for this structure. The unit cell contents were defined, giving a Z value of 4. Since the multiplicity for the general positions in this space group is 2, a Z value of 4 meant that there were two independent molecules per motif, or two dimers (four molecules) in each unit cell. All atoms are related by inversion only (there are no glide planes, screw axis, mirror planes, etc.).

3.5.3 Data collection and refinement

Once the space group was determined a direct methods structure solution was performed using SHELXTL, analogous to the two aforementioned crystal structures. The initial projection indicated the heaviest atoms as S(1) and S(2). Other atoms were

renamed when confidence was high in their positions, and SHELXS was run repeatedly until all atoms (except hydrogen) were located on difference Fourier maps.

All atoms (except fluorine) were made anisotropic and an initial least squares refinement was completed. The hydrogen atoms were localised geometrically, and a riding model was assumed for refinement. Temperature factors were set to 1.2 (Ar-H) times the equivalent isotropic temperature factor of corresponding carbon atoms.

Rotational disorder was found in the two CF_3-groups due to the size of the fluorine atoms, and a second set of fluorine atoms were located for each group (labelled 1A through 6A). Then the distances between the carbon/fluorine atoms and the fluorine/fluorine atoms were restrained. The fluorine atoms were made anisotropic. The fractional occupancies were refined to give 0.89 for F(1)–F(3), 0.11 for F(1A)–F(3A), 0.93 for F(4)–F(6), and 0.07 for F(4A)–F(6A), and thereafter fixed. The whole model was allowed to refine to convergence using the recommended weighting scheme. Agreement factors of $R_1 = 0.0412$, $wR_2 = 0.1309$ were found. 4269 independent reflections were found from the 13901 reflections collected, which gave 13x oversampling of the 309 parameters to refine.

All Data Tables are collected in Chapter 6, Section 6.10. Data collection and refinement parameters are listed in Table 6.17. Atom coordinates as well as bond lengths and angles for **8c** are listed in Tables 6.18, 6.19, and 6.21. Table 6.20 contains the anisotropic thermal parameters for **8c**.

3.5.4 Discussion

Figure 3.11 is an ORTEP diagram showing the motif in this crystal structure.

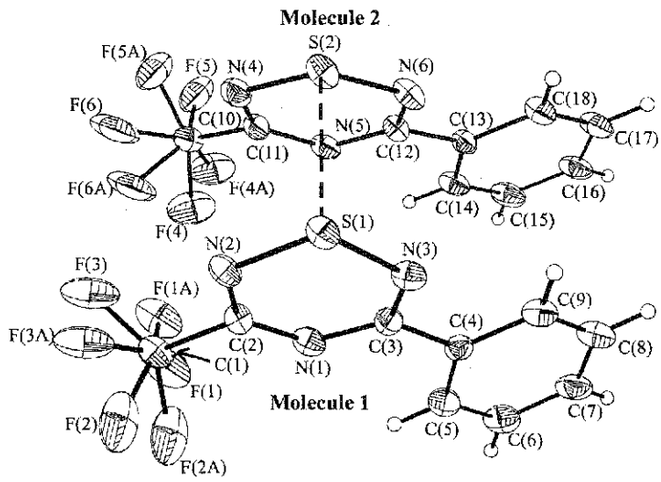

Figure 3.11 Thermal ellipsoid plot (25% probability) and atom numbering scheme for **8c**. Dashed line indicates the close contact between sulfur atoms.

The unit cell contents are shown in Figure 3.12, showing the 2 motifs or four thiatriazine radicals in the unit cell.

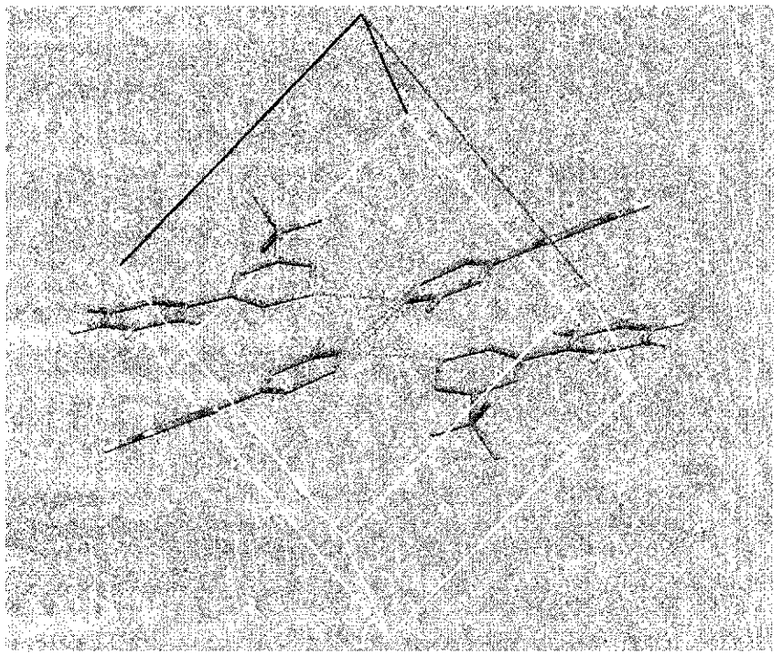

Figure 3.12 Unit cell diagram of **8c**.

As with **7c** and **10**, the two C_2N_3S rings exhibit shallow boat conformations, but **8c** is more distorted than **7c**. In Molecule 1, S(1) is displaced 0.0640(23) Å, while N(1) is displaced 0.0207(23) Å from the mean plane of the central four atoms (N(3), C(3), C(2), and N(2)), which are coplanar to within 0.0101 Å. In Molecule 2, S(2) is displaced 0.0727(23) Å, while N(5) is displaced 0.0475(27) Å from the mean plane of the central four atoms (N(6), C(12), C(11), and N(4)), which are coplanar to within 0.0010 Å. The dimers consist of cofacially bonded C_2N_3S units. The shortest contact between C_2N_3S rings is through sulfur atoms, with a distance of 2.6402(7) Å. This is longer than a normal disulfide linkage but within range of other known thiatriazines such as **10**, whose shortest contact in the C_2N_3S rings is through the sulfur atoms, with a distance of 2.666(3) Å, and 3,5-bis(dimethylamino)-1,2,4,6-thiatriazine, whose shortest contact is again through the sulfur atoms at 2.5412(8) Å. By contrast, in **7c** the shortest contact is between the sulfur and nitrogen atoms at 2.957 Å. However, if one considers the mean separation between each of the six atoms in the thiatriazine core of all three structures, one gets 3.020 Å in **7c**, 3.193 Å in **8c**, and 3.160 Å in the 3,5-bis(dimethylamino)-1,2,4,6-thiatriazine structure.

The two mean planes of **8c** intersect with a dihedral angle of 17°. In comparison **10** has a dihedral angle of 14° (which is quite similar), while 3,5-bis(dimethylamino)-1,2,4,6-thiatriazine has a dihedral angle of only 6°. In **7c** of course, the dihedral angle is 0°, as mentioned earlier.

An extended packing diagram is given in Figure 3.13, and a more simplified schematic drawing of this complex packing arrangement is shown in Figure 3.14.

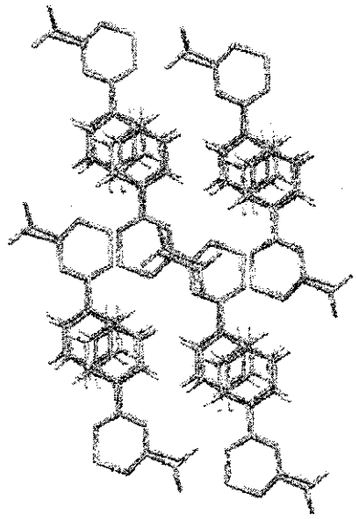

Figure 3.13 Crystal packing diagram of **8c** viewed perpendicular to the [1,1,1] axis, along the body diagonal.

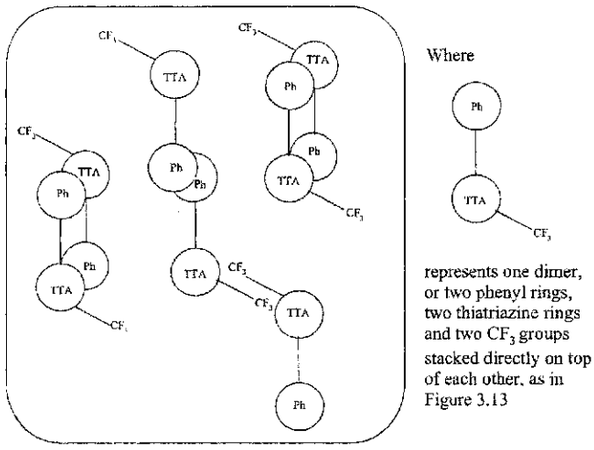

Figure 3.14 Simplified packing diagram for **8c**.

It is interesting to note that the stacking alternates from the C_2N_3S ring over top of the phenyl ring in one column, to the phenyl rings over top of each other in another, and then back again. When compared with 3,5-bis(diphenyl)-1,2,4,6-thiatriazine **10**, the

packing seems to only be with the dimers in a cofacial fashion with alternating phenyl and C_2N_3S rings. Again with both molecules there is a larger gap between pairs of dimers, so that no real electronic communication can take place in any one dimension.

Crystal structures are known for 1,2,4,6-thiatriazines with oxidation states of +1, 0, and −1. I am only interested in comparing structures with similar neutral oxidation states. Hence only the 3,5-bis(diphenyl)-1,2,4,6-thiatriazine **10** and 3,5-bis(dimethylamino)-1,2,4,6-thiatriazine are available for comparison. Comparable bond lengths and angles are presented in Tables 3.2 and 3.3, respectively.

Table 3.2 Comparison of bond lengths[1] in 1,2,4,6-thiatriazine radicals with oxidation state 0.

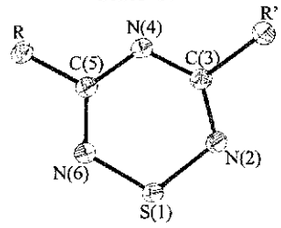

R	R'	S(1)-N(2)	N(2)-C(3)	C(3)-N(4)
Ph	Ph	1.602(6)	1.316(9)	1.34(1)
		1.614(6)[2]	1.34(1)	1.33(1)
NMe_2	NMe_2	1.6124(20)	1.3577(30)	1.3434(29)
		1.6113(19)[2]	1.3482(28)	1.3504(27)
Ph	CF_3	1.6411(16)	1.3192(21)	1.3207(24)
		1.6402(18)[2]	1.3182(24)	1.3223(25)
Ph	CCl_3	1.6400(22)	1.3033(36)	1.3402(34)

R	R'	N(4)-C(5)	C(5)-N(6)	N(6)-S(1)	Ref
Ph	Ph	1.34(1)	1.32(1)	1.627(6)	4
		1.33(1)	1.32(1)	1.624(6)	
NMe_2	NMe_2	1.3515(28)	1.3519(28)	1.6063(19)	12
		1.3454(28)	1.3609(28)	1.6117(20)	
Ph	CF_3	1.3580(24)	1.3285(22)	1.6227(17)	12
		1.3600(23)	1.3274(22)	1.6169(17)	
Ph	CCl_3	1.3504(32)	1.3291(34)	1.6280(23)	12

1. Bond lengths are measured in Angstroms (Å).
2. There are two molecules per motif.

No attempt has been made to average these bonds, as there is considerable variability from structure to structure. The asymmetric substitution pattern in **7c** and **8c** is clearly visible in the bond lengths. There is a slight tendency for the N=S=N bonds to shorten and the C–N–C bonds to lengthen with the electron releasing Me_2N groups. Correspondingly, S–N bonds lengthen and C–N bonds shorten in the proximity of electron withdrawing CF_3 groups. Beyond this few generalizations are possible.

Table 3.3 Comparison of bond angles(°) in 1,2,4,6-thiatriazine radicals with oxidation state 0.

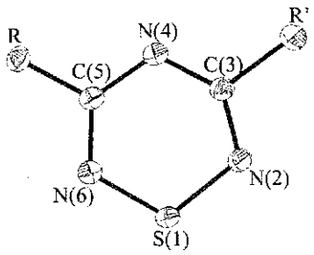

R	R'	<N(6)S(1)N(2)	<S(1)N(2)C(3)	<N(2)C(3)N(4)
Ph	Ph	110.7(4)	117.2(6)	127.7(8)
		110.8(3)[1]	116.7(6)	127.5(8)
NMe_2	NMe_2	111.71(10)	115.07(16)	128.08(21)
		111.75(10)[1]	116.05(15)	127.75(20)
Ph	CF_3	109.26(8)	115.39(14)	131.78(17)
		109.55(8)[1]	114.76(14)	132.26(18)
Ph	CCl_3	108.64(12)	117.02(19)	130.14(24)

R	R'	<C(3)N(4)C(5)	<N(4)C(5)N(6)	<C(5)N(6)S(1)	Ref
Ph	Ph	119.2(7)	128.1(8)	116.2(6)	4
		119.6(7)	128.3(8)	116.6(6)	
NMe_2	NMe_2	118.56(19)	127.97(20)	115.84(16)	12
		118.80(18)	127.87(20)	115.29(15)	
Ph	CF_3	117.67(15)	126.55(17)	119.09(14)	12
		117.53(16)	126.02(17)	119.48(14)	
Ph	CCl_3	118.36(23)	126.35(23)	119.27(18)	12

1. There are two molecules per motif.

The S–N bond lengths tend to be around 1.6 Å. Typical S–N single bond lengths are found in $S_4N_4H_4$ to be 1.665 Å, and N=S bond lengths are found to be 1.616 Å from S_4N_4. C–N bond lengths in the ring tend to fall anywhere between 1.32 and 1.36 Å. A typical heterocyclic C=N bond length is approximately 1.352 (5) Å.[13] They are definitely longer than an average C=N double bond (~1.270 (15) Å)[14], and shorter than the average C–N single bond (1.472 (5) Å). Just as for the bond lengths, we find that the bond angles are significantly less symmetrical with asymmetric substitution in **7c** and **8c**. Thus, the internal angles at the carbon of attachment of a CX_3 group are noticeably larger than for either phenyl or dimethylamino. Correspondingly, the internal angles at sulfur in **7c** and **8c** are noticeably smaller than those of phenyl and dimethylamino.

3.5 Conclusions

I have reported four new crystal structures. The imidoylamidines are novel, and show surprisingly strong intramolecular hydrogen bonding and relatively weak intermolecular hydrogen bonding. Two new neutral thiatriazine crystal structures are reported. **8c** has a face-to-face dimer similar to previously known thiatriazine radical structures, but packing between the dimers is unique. **7c** is the first example of a head-to-tail thiatriazine dimer structure. Unfortunately for both structures, no evidence was found for the proper stacking required for metallic conductivity. However, **8c** does display interstack contacts between the two dimers (Figure 3.12) that demonstrates that the essential interstack contacts can in fact form. This raises hopes that future crystal engineering will yet lead to an infinitely stacked thiatriazine radical.

References

1. Boeré, R. T.; Cordes, A. W.; Hayes, P. J.; Oakley, R. T.; Reed, R. W.; Pennington, W. T. *Inorg. Chem.* **1986**, *25*, 2445.

2. Cordes, A. W.; Oakley, R. T.; Reed, R. W. *Acta Cryst.* **1986**, *C42*, 1889.

3. Cordes, A. W.; Hayes, P. J.; Josephy, P. D.; Koenig, H.; Oakley, R. T.; Pennington, W. T. *J. Chem. Soc., Chem. Commun.* **1984**, 1021.

4. Hayes, P. J.; Oakley, R. T.; Cordes, A. W.; Pennington, W. T. *J. Am. Chem. Soc.* **1985**, *107*, 1346.

5. Oakley, R. T.; Reed, R. W.; Cordes, A. W.; Craig, S. L.; Graham, J. B. *J. Am. Chem. Soc.* **1987**,*109* , 7745.

6. Privett, A. J.; Craig, S. L.; Jeter, D. Y.; Cordes, A. W.; Oakley, R. T.; Reed, R. W. *Acta Crystallogr., Sect. C.* **1987**, *43*, 2023.

7. Robinson, V.; Taylor, G. E.; Woodward, P.; Bruce, M. I.; Wallis, R. C. *J. Chem. Soc. Dalton Trans.* **1981**, 1169.

8. Hursthouse, M. B.; Mazid, M. A.; Robinson, S. D.; Sahajpal, A. *J. Chem. Soc., Dalton Trans.* **1994**, *24*, 3615.

9. Aris, D. R.; Barker, J.; Phillips, P. R.; Alcock, N. W.; Wallbridge, G. H. *J. Chem. Soc., Dalton Trans.* **1997**, 909.

10. Greenwood, N. N.; Earnshaw, A. *Chemistry of the Elements, 2nd Edition*; Reed Educational and Professional Publishing Ltd.: Oxford, 1997; p 60.

11. Silverstein, R. M.; Webster, F. X. *Spectrometric Identification of Organic Compounds.*; John Wiley & Sons, Inc: New York, 1998.

12. Boeré, R. T. *Unpublished Data* .

13. *CRC Handbook of Chemistry and Physics, 70th Edition*; Weast, R. C.; CRC Press: Boca Raton, FL, 1989; p F-188.

14. Patai, S. *The Chemistry of Amidines and Imidates.*; John Wiley and Sons: New York, 1975.

Chapter 4

Electron paramagnetic resonance (EPR) spectroscopy and density functional theory (DFT) calculations of the 1,2,4,6-thiatriazine radicals

4.1 Introduction

The reduction of all ten 1-chloro-1,2,4,6-thiatriazine compounds **5a-e**, **6a-e** to their radicals **7a-e**,**8a- e** were successfully performed through the use of triphenylantimony in dried degassed acetonitrile. Characterization of these radicals using EPR analysis gave insight as to the unpaired electron's spin distribution on the thiatriazine core, as well as sensitivity to external electron donating and withdrawing substituents.

4.2 Electron paramagnetic resonance (EPR)

The background information presented here is based upon information obtained from undergraduate lectures. I have found Weil's book on EPR to be an excellent source of further information.[1] Electron paramagnetic resonance (EPR) is a characterization technique used for compounds that contain one or more unpaired electrons. EPR and nuclear magnetic resonance (NMR) are similar in the fact that they both involve electromagnetic radiation passing through a sample of matter contained in a homogenous magnetic field. With NMR the origin of the signal coming from the molecule is the nucleus, whereas with EPR it is the unpaired electron. Each electron possesses an intrinsic magnetic-dipole moment that arises from its spin. In most systems electrons occur in pairs such that the net moment is zero. Hence only species that contain one or more unpaired electrons possess the net

spin moment necessary for suitable interaction with an electromagnetic field. EPR is used to effectively map an unpaired electrons' distribution and hence determine the extent to which it is delocalized over the molecule. This type of spectroscopy (detection of one or more unpaired electrons) occurs in the microwave frequency range due to a larger energy gap than that for NMR. The uses of EPR vary from characterization of various conducting materials and polymers to magnetic resonance imaging.

It is known that when a magnetic field B_0 is applied an electron can assume two different spin orientations along the field's direction. The equation

$$\Delta E = h\upsilon_0 = g\mu_B B_0 \qquad [4.1]$$

is used to determine the size of the energy gap between these two spin orientations.

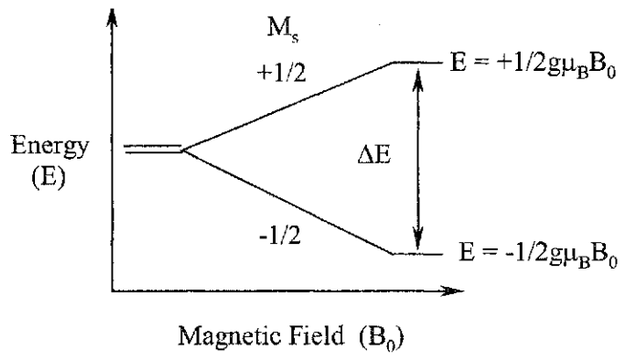

Figure 4.1. Energy gap between the +1/2 and –1/2 spin orientations.

g is called the Landé splitting energy or the "g value." For a free electron this value is 2.0023, and can be used for comparison between the magnetic environments of measured spectra versus that of the free electron. μ_B is the Bohr magneton and B_0 is the applied magnetic field. The size of the energy gap corresponds to photon energies

in the microwave region of the electromagnetic spectrum when magnetic fields of 1 – 10 Tesla are used. Lines or bands in a spectrum represent transitions between energy levels of the absorbing species. EPR spectra are traditionally recorded as the first derivative of the absorption peak (dispersion mode), and the electron spin energy levels are often split into multiplets called their hyperfine structure. These are due to the interaction of the nuclear spins of attached nuclei (similar to NMR) where a magnetic nucleus of spin quantum number I can adopt $2NI + 1$ different orientations and hence give rise to $2NI + 1$ different contributions to the local field. N is the number of equivalent nuclei the electron couples to, and I is the nuclear spin.

4.3 Experimental

In all cases a small crystal of pure thiatriazine was placed in a 4mm pyrex tube, and deoxygenated dichloromethane was added by vacuum transfer. The tubes were flame-sealed before measurements were taken. The samples were progressively diluted by vacuum transfer until severe signal-to-noise limitations set in, or until the spectrum became invariant. At higher concentrations all the spectra lost a substantial part of their fine structure. Data were collected at the University of Calgary on a Bruker EMX10 spectrometer.

4.4 Results

Experimental EPR spectra were obtained for all 10 compounds (**7a-e** & **8a-e**). The spectra are very complex, indicative of inequivalent hyperfine coupling (hfc) to the symmetry non-equivalent nitrogen atoms. For such cases where the nitrogen

atoms are equivalent, the formula $2NI + 1$ predicts $2(3)1 + 1 = 7$ lines of unequal intensity. 1:1:1 triplets of equal intensity are clearly visible in spectra for compounds **7a-e**, for example in Figure 4.2. This is indicative of at least one unique nitrogen, for which the formula predicts $2(1)1 + 1 = 3$ lines of equal intensity. The spectra were successfully simulated as a 1:1:1 triplet of 1:1:1 triplets of 1:1:1 triplets using WINEPR SimFonia software and the hyperfine coupling constants were obtained from the simulations. Figure 4.2 shows the excellent agreement between the simulation and the experimental spectrum for **7d** and similar agreements were obtained for the other members of this series.

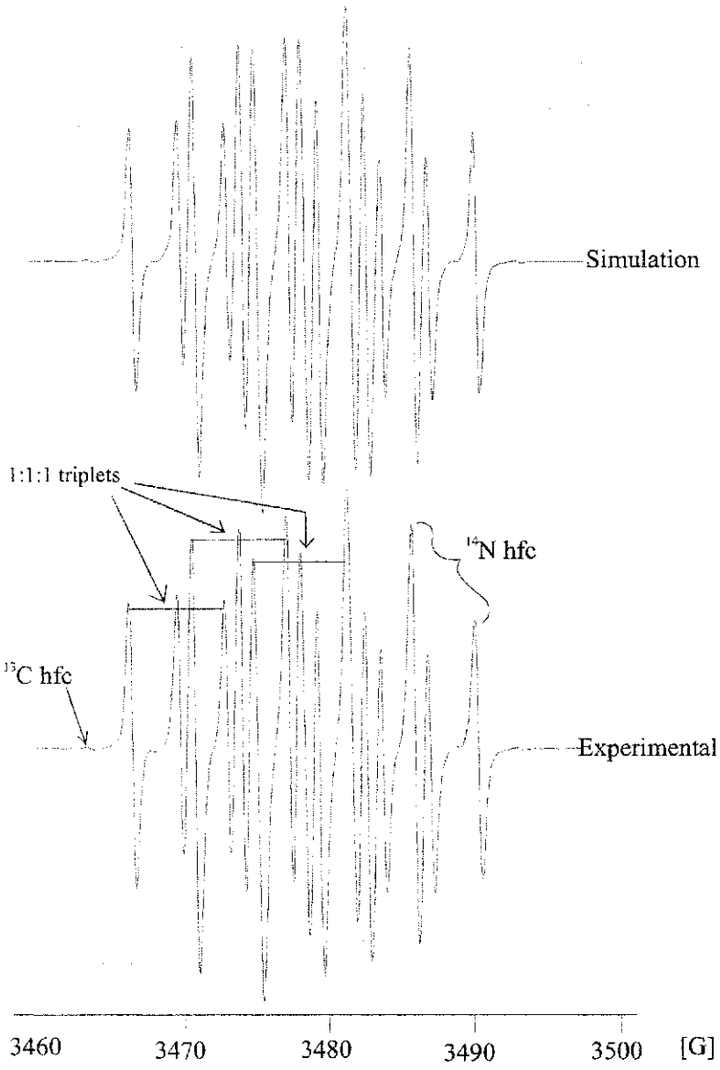

Figure 4.2 EPR spectrum of **7d** in CH_2Cl_2.

The spectra of the trifluoromethyl radicals **8a-e** are even more complex because of additional coupling to the fluorine atoms of the CF_3 group. An example of the experimental and simulated spectrum of **8d** is shown in Figure 4.3.

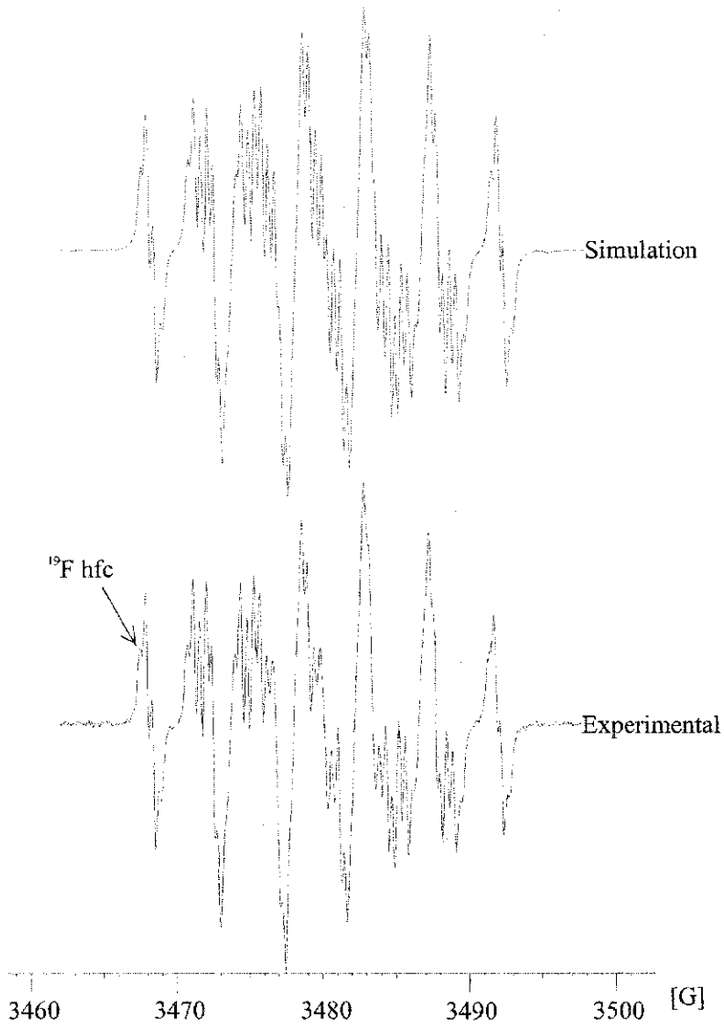

Figure 4.3 EPR spectrum of **8d** in CH_2Cl_2.

The fluorine atoms cause each subpeak to split into small quartets. Here too, excellent agreement was obtained between the experimental and simulated EPR spectra for all five compounds. A compilation of all hfc constants obtained from the simulations is presented in Table 4.1.

4.5 Density Functional Theory (DFT) calculations

In order to assign the hfc constants to the individual nitrogen nuclei in the thiatriazine ring, it was necessary to perform quantum mechanical calculations. A recent comparison of *ab initio* and DFT methods in calculating molecular geometry, isotropic hyperfine coupling constants, and redox processes for several heterocyclic radical ring systems (including the 1,2,4,6-thiatriazine) was done[2,3], which determined that the best results were obtained using the UB3LYP/6-31G(d) method. UB3LYP/6-31G(d) geometry optimizations were therefore performed on all ten 1,2,4,6-thiatriazine radicals, and theoretical hyperfine coupling constants were calculated. All calculations were performed by Meg O'Shea and Dr. René Boeré. The optimized geometries were found to be consistent with the known structures of thiatriazine radicals as determined from X-ray crystallographic studies of the dimer in the solid-state. The results of the calculated hfc constants, scaled by a factor (see below) are also included in Table 4.1.

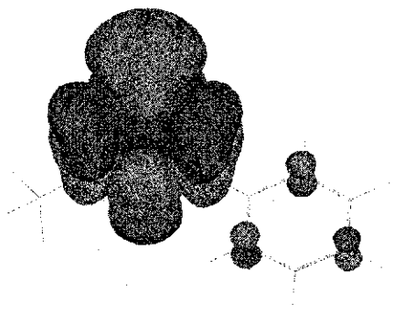

Figure 4.4 Shaded surface plot of the π-SOMO of **8c**.

For each thiatriazine the unpaired electron occupies a π-SOMO, which is delocalized over the heterocyclic core. Figure 4.4 shows this orbital for **8c**. The

largest coefficient is that of sulfur, but there is considerable unpaired electron density on each of the three nitrogen atoms, and a lesser degree on the carbon atoms. The small coefficients on three of the phenyl carbon atoms are indicative of spin leakage onto the aryl rings. There is no experimental evidence however, for hyperfine coupling to aryl ring atoms, and it may be expected that free rotation of the aryl rings

Table 4.1 Experimental and calculated EPR data of **7a-e**, **8a-e**.

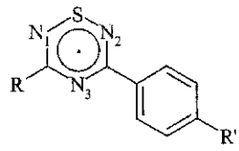

Cmpd	R	R'		a_{N1}	a_{N2}	a_{N3}	a_C	a_S	a_F
7a	CCl_3	OCH_3	Exptl.	3.177	4.374	4.374	5.500	[3]	
			DFT[1]	3.055	4.349	4.509	-5.485	5.432	
7b	CCl_3	CH_3	Exptl.	3.240	4.370	4.374	5.600	[3]	
			DFT[1]	3.130	4.440	4.440	-5.652	5.405	
7c	CCl_3	H	Exptl.	3.275	4.326	4.435	5.500	[3]	
			DFT[1]	3.165	4.417	4.482	-5.725	5.411	
7d	CCl_3	Cl	Exptl.	3.260	4.227	4.446	5.700	[3]	
			DFT[1]	3.168	4.380	4.486	-5.729	5.439	
7e	CCl_3	CF_3	Exptl.	3.350	4.100	4.560	5.800	[3]	
			DFT[1]	3.139	4.268	4.470	-5.563	5.413	
8a	CF_3	OCH_3	Exptl.	3.100	4.350	4.350	5.800	[3]	0.420[2]
			DFT[1]	3.176	4.470	4.266	-5.518	5.581	
8b	CF_3	CH_3	Exptl.	3.200	4.370	4.375	5.800	[3]	0.420[2]
			DFT[1]	3.236	4.353	4.306	-5.625	5.462	
8c	CF_3	H	Exptl.	3.200	4.240	4.500	5.800	[3]	0.420[2]
			DFT[1]	3.333	4.294	4.417	-5.756	5.412	
8d	CF_3	Cl	Exptl.	3.260	4.190	4.510	5.500	[3]	0.410
			DFT[1]	3.267	4.275	4.347	-5.606	5.487	
8e	CF_3	CF_3	Exptl.	3.350	4.120	4.530	5.500	[3]	0.400[2]
			DFT[1]	3.320	4.160	4.412	-5.665	5.464	

1. Calculated hfc in Gauss from UB3LYP-DFT calculations, multiplied by a scaling factor of 0.81.
2. The F hfc is to the three fluorine atoms in the directly bound CF_3 group.
3. Sulfur hfc was not observable due to the very small natural abundance of this isotope.

in solution reduces the extent of unpaired electron density delocalization onto the aryl rings. The appearances of the other nine π-SOMOs are visually indistinguishable from the one shown in Figure 4.4.

4.6 Discussion

In each case, there are three distinct a_N values, except for **7a** and **8a** where two of the values are indistinguishable. Such accidental degeneracy of symmetry non equivalent nitrogen atoms is fairly common. For example in **10**, where the N=S=N and C–N–C nitrogen nuclei are in distinctly different environments, all three nitrogen atoms appear to have identical hfc of 3.97 G. However, it should be noted that the linewidth of the spectra are quite large, making small differences in a_N difficult to distinguish. Much more convincing is the trend in the hfc with *para* R-substituents, such that as the R group becomes more strongly electron withdrawing a_{N1} and a_{N3} increase while a_{N2} decreases. As controls we can cite the powerfully π-electron donating NMe_2 groups directly bound in 3,5-bis(dimethylamino)-1,2,4,6-thiatriazinc[4] (Table 4.2), in which $a_{N1} = a_{N2}$ is twice as large as a_{N3}. Conversely with the powerfully electron withdrawing, directly bound CF_3 and CCl_3 groups in 3,5-bis(trifluoromethyl)-1,2,4,6-thiatriazine[5] and 3,5-bis(trichloromethyl)-1,2,4,6-thiatriazine[4], a_{N3} is found to be larger by about 40% than a_{N1} and a_{N2}. The hyperfine coupling constants of compounds **7a-e** and **8a-e** are therefore intermediate, as expected. However small changes in the relative a_N values occur and accurately reflect the electron withdrawing abilities of the remote substituents. This can be

understood as charge drift away from the N=S=N group in the radical, towards the C–N–C section of the molecule.

The sum of the hyperfine coupling to nitrogen in all ten rings is remarkably consistent. The distribution of the coupling changes with substituent, but the total is almost invariant. A similar result occurred for the hfc constants obtained from the UB3LYP/6–31G(d) calculations, except that all values were larger. It was found that a consistent set of calculated and experimental results could be obtained by applying a scaling factor of 0.81 to the calculated values. The calculated values were used to assign the experimental values to specific nuclei.

Table 4.2 All EPR data for 1,2,4,6-thiatriazines.

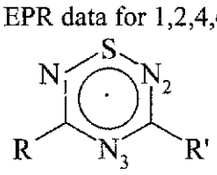

R	R'	a_{N1}	a_{N2}	a_{N3}	Add'l hfc
CCl_3	4-$CH_3OC_6H_4$	3.177	4.374	4.374	5.5 (^{13}C)
CCl_3	4-$CH_3C_6H_4$	3.240	4.370	4.374	5.6 (^{13}C)
CCl_3	C_6H_5	3.275	4.326	4.435	5.5 (^{13}C)
CCl_3	4-ClC_6H_4	3.260	4.227	4.446	5.7 (^{13}C)
CCl_3	4-$CF_3C_6H_4$	3.350	4.100	4.560	5.8 (^{13}C)
CF_3	4-$CH_3OC_6H_4$	3.100	4.350	4.350	5.8 (^{13}C), 0.42 (^{19}F)
CF_3	4-$CH_3C_6H_4$	3.200	4.370	4.375	5.8 (^{13}C), 0.42 (^{19}F)
CF_3	C_6H_5	3.200	4.240	4.500	5.8 (^{13}C), 0.42 (^{19}F)
CF_3	4-ClC_6H_4	3.260	4.190	4.510	5.5 (^{13}C), 0.41(^{19}F)
CF_3	4-$CF_3C_6H_4$	3.350	4.120	4.530	5.5 (^{13}C), 0.40 (^{19}F)
CF_3[1]	CF_3	3.35	3.35	4.59	0.42 (^{19}F)
CCl_3[2]	CCl_3	3.59	3.59	4.94	
Cl[1]	Cl	3.73	3.73	4.44	0.71 (^{35}Cl)
4-$CH_3OC_6H_4$[1]	4-$CH_3OC_6H_4$	3.65	3.65	3.65	
C_6H_5[1]	C_6H_5	3.99	3.99	3.99	
4-$NO_2C_6H_4$[1]	4-$NO_2C_6H_4$	3.72	3.72	4.27	
NMe_2[2]	NMe_2	4.14	4.14	2.25	0.71 a(NMe_2)

1. Data from reference 5
2. Data from reference 4

The directly bound CF_3 group causes further splitting of the EPR signals of **8a-e**, but the a_F values are small. The quartet pattern implies a rotational average of all three fluorine nuclei, as expected for CF_3 groups. As mentioned in Chapter 3, rotational motion of the CF_3 groups even occurs in the solid state at room temperature. I interpret the small a_F values to be due to a relatively weak interaction between the fluorine atomic orbitals and the thiatriazine ring π-system. Similar a_F values have been reported for 3,5-bis(trifluoromethyl)-1,2,4,6-thiatriazine (Table 4.2).

Small satellite peaks occur outside the main lines from coupling to nitrogen (and fluorine). The best fit in the simulations of these very weak lines was to assign them to two carbon nuclei with the same hfc constant. As expected from the symmetry of the molecule, the DFT calculations provide two different numbers for the two carbons in the ring. However, the 1% abundant ^{13}C signal is so weak that it is not possible to distinguish these peaks in the experimental data and they have been averaged. Coupling to sulfur is more complex because it has a 3/2 spin. There is some evidence in some of the EPR spectra for such coupling, but the signal to noise ratio does not allow me to assign that coupling. I would need to use isotopically enriched sulfur to observe that coupling.

4.7 Conclusion

The EPR spectra for **7a-e** and **8a-e** are highly diagnostic as to the structure of the thiatriazine radicals in solution. Thus, although these compounds crystallize as dimers in the solid-state (Chapter 3), they dissociate in solution in dichloromethane, at least at low concentrations. At higher concentrations the EPR spectra are

concentration broadened, a well-known phenomenon. UB3LYP/6-31G(d) gas-phase calculations worked well in predicting the isotropic hyperfine coupling constants of these radicals, allowing us to assign the constants to individual atoms in the heterocyclic core. A small but very distinct influence on the nitrogen hyperfine coupling constants from the remote R-substituents has clearly been demonstrated. EPR spectroscopy can therefore be used to monitor the electronic influence of the substituents on the heterocyclic core.

References

1. Weil, J. A.; Bolton, J. R.; Wertz, J. E. *Electron Paramagnetic Resonance*; John Wiley & Sons: New York, 1994.

2. Kaszynski, P. *J. Phys. Chem. A* **2001**, *105*, 7626.

3. Kaszynski, P. *J. Phys. Chem. A* **2001**, *105*, 7615.

4. Boeré, R. T. *Unpublished Data* .

5. Boeré, R. T.; Oakley, R. T.; Reed, R. W.; Westwood, N. P. C. *J. Am. Chem. Soc.* **1989**, *111*, 1180.

Chapter 5

Electrochemistry of the 1,2,4,6-thiatriazine radicals

5.1 Introduction

Electrochemistry involves the coupling of electricity to chemical changes of a species or compound. These chemical changes must be oxidation and/or reduction (redox) processes. A redox reaction occurs when there is a transfer of one or more electrons from one species to another. This broad definition includes processes of practical interest (power generation i.e. "batteries", synthesis, winning elements from their ores), as well as purely analytical methods. In this work only analytical electrochemistry is in view. Further, within analytical electrochemistry the distinction can be made between techniques aimed at quantitative determination of the analyte and diagnosis of the analyte. The work reported here is purely diagnostic.

The information given below is largely based upon a standard textbook presentation.[1] When electrons in a redox reaction can be made to flow through an electric circuit, insight into the reaction can be learned through measurement of the voltage and the current in the circuit. My goal was to use electrochemistry to diagnose the redox reactions that 1,2,4,6-thiatriazine radicals undergo in solution. Within the context of the thesis, the specific goal of the electrochemical study was to examine the influence of the remote aryl substitutes 'X' in compounds **7a-e** and **8a-e** on the redox processes.

As mentioned in Chapter 1, one of the chief design factors sought in both kinds of molecular metals (i.e. RICs and NRCs) is weak electron-electron (coulombic) repulsion, since this can be correlated with minimization of ionic fluctuation during current flow

through the solid. A chemical expression of weak coulombic repulsion is a low disproportionation energy, i.e. for the reaction:

$$2\ \text{Radical} \leftrightarrow \text{Oxidized form} + \text{Reduced form} \qquad [5.1]$$

the (unfavorable) free energy should be minimized. An estimate of the size of this process in the solid state can be obtained from solution electrochemistry.[2] The electrochemical cell potential, E_{cell} for the above reaction (1) has been obtained for classical charge-transfer type RICs. The cell potentials have been expressed as positive numbers, i.e., $|E_{process1} - E_{process2}|$, recognizing that this value should be as small as possible for conducting systems. In doing so, we are effectively using the so-called 'European' sign convention for electrode processes.[3] A key objective of the thesis was to determine reliable E_{cell} values for the 1,2,4,6-thiatriazines.

5.2 Electroanalytical techniques

Voltammetry describes a family of electroanalytical techniques with the common characteristics that the potential of the working electrode is controlled (typically with a potentiostat) and the current flowing through the circuit is measured. Linear-sweep voltammetry (LSV) is one of the most common techniques in which the potential is scanned linearly in time. By far the most common LSV technique has been polarography, which through the use of the dropping mercury electrode was primarily suited to the investigation of reduction processes.[4] More recent work has tended to use cyclic voltammetry (CV), and work in both oxidizing and reducing regimes.[5] Polarography is most suited to quantitative analysis of analyte with known redox

potentials, whereas cyclic voltammetry is better suited as a diagnostic tool for the investigation of redox processes.

5.2.1 Cyclic Voltammetry (CV)

In Cyclic Voltammetry (CV) the current flowing through the circuit is measured as a function of the potential of the working electrode. This current is proportional to the applied voltage and to the concentration of analyte in the monolayer directly surrounding the electrode. The potential of a small, stationary working electrode is changed linearly with time starting from a potential where no electrode reaction occurs and moving to potentials where reduction or oxidation of an analyte (our material being studied) occurs.

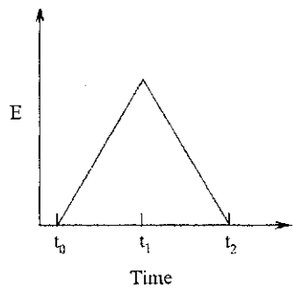

Figure 5.1 Waveform for cyclic voltammetry.

After traversing the potential region in which one or more electrode reactions take place, the direction of the linear sweep is reversed and the electrode reactions of intermediates and products, formed during the forward scan, can often be detected. This cycle can be repeated a number of times. The waveform of this process is shown in Figure 5.1. The result of applying this waveform to a reversible electrode process is represented in Figure 5.2, where $t_0 - t_2$ are the same times as in Figure 5.1.

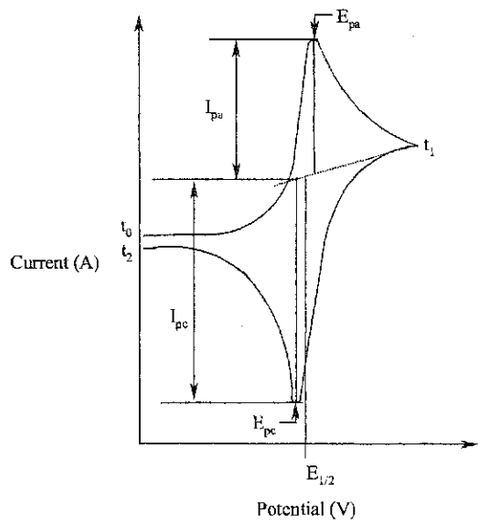

Figure 5.2 Idealized cyclic voltammogram trace for an oxidation reaction followed by return to the initial conditions. I_{pa} is the peak anodic current and I_{pc} is the peak cathodic current. E_{pa} and E_{pc} are the potentials at which these currents are observed. $E_{1/2}$ is the half wave potential, and $t_0 - t_2$ are defined in Figure 5.1.

In CV there is no stirring of the solution containing the analyte during the experimental run. This means that once the potential is such that the analyte is able to be oxidized (or reduced), only the analyte near the electrode surface will be affected. Diffusion is the only process bringing new analyte in to be oxidized, and if the time frame of the experiment is fast enough very little new analyte will be brought to the electrode surface. In polarography the time frame is longer, hence diffusion allows the current to stay at a constant value throughout the appropriate potential range. In CV the current drops, which reflects the inability to diffuse in enough new analyte to stay at a maximum in the allowed time frame. This also means that, if the potential is reversed, the material that has been oxidized can now be reduced back to its original form. This re-reduction is shown occurring from $t_1 - t_2$ in Figure 5.2. The exact inverse occurs when an initial species is first reduced and then reoxidized.

Cyclic voltammetry is commonly performed in a single-compartment cell, and is most commonly performed with a three electrode configuration. All three are immersed in a solution containing the analyte and electrolyte. The first electrode, called the working electrode, has a potential which is varied linearly with time. The second electrode, called the reference electrode, has a potential that remains constant throughout the experiment. The third electrode, called the counter electrode, serves to conduct current from the source through the solution to the working electrode. The signal source is a variable dc power supply which is in series with a variable resistor. The resulting current is recorded as a function of the potential difference between the working and reference electrodes. Electrodes can be manufactured from a variety of inert materials, including platinum, gold, and glassy carbon (graphite). Our cell employs all platinum electrodes. The time scale of the experiment is controlled by a variable scan rate (or sweep rate), such that the total potential range can be traversed between $10^2 - 10^5$ s. A supporting electrolyte (in our case, $N^nBu_4PF_6$), dissociates into ions once in solution, and is present as the charge carrier in solution. The electrolyte itself must be redox-inert over the potential range of interest.

A CV can show multiple redox processes, and can show those processes to be either reversible, quasi-reversible, or irreversible. A redox process is said to be electrochemically reversible if the surface concentrations of the analyte and either its reduced or oxidized forms are maintained at the values required by the Nernst equation throughout the experiment. If a reaction is reversible, the Nernst equation relates the current and potential in the following manner:

$$E = E_{1/2} - \frac{C}{n}\log\frac{I}{I_d - I} \qquad [5.2]$$

Where E is the applied potential (in mV), $E_{1/2}$ is the half wave potential, C in aqueous ionic solution at 298.15 K is 0.05916V, n is the number of moles of electrons transferred in the balanced equation for the reaction, I is the current, and I_d is the diffusion current. Strictly speaking, in CV the current is proportional to the rate of change of analyte concentration rather than due to any actual diffusion process. However, the resulting equations are of similar form to Equation [5.2] and will not be developed in any further detail. Thus, a reversible single-electron process in CV has a peak potential separation ΔE_p ($E_{pc} - E_{pa}$) = ~59.16 mV in water at all scan rates at 25°C. For non-aqueous solutions the range is found to be much larger, and values around 100 – 200 mV are typical. As well, for a reversible process the peak current ratio = 1 at all scan rates, and the peak current function is independent of scan rate. A process is said to be electrochemically quasi-reversible if a return wave is observed but the peak potential separation is greater than the above values and the peak current ratio deviates significantly from 1. A process is said to be electrochemically irreversible if a return wave cannot be observed at a given scan rate.

5.2.2 Osteryoung square wave voltammetry (OSWV)

Osteryoung square wave voltammetry (OSWV) is one of several types of pulse voltammetry (which also include Normal pulse, Differential pulse, and Staircase voltammetry). OSWV retains much of the diagnostic capability of traditional cyclic voltammetry, but differs from CV in that the current is measured at a constant potential (instead of with a linear change in potential with time).[6] In OSWV the potential becomes independent of time, which makes the non-faradaic (background) current negligible in the

experimental run. Because the signal to noise is greater than in CV the sensitivity of the OSWV experiment is much higher and detection limits reach 10^{-7} to 10^{-8} M.[6] The time frame of the experiment in OSWV is shortened, especially with regards to sampling time of the analyte. The waveform of this process is shown in Figure 5.3.

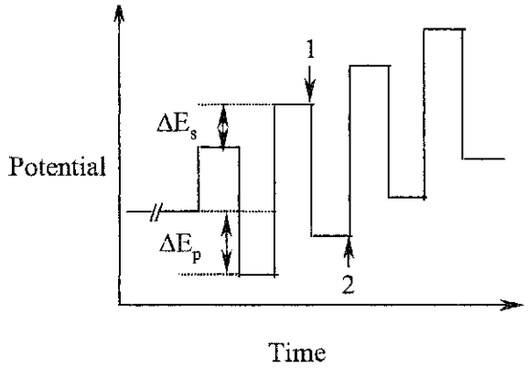

Figure 5.3 Waveform for osteryoung square wave voltammetry (OSWV). ΔE_s is the step height or potential increase over each cycle, ΔE_p is the pulse amplitude, and 1 & 2 are points at which the current is sampled. Diagram is not drawn to scale.

The step height (ΔE_s) is a lot smaller (~10mV) than the amplitude of the pulse (~50mV), causing the overall increase in potential to be gradual (not a steep slope). The forward (or positive) pulse produces a cathodic current (i_1), while the reverse (negative) pulse produces an anodic current (i_2), and the difference between the two is plotted to give Δi for the reaction.[7] This is shown in Fig. 5.4. In a reversible electrochemical process the size of the forward pulse is large enough to allow for the onset of oxidation of the analyte and the reverse pulse is large enough to allow for reduction of the material oxidized on the forward pulse. As in CV, decay of the oxidized material in the

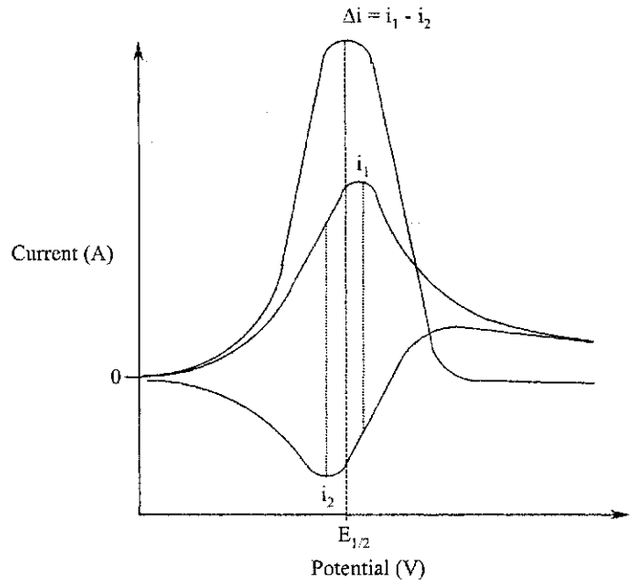

Figure 5.4 Forward (i_1) and reverse (i_2) current for an idealized square wave voltammogram (Δi) in a reversible reaction.

monolayer can cause the reduction current (i_2) to be smaller than theory predicts. This causes Δi to be smaller and the differential peak becomes lower. The maximum in the OSWV peak corresponds approximately to the conventional $E_{½}$ of the process. In this work the maximum on the Δi curve has been taken as $E_{½}$ of the process, and provides independent corroboration of the redox potentials measured from the CV data. OSWV was attempted because of the known tendency of the thiatriazine radicals to dimerize in solution at moderate to high concentration. Thus it was desirable to measure the redox potentials at the very lowest concentrations possible where dimerization is expected to be at a minimum.

5.2.3 Solvents

Except for the earliest work, in which protic solvents were common, the majority of the previous electrochemical data on redox-active heterocycles[2] has been recorded in

aprotic non-aqueous solvents, of which acetonitrile (CH_3CN) is the most common. Other solvents which have been used are dichloromethane (CH_2Cl_2), 1,2-dichloroethane, dimethylformamide (DMF), trifluoroacetic acid and sulfur dioxide. Early work in protic solvents was rendered unreliable by redox-induced degradation reactions involving the solvent medium. As a rule compounds containing bonds between the Group 15/16 elements are susceptible to hydrolysis, so protic solvents should be avoided to suppress decomposition reactions, and carefully dried solvents should be used at all times.

The importance of solvent effects has recently been emphasized by careful comparative work in more than one solvent. Thus for the 1,2,3,5-dithiadiazole ring system it has been demonstrated that, starting with the neutral radicals in solution, the $E_{1/2}$ for the +1/0 process differs by ~0.2 V between CH_3CN and CH_2Cl_2, while the 0/–1 wave is almost unaffected by the change in solvent.[8,9] It is obvious that the comparison of data obtained in different solvent systems should be practiced with caution, and the same applies to different electrolyte systems as well.[10]

As of yet there is no universal consensus on the correct referencing of electrochemical data in non-aqueous solutions. The vast majority of the data for organic polarography and cyclic voltammetry is reported against the saturated calomel electrode (SCE), usually in a half-cell containing the same solvent and electrolyte system as the working half-cell. In this work I have elected to use a single-compartment three-electrode system with a pseudo-reference electrode, along with an internal standard for the redox potentials. These standards are calibrated in careful measurement against the SCE, and the potentials are then converted to the SCE scale. The most commonly used internal redox reference is the ferrocene/ferrocenium couple (Fc/Fc^+), which with 0.1 M

$N^nBu_4PF_6$ (TBAFP) appears at + 0.38 V versus SCE in CH_3CN solution, and 0.5 M TBAFP appears at + 0.48 V in CH_2Cl_2.[9] We have opted for ferrocene as our internal reference in all electrochemical work presented here. The accuracy of this approach has been substantiated by previous work. Nearly identical potential values were obtained for a series of 1,2,3,5-dithiadiazole rings by this method compared to measurements made on the same compounds in a two-electrode cell using a pressure-equalized Ag/Ag^+ reference electrode, which was itself calibrated externally to an SCE electrode.[11]

5.2.4 Specialized electrochemical cell

The study of redox active heterocycles requires, from time to time, the handling of high concentrations of free radicals in solution. In addition, many Group 15/16 linkages are highly susceptible to hydrolysis by adventitious moisture, as is the case with our 1,2,4,6-thiatriazine radicals. The development of several specialized electrochemical cells has helped the progress of diagnostic electrochemistry on these and other compounds with similar limitations. The cell, which was developed and used in our case for handling very air-sensitive inorganic materials, is described in Figure 5.5.

As shown in Figure 5.5, A is the chamber for electrolyte and solvent, B is the working cell compartment with internal cold finger, C is the break seal with analyte, D is the break seal with internal reference, E are the weights used to crush the breakseals, F is the counter electrode, G is the working electrode, H is the reference electrode, and I is the tap with transfer line to connect to a vacuum line. This design uses break-seal technology to produce an all-glass cell (except for a single Teflon stopcock). During cell operation, the electrolyte and solvent are first introduced into the working compartment to obtain background scans and measure the actual solvent window for the experiment being

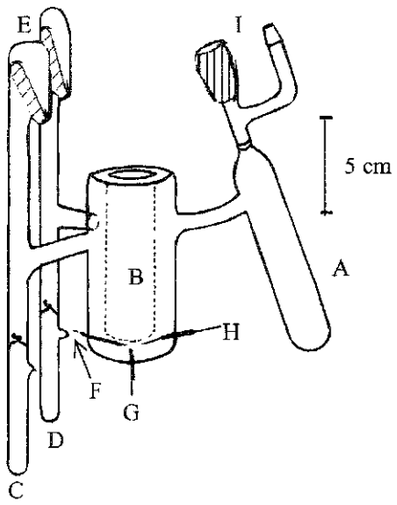

Figure 5.5 Specialized electrochemical cell design. Break-seals can be loaded in a glove box and are fused to the cell prior to rigorous vacuum drying and loading of electrolyte and solvent.

performed. The analyte is then introduced by washing the contents of the first break-seal into the working cell, and later the internal reference can also be added in the same way. It is even possible to add the analyte and/or reference in portions to prevent one or the other from swamping the signals. The internal cold-finger allows the experiment to be cooled below ambient temperature. This cell can also operate under mild pressure, e.g. using sulfur dioxide as the solvent.

5.3 Experimental

I have opted to do a comparative study in both CH_3CN and CH_2Cl_2. The same procedure was followed for all ten radicals in both solvents (CH_3CN and CH_2Cl_2). Crystals of sufficient purity of **7a-e**, **8a-e** were collected, weighed, and loaded into individual break seal tubes. These were then sealed under vacuum. A known mass of

ferrocene was also weighed and loaded into a break seal tube, and then sealed under vacuum. Both break seals (one of analyte, one of ferrocene) were attached to the electrochemical cell by glass blowing, and checked for possible leaks. Once the cell was complete it was rigorously cleaned and dried under vacuum to ensure no air or moisture was present. A known quantity of the electrolyte $N^nBu_4PF_6$ (TBAFP) was added to the chamber (A in Figure 5.5), and the cell was placed on the vacuum line with the chamber immersed in a 70°C oil bath overnight to fully dry the electrolyte. The solvent was attached to the vacuum line and freeze–thaw degassed several times to remove all traces of oxygen. Then a predetermined volume of the solvent was transferred into the electrolyte chamber of the electrochemical cell by vacuum line transfer. The tap was closed and the cell was removed from the vacuum line in order to run the experiment. All experiments were performed on a BAS CV50 potentiostat. Cyclic voltammetric studies (scan rates $v = 100 - 10000$ mVs^{-1}) and Osteryoung square wave voltammetric studies (square wave amplitude = 25mV, frequency = 15 Hz, step size = 4mV) were performed.

5.4 Results and discussion

The electrochemical data is reported in full detail in Tables 5.1, 5.2, and 5.3 for all radicals studied in this thesis. The procedure used for each run was to slowly add analyte to the electrolyte solution while monitoring with both CV and OSWV. If noticeable changes in the electrochemical response occurred with increasing analyte concentration, then the effect of varying scan rate over a wide range was also investigated. When either all the analyte had been added (for **8a-e**) or the solutions appeared to be saturated (for **7a-**

e), ferrocene was carefully added to avoid swamping the analyte signals. The data compiled in Tables 5.1 to 5.3 represents a careful distillation of all the electrochemical experiments that were performed, and is typically reported at scan rates of 100 or 200 mVs^{-1}. Table 5.1 summarizes all the data for **7a-e**. The appearance of the electrochemical response of **8a-e** changed dramatically from low concentration to higher concentration, which was also apparent from the color change of the solution (from a pale yellow to brown). Table 5.2 presents the high concentration data ($6.3 \times 10^{-3} - 1.1 \times 10^{-2}$ M), while Table 5.3 summarizes the results at lower concentration. From the current response of the CV and OSWV data, the active concentrations are estimated to be 10 – 20 times lower than the nominal concentration values which are listed in Table 5.3. Tables 5.4 – 5.6 are more concise data tables listing key 0/–1, +1/0, and E_{cell} potentials from the CV data listed in Tables 5.1 – 5.3.

Table 5.1 Electrochemical data for X-$C_6H_4C_2N_3SCCl_3$ thiatriazines

X		OCH_3		CH_3		H		Cl		CF_3	
Solvent		CH_3CN[2]	CH_2Cl_2[3]	CH_3CN[2]	CH_2Cl_2[3]	CH_3CN[2]	CH_2Cl_2[3]	CH_3CN[2]	CH_2Cl_2[3]	CH_3CN[2]	CH_2Cl_2[3]
Conc., M		3.5×10^{-3}	7.2×10^{-3}	7.4×10^{-3}	8.4×10^{-3}	6.2×10^{-3}	5.8×10^{-3}	3.9×10^{-3}	6.4×10^{-3}	5.3×10^{-3}	6.2×10^{-3}
Scan Rate (mV/s)		100	200	200	100	100	100	100	200	200	200
+1/0											
CV	E_c, V	0.969	-	-	1.175	1.070	1.244	1.109	-	1.161	1.269
	E_a, V	1.045	1.186	1.035	1.287	1.138	1.316	1.183	1.284	1.223	1.361
	$E_{1/2}$, V	1.007	-	-	1.231	1.104	1.280	1.146	-	1.192	1.315
	i_p, μA	100	144	78	391	70	250	97	154	115	278
OSWV	E, V	1.016	1.148	1.052	1.208	1.104	1.188	1.128	1.236	1.184	1.384
	$w_{1/2}$, mV	202	139	114	125	141	102	112	219	129	248
	i_p, μA	93	41	145	295	85	262	85	124	78	96
0/-1											
CV	E_c, V	-0.243	-0.326	-0.159	-0.283	-0.138	-0.181	-0.063	-0.150	0.017	-0.161
	E_a, V	-	-	-	-	-	-	-	-	-	-
	$E_{1/2}$, V	-	-	-	-	-	-	-	-	-	-
	i_p, μA	51	138	78	247	56	153	60	194	51	209
OSV	E, V	-0.180	-0.232	-0.178	-0.172	-0.136	-0.108	-0.020	-0.072	-0.016	-0.096
	$w_{1/2}$, mV	149	216	337	170	250	120	342	136	231	194
	i_p, μA	41	48	25	163	19	156	21	63	6	62
E_{cell} (CV)		1.212[1]	[1.512][1]	[1.194][1]	1.458[1]	1.208[1]	1.424[1]	1.172[1]	[1.434][1]	1.144[1]	1.430[1]
E_{cell} (OSWV)		1.196	1.380	1.230	1.380	1.240	1.296	1.148	1.308	1.200	1.480

1. $E_{cell} = E_{c1} - E_{c2}$ except [] where both processes are irreversible; the latter are approximate values only.
2. At a Pt-electrode in CH_3CN containing 0.1 M $N^nBu_4PF_6$ electrolyte, referenced to SCE such that $E_{½} = +0.38$ V for $[Cp_2Fe]^{+1/0}$.
3. At a Pt-electrode in CH_2Cl_2 containing 0.5 M $N^nBu_4PF_6$ electrolyte, referenced to SCE such that $E_{½} = +0.48$ V for $[Cp_2Fe]^{+1/0}$.

Table 5.2 Electrochemical data for X-$C_6H_4C_2N_3SCF_3$ thiatriazines at the full indicated concentrations.

X		OCH_3		CH_3		H		Cl		CF_3	
Solvent		CH_3CN[2]	CH_2Cl_2[3]	CH_3CN[2]	CH_2Cl_2[3]	CH_3CN[2]	CH_2Cl_2[3]	CH_3CN[2]	CH_2Cl_2[3]	CH_3CN[2]	CH_2Cl_2[3]
Conc., M		$7.3x10^{-3}$	$1.0x10^{-2}$	$6.3x10^{-3}$	$8.7x10^{-3}$	$1.0x10^{-2}$	$1.1x10^{-2}$	$1.1x10^{-2}$	$9.0x10^{-3}$	$6.7x10^{-3}$	$6.7x10^{-3}$
Scan Rate (mV/s)		200	200	100	200	200	200	200	200	200	200
+1/0											
CV	E_c, V	1.007	1.148	1.096	1.217	1.119	1.258	1.160	1.268	1.236	1.361
	E_a, V	1.143	1.258	1.188	1.345	1.267	1.398	1.274	1.456	1.342	1.483
	$E_{1/2}$, V	1.075	1.203	1.142	1.281	1.193	1.328	1.217	1.362	1.289	1.422
	i_p, μA	588	640	653	934	1009	1156	1188	642	706	485
OSWV	E, V	1.072	1.208	1.160	1.292	1.204	1.332	1.232	1.364	1.296	1.416
	$w_{1/2}$, mV	125	152	124	192	146	144	128	172	132	183
	i_p, μA	408	441	586	283	527	607	741	263	497	224
0/-1											
CV	E_c, V	-0.247	-0.176	-0.216	-0.176	-0.217	-0.154	-0.165	-0.152	-0.126	-0.097
	E_a, V	-0.133	-0.072	-0.132	-0.060	-0.099	-0.038	-0.070	0.008	-0.038	0.029
	$E_{1/2}$, V	-0.190	-0.124	-0.174	-0.118	-0.158	-0.096	-0.118	-0.072	-0.082	-0.034
	i_p, μA	877	809	382	786	466	947	562	562	499	459
OSWV	E, V	-0.192	-0.124	-0.168	-0.112	-0.164	-0.092	-0.120	-0.068	-0.084	-0.036
	$w_{1/2}$, mV	124	124	119	182	137	130	122	154	119	131
	i_p, μA	189	526	355	224	297	559	339	256	319	245
E_{cell} (CV)		1.265[1]	1.327[1]	1.316[1]	1.399[1]	1.351[1]	1.424[1]	1.335[1]	1.434[1]	1.371[1]	1.456[1]
E_{cell} (OSWV)		1.264	1.332	1.328	1.404	1.368	1.424	1.352	1.432	1.380	1.452

1. $E_{cell} = E_{1/2} - E_{1/2}$
2. At a Pt-electrode in CH_3CN containing 0.1 M $N^nBu_4PF_6$ electrolyte, referenced to SCE such that $E_{½} = +0.38$ V for $[Cp_2Fe]^{+1/0}$.
3. At a Pt-electrode in CH_2Cl_2 containing 0.5 M $N^nBu_4PF_6$ electrolyte, referenced to SCE such that $E_{½} = +0.48$ V for $[Cp_2Fe]^{+1/0}$.

Table 5.3 Electrochemical data for X-$C_6H_4C_2N_3SCF_3$ thiatriazines at below the indicated concentrations.

X		OCH_3		CH_3		H		Cl		CF_3	
Solvent		CH_3CN[2]	CH_2Cl_2[3]	CH_3CN[2]	CH_2Cl_2[3]	CH_3CN[2]	CH_2Cl_2[3]	CH_3CN[2]	CH_2Cl_2[3]	CH_3CN[2]	CH_2Cl_2[3]
Conc., M		$7.3x10^{-3}$	$1.0x10^{-2}$	$6.3x10^{-3}$	$8.7x10^{-3}$	$1.0x10^{-2}$	$1.1x10^{-2}$	$1.1x10^{-2}$	$9.0x10^{-3}$	$6.7x10^{-3}$	$6.7x10^{-3}$
Scan Rate (mV/s)		100	200	100	200	200	200	200	200	200	200
+1/0											
CV	E_c, V	-	-	-	-	-	-	-	-	-	-
	E_a, V	0.982	1.151	1.045	1.195	1.113	1.218	1.114	1.271	1.213	1.334
	$E_{1/2}$, V	-	-	-	-	-	-	-	-	-	-
	i_p, μA	19	53	16	12	39	19	48	57	60	16
OSWV	E, V	0.924	1.072	0.992	1.120	0.992	1.084	0.976	1.136	1.036	1.216
	$w_{1/2}$, mV	205	174	142	160	262	142	194	142	219	155
	i_p, μA	20	32	15	6	16	8	21	25	24	9
0/-1											
CV	E_c, V	-0.222	-0.159	-0.211	-0.148	-0.192	-0.122	-0.151	-0.107	-0.130	-0.066
	E_a, V	-0.158	-0.089	-0.137	-0.088	-0.124	-0.070	-0.084	-0.035	-0.034	-0.002
	$E_{1/2}$, V	-0.190	-0.124	-0.174	-0.118	-0.158	-0.096	-0.118	-0.072	-0.082	-0.034
	i_p, μA	18	98	22	19	29	34	98	107	126	25
OSWV	E, V	-0.192	-0.124	-0.168	-0.112	-0.164	-0.092	-0.120	-0.068	-0.084	-0.036
	$w_{1/2}$, mV	102	101	113	106	175	95	94	94	112	100
	i_p, μA	71	151	35	22	34	24	94	91	98	30
E_{cell} (CV)		1.140[1]	1.240[1]	1.182[1]	1.283[1]	1.237[1]	1.288[1]	1.198[1]	1.306[1]	1.247[1]	1.336[1]
E_{cell} (OSWV)		1.116	1.196	1.160	1.232	1.156	1.176	1.096	1.204	1.120	1.252

1. $E_{cell} = E_{a1} - E_{a2}$.
2. At a Pt-electrode in CH_3CN containing 0.1 M $N^nBu_4PF_6$ electrolyte, referenced to SCE such that $E_{½}$ = +0.38 V for $[Cp_2Fe]^{+1/0}$.
3. At a Pt-electrode in CH_2Cl_2 containing 0.5 M $N^nBu_4PF_6$ electrolyte, referenced to SCE such that $E_{½}$ = +0.48 V for $[Cp_2Fe]^{+1/0}$.

5.4.1 5-Aryl-3-trichloromethyl-1,2,4,6-thiatriazine radicals **7a-e**

The electrochemical study of these compounds was hindered by the very low solubility of the crystalline radical, especially in CH_3CN. Therefore the concentrations listed in Table 5.1 do not accurately reflect the molarity of analyte in solution, as more radical was added than would usually dissolve in solution.

There were two redox processes noted for each compound. The reduction of the 7π radicals to the 8π anions was in all cases irreversible. The CV of **7c** presented in Figure 5.6 is typical of the results obtained for this series.

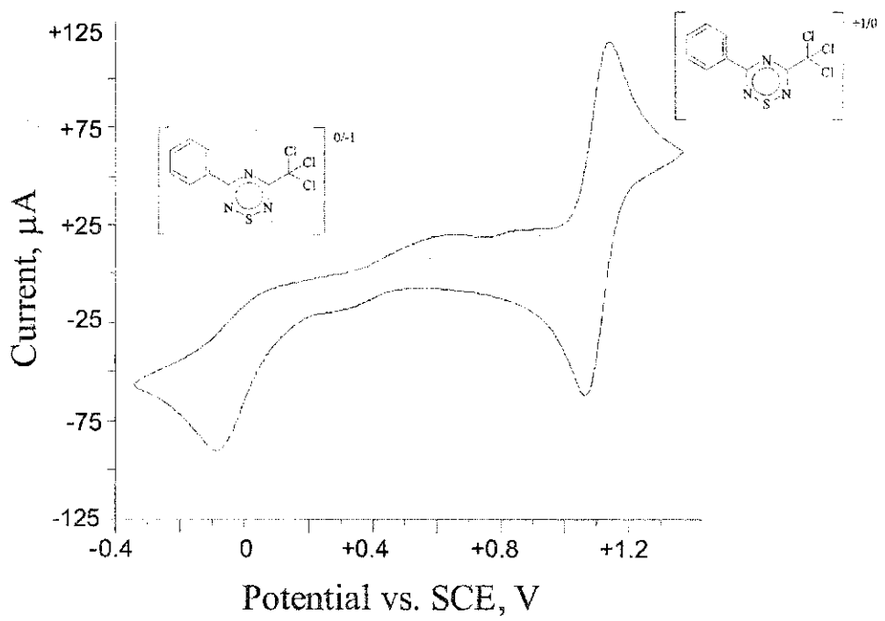

Figure 5.6 CV of a saturated solution of **7c** in CH_3CN solution (0.1 M $N^nBu_4PF_6$).

Faster scan rates generally did not seem to improve the reversibility of the 0/–1 process, except in the case of **7e**, which at normal scan rates (~100 – 200mVs^{-1}) resembles the typical response similar to Figure 5.6. When the scan rates were increased

to 1000 -- 5000 mVs^{-1} both the 0/–1 and the +1/0 processes of **7e** became reversible, as shown in Figure 5.7.

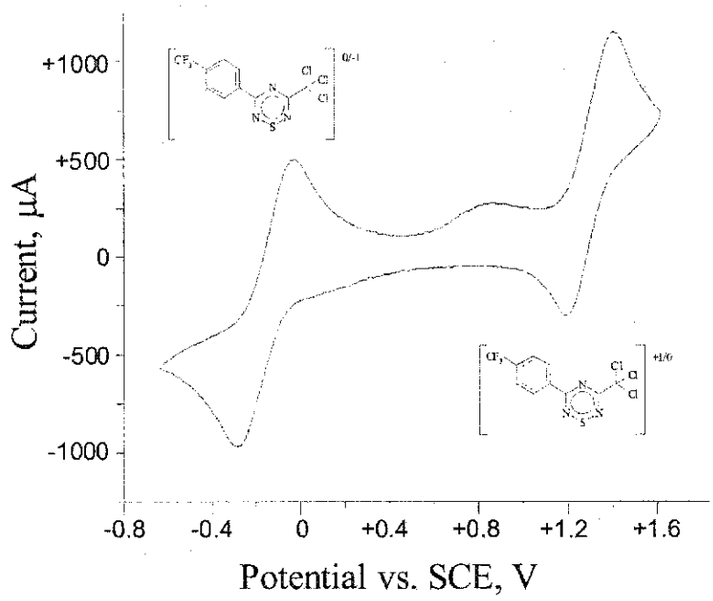

Figure 5.7 CV of a saturated solution of **7e** in CH_2Cl_2 (0.5 M $N^nBu_4PF_6$) at a scan rate of 5120mVs^{-1}.

The oxidation of the 7π radical to the 6π cation was reversible in CH_3CN in all cases except **7b**, and reversible in CH_2Cl_2 in all cases except **7a** and **7d**. Running the CV's at faster scan rates failed in all cases to give reversible waves. The OSWV data showed similar results in all cases, with a small wider peak for the 0/–1 process (representing an irreversible process) and a tall sharp peak for the +1/0 process. A typical OSWV trace is shown in Figure 5.8.

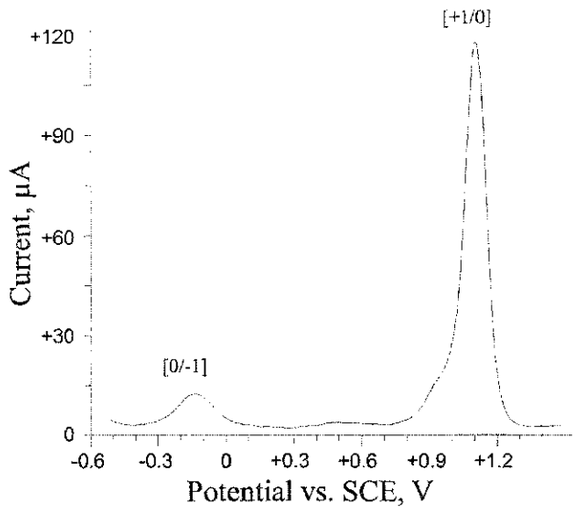

Figure 5.8 OSWV diagram of **7c**.

From the wealth of electrochemical data I have distilled the key potentials and the E_{cell} values in Table 5.4. Note that for the 0/–1 process the potentials are cathodic peak values. In most cases for the +1/0 processes $E_{1/2}$ values are listed. This explains why the differences between the two processes are not always equivalent to the E_{cell} values. For example, the E_{cell} value for **7a** in CH_3CN solution is 1.212 V, which is obtained by the difference between the E_c's of 0.969 V for the +1/0 process and –0.243 V for the 0/–1 process.

The potential ranges for the reduction of **7a-e** are from –0.243 to +0.017 V vs. SCE in CH_3CN and –0.326 to –0.120 V vs. SCE in CH_2Cl_2. The potential ranges for oxidation are from 1.007 to 1.192 V vs. SCE in CH_3CN and 1.186 to 1.356 V vs. SCE in CH_2Cl_2. The range of potentials for reduction have an overall change of 0.260 V (in CH_3CN) and 0.206 V (in CH_2Cl_2) for the 0/–1 process, and of 0.185 V (in CH_3CN) and 0.170 V (in CH_2Cl_2) for the +1/0 process. This ability of the substituents to alter the

Table 5.4. Voltammetric data for compounds **7a-e**.

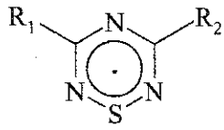

Compound	R_1 =	R_2 =	+1/0 $E_{1/2}$ / V	0/-1 E / V	E_{cell} / V
CH_3CN Solution					
7a	4-$CH_3OC_6H_4$	CCl_3	1.007	–0.243[2]	1.212[3]
7b	4-$CH_3C_6H_4$	CCl_3	1.035[1]	–0.159[2]	[1.194[4]]
7c	C_6H_5	CCl_3	1.104	–0.138[2]	1.208[3]
7d	4-ClC_6H_4	CCl_3	1.146	–0.063[2]	1.172[3]
7e	4-$CF_3C_6H_4$	CCl_3	1.192	0.017[2]	1.144[3]
		Δ	0.185	0.260	0.068
CH_2Cl_2 Solution					
7a	4-$CH_3OC_6H_4$	CCl_3	1.186[1]	–0.326[2]	[1.512[4]]
7b	4-$CH_3C_6H_4$	CCl_3	1.231	–0.283[2]	1.458[3]
7c	C_6H_5	CCl_3	1.254	–0.185[2]	1.424[3]
7d	4-ClC_6H_4	CCl_3	1.284[1]	–0.150[2]	[1.434[4]]
7e	4-$CF_3C_6H_4$	CCl_3	1.356	–0.120[5]	1.430[3]
		Δ	0.170	0.206	0.088

1. Irreversible behaviour, E_a given.
2. Irreversible behaviour, E_c given.
3. $E_{cell} = E_c$ oxid – E_c red.
4. $E_{cell} = E_a$ oxid – E_c red.

redox potentials I have referred to previously as the 'tunability' of the redox-active heterocycle. This tunability is markedly larger than that reported for the 1,2,3,5-dithiadiazoles, substituted with the exact same substituent as **7a-e**, where tunability is only ~0.1V for both the 0/–1 and +1/0 processes. The thiatriazine ring system can therefore be tuned between 1.5 – 3 times more effectively by remote substituents.

The E_{cell} values for **7a-e** (i.e. the potential range over which the ring is stable as a 7π species) show considerable scatter. For **7** the average E_{cell} is 1.19 ± 0.03 V in CH_3CN and 1.44 ± 0.01 V in CH_2Cl_2. The larger E_{cell} in CH_2Cl_2 is a consequence of both higher oxidation and lower reduction potentials. In contrast to the 1,2,3,5-dithiadiazoles, which

portrayed fully reversible 0/–1 and the +1/0 processes[2], **7a-e** gave only reversible +1/0 waves and irreversible 0/–1 waves. However, **7e** becomes reversibile in both processes at higher scan rates in CH_2Cl_2. This suggests that all of these compounds may exhibit reversibility at fast enough scan rates. As well, the E_{cell} value obtained from the fast scan of **7e** was 1.47 V, very similar to its E_{cell} value at lower scan rates, and very close to the average E_{cell} for all five compounds. This result serves to confirm the validity of the E_{cell} values for **7a-e** despite the difficulties with reversibility at normal scan rates.

5.4.2 5-Aryl-3-trifluoromethyl-1,2,4,6-thiatriazine radicals **8a-e**

This series was more soluble in both solvents (CH_3CN and CH_2Cl_2), which allowed us to gain information about these compounds at higher concentrations than with **7a-e**. They also seemed to behave more consistently in solution and displayed more predictable patterns. At very low concentration (which was evidenced by a pale yellow color in solution) the CV has a reversible reduction process and an irreversible oxidation process. This is exactly the opposite of the **7a-e** series, the reasons for which are not clear. As the concentration increased (evidenced by a darker brown solution) a second oxidation process appeared at a more positive potential and this second process was reversible under all the conditions used in this study. In Figure 5.9, I show overlapping traces at three different concentrations of **8e**. At the lowest concentration, a small irreversible oxidation wave appears. At intermediate concentration, this peak is present at approximately the same height, but a second quasi-reversible process grows in. At the highest concentration, the first process is just a residual shoulder on the reversible wave at higher potential. I attribute the electrochemical response at low concentration to be that of a monomeric thiatriazine radical, and at higher concentration to be that of the

dimer, with monomer and dimer in equilibrium. Such an equilibrium has been witnessed previously for **10**.[2] Much the same thing occurred for all five compounds. In each case however, there was only a single, reversible, reduction process at all concentrations studied. Therefore the assumption was made that at higher concentrations the reduction process for both the monomer and dimer occur at approximately the same potentials (they overlap one another).

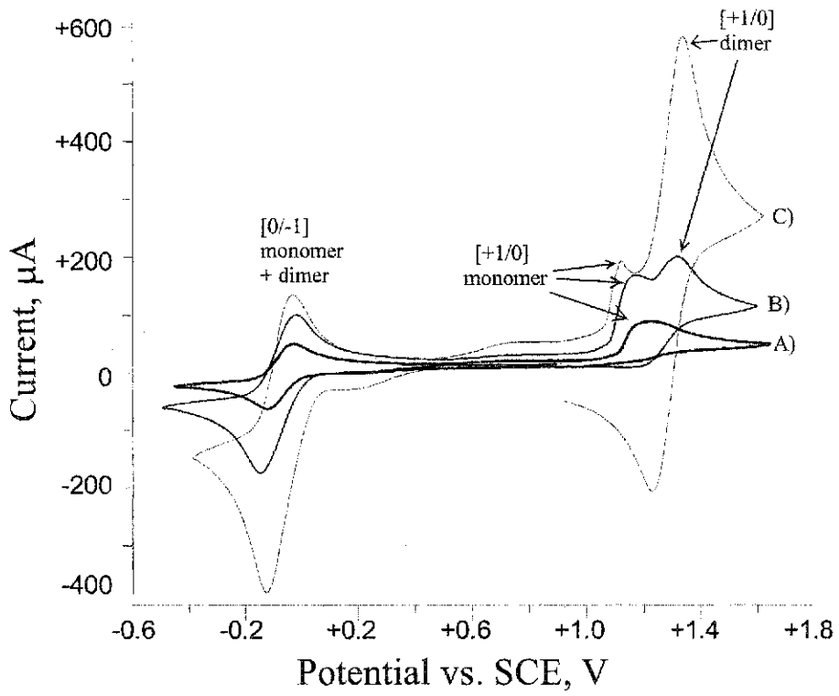

Figure 5.9 Overlapping CV's of the oxidation and reduction potentials of **8e** in CH_3CN solution (0.5M $N^nBu_4PF_6$) at A) dilute concentration, B) moderate concentration, and C) high concentration.

The Osteryoung method is particularly suited to low concentrations of analyte. Indeed, as shown in Figure 5.10, both redox processes are clearly visible at very dilute concentration. The distortion of the peak shape for the +1/0 process, as well as its lower height, indicates the irreversible redox process. Increasing the concentration produced

changes in the OSWV traces comparable to those observed by CV. In Figure 5.11, which corresponds to trace C) in Figure 5.9, the monomer +1/0 process appears as a shoulder to the sharp, reversible peak for the dimer +1/0 process.

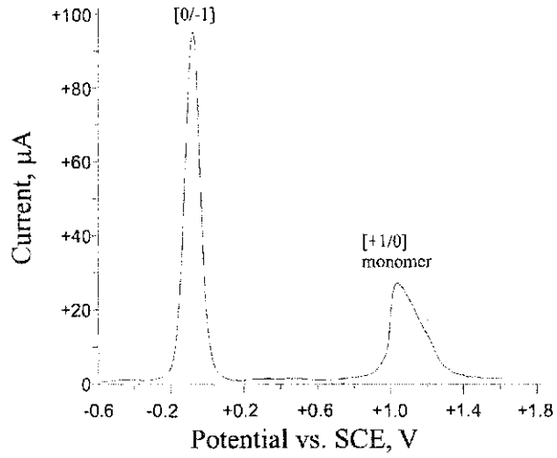

Figure 5.10 OSWV of **8e** in CH_3CN solution (0.5M $N^nBu_4PF_6$) at dilute concentration, corresponding to trace A) in Figure 5.9.

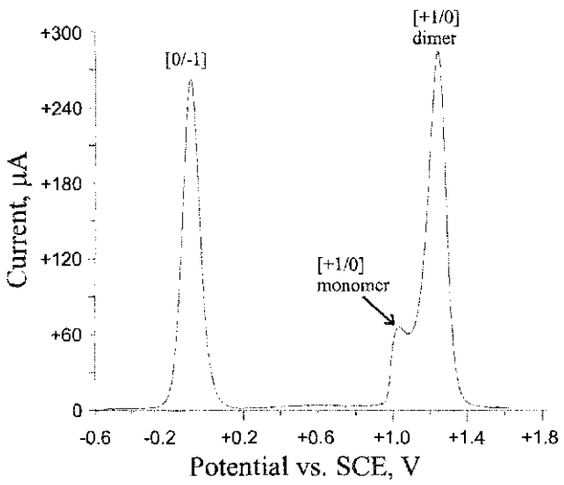

Figure 5.11 OSWV of **8e** in CH_3CN solution (0.5M $N^nBu_4PF_6$) at higher concentration (6.7×10^{-3} M), corresponding to trace C) in Figure 5.9.

In view of the distinct difference in behavior at low concentration (presumed monomer) and high concentration (presumed dimer), I have separated the electrochemical data into two sets of tables. Summarized voltammetric data ascribed to monomer and dimer are presented in Tables 5.5 and 5.6 respectively. The potential ranges for the reduction of **8a-e** at low concentrations are from –0.202 to –0.078 V vs. SCE in CH_3CN and –0.135 to –0.028 V vs. SCE in CH_2Cl_2. The range of potentials for oxidation are from 0.970 to 1.218 V vs. SCE in CH_3CN and 1.140 to 1.308 V vs. SCE in CH_2Cl_2. These have an overall change of 0.248 V (in CH_3CN) and 0.168 V (in CH_2Cl_2). The range of potentials for reduction have an overall change of 0.124 V (in CH_3CN) and 0.107 V (in CH_2Cl_2) for the 0/–1 process. These ranges are of similar magnitude to those

Table 5.5 Voltammetric data for compounds **8a-e** at low concentration.

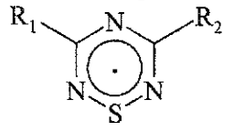

Compound	R_1 =	R_2 =	+1/0 E / V	0/–1 $E_{1/2}$ / V	E_{cell} / V
CH_3CN Solution					
8a	4-$CH_3OC_6H_4$	CF_3	+0.970[1]	–0.202	1.140
8b	4-$CH_3C_6H_4$	CF_3	+1.047[1]	–0.172	1.182
8c	C_6H_5	CF_3	+1.113[1]	–0.158	1.237
8d	4-ClC_6H_4	CF_3	+1.114[1]	–0.118	1.198
8e	4-$CF_3C_6H_4$	CF_3	+1.218[1]	–0.078	1.247
		Δ	0.248	0.124	0.107
CH_2Cl_2 Solution					
8a	4-$CH_3OC_6H_4$	CF_3	+1.140[1]	–0.135	1.240
8b	4-$CH_3C_6H_4$	CF_3	+1.191[1]	–0.112	1.283
8c	C_6H_5	CF_3	+1.213[1]	–0.102	1.288
8d	4-ClC_6H_4	CF_3	+1.271[1]	–0.072	1.306
8e	4-$CF_3C_6H_4$	CF_3	+1.308[1]	–0.028	1.336
		Δ	0.168	0.107	0.096

1. Irreversible behaviour, E_a given.

found for **7a-e**, but note that the larger ranges apply for both series of compounds to the irreversible redox processes.

The E_{cell} values for monomeric **8a-e** are less independent of substituent type than was seen for **7a-e**, and this is reflected in larger error limits for the average values. For **8a-e** the average E_{cell} is 1.20 ± 0.04 V in CH_3CN and 1.29 ± 0.04 V in CH_2Cl_2. The value in CH_3CN is indistinguishable from that of **7a-e**, but the value in CH_2Cl_2 is noticeably smaller. The reduction potentials are distinctly less negative in CH_2Cl_2 than in CH_3CN, as well as less negative than the corresponding values in CH_2Cl_2 for **7a-e**. Overall the 0/–1 process appears to be less affected by substituent type for **8a-e** rather than **7a-e**.

Table 5.6 Voltammetric data for compounds **8a-e** at high concentration.

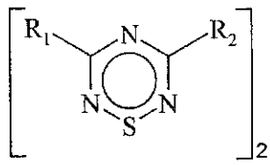

Compound	R_1 =	R_2 =	+1/0 $E_{1/2}$ / V	0/–1 $E_{1/2}$ / V	E_{cell} / V
CH_3CN Solution					
8a	4-$CH_3OC_6H_4$	CF_3	+1.075	–0.190	1.265
8b	4-$CH_3C_6H_4$	CF_3	+1.142	–0.174	1.316
8c	C_6H_5	CF_3	+1.193	–0.158	1.351
8d	4-ClC_6H_4	CF_3	+1.217	–0.118	1.335
8e	4-$CF_3C_6H_4$	CF_3	+1.289	–0.082	1.371
		Δ	0.214	0.108	0.106
CH_2Cl_2 Solution					
8a	4-$CH_3OC_6H_4$	CF_3	+1.203	–0.124	1.327
8b	4-$CH_3C_6H_4$	CF_3	+1.281	–0.118	1.399
8c	C_6H_5	CF_3	+1.328	–0.096	1.424
8d	4-ClC_6H_4	CF_3	+1.362	–0.072	1.434
8e	4-$CF_3C_6H_4$	CF_3	+1.422	–0.034	1.456
		Δ	0.219	0.090	0.129

The potential ranges for the reduction of **8a-e** at high concentrations are from – 0.190 to – 0.082 V vs. SCE in CH_3CN and – 0.124 to – 0.034 V vs. SCE in CH_2Cl_2. The range of potentials for oxidation are from 1.075 to 1.289 V vs. SCE in CH_3CN and 1.203 to 1.422 V vs. SCE in CH_2Cl_2. These have an overall change of 0.214 V (in CH_3CN) and 0.219 V (in CH_2Cl_2). The range of potentials for reduction have an overall change of 0.108 V (in CH_3CN) and 0.090 V (in CH_2Cl_2) for the 0/–1 process. The E_{cell} values for dimeric **8a-e** are even less independent of substituent type than was seen for monomeric **8a-e**. This can be attributed to the small effect of substituents on the 0/–1 process, especially in CH_2Cl_2 solution. The average values are 1.33 ± 0.04 V in CH_3CN and 1.41 ± 0.05 V in CH_2Cl_2. Especially in the latter solvent I find the important result that the E_{cell} value increases (by 0.13 V) from the most donating to the most withdrawing substituent.

For a monomeric neutral thiatriazine radical, the redox process is assumed to involve removal from, or addition to the π-SOMO (Figure 4.4), and can be represented as:

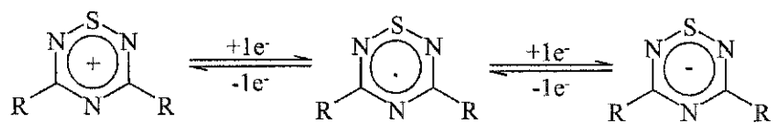

Since the same redox orbital is involved in the electrochemical oxidation and reduction reactions, one expects the substituents R to influence both redox processes by the same amount, so long as the influence is purely inductive. Exactly this has been observed in electrochemical investigations of more than twenty 1,2,3,5-dithiadiazoles.[9,2] However, unlike the dithiadiazole, the redox orbital of the thiatriazine (the SOMO, Figure 4.4) does not have a node at the substituent-bearing carbon atoms. It is to be expected, therefore,

that resonance effects can have a significant influence. These are expected to affect the oxidation and reduction processes differently. For example, if a methoxy group donates an electron pair to the phenyl ring, negative charge is placed in close proximity to the thiatriazine ring.

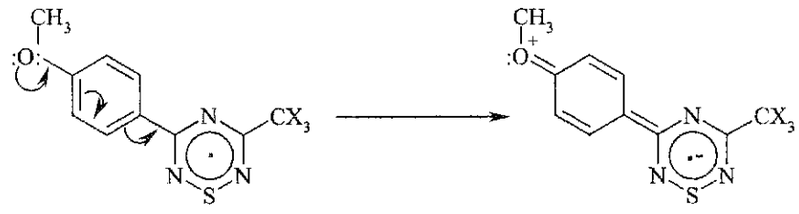

Now the formation of a cation or an anion at the ring is expected to have different energetic consequences.

Another factor that cannot be discounted is the effect of dimer formation on the redox processes. In a dimeric thiatriazine the redox process can be represented as:

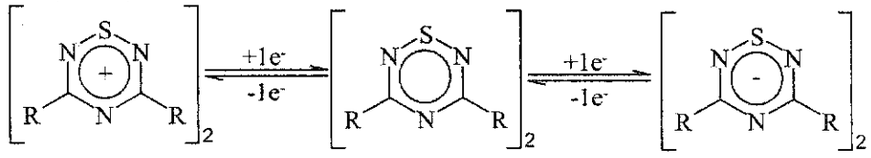

It has been shown that the formation of thiatriazine dimers is the result of diffuse side-on overlap of the π-orbitals of the individual thiatriazine rings[12]. Analysis of a semi-empirical MO calculation indicates that the only net "bonding" interaction results from the in-phase and out-of-phase combination of the SOMO π_4 (Figure 5.12). The dimer is a diamagnetic species and hence oxidation occurs from a different orbital (the in-phase combination) than reduction (the out-of-phase combination). It is therefore to be expected that the substituents influence these distinct orbitals by different amounts. The

'drift' in E_{cell} values could therefore also be a consequence of a redox process operating on a dimeric molecule.

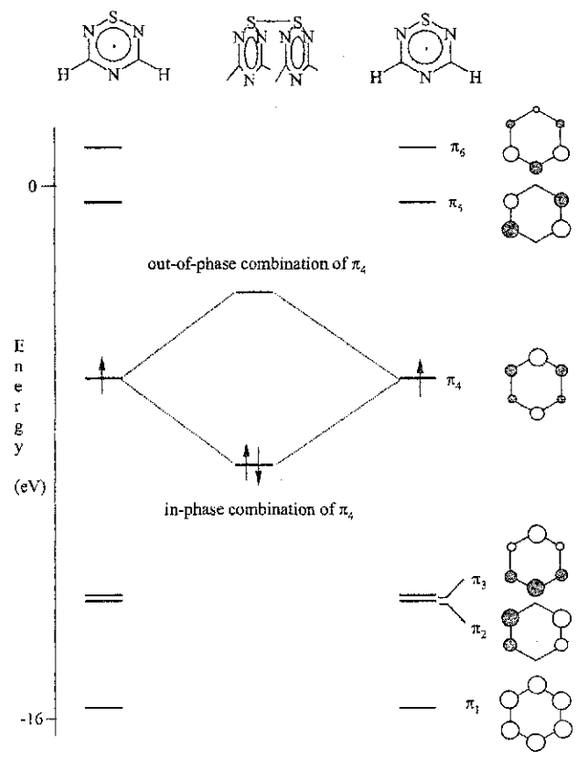

Figure 5.12 Schematic MO diagram for thiatriazine dimer formation.

5.4.3 Correlation of redox potentials with gas phase calculations

It is always desirable to look for additional confirmation of experimental results. The electrochemistry described in this thesis was particularly difficult (compounds were difficult to prepare, highly reactive, some were very insoluble, while the soluble species gave rise to predominately dimeric species in solution). Previous studies have shown that quantum calculations, when judiciously used, can provide corroboration of electrochemical results.[2]

Fully geometry optimized calculations at the B3LYP/6–31G(d) level of theory were performed for the monomeric cation, anion, and neutral thiatriazine derivatives. No attempt was made to model the weakly bound dimeric molecules. The energies of these optimized molecules were then used to define the theoretical redox reactions:

$$+1/0 \text{ process: } E_{cation} - E_{radical} = E_{oxidation} \qquad [5.3]$$

$$0/-1 \text{ process: } E_{anion} - E_{radical} = E_{reduction} \qquad [5.4]$$

For example, the +1/0 process of **7a** was calculated as follows:

$$-65394.298 - (-65401.437) = +7.140\ eV$$

Tables 5.7 and 5.8 list all the calculated energies for **7a-e** and **8a-e** respectively. I have chosen the most reliable experimental data for comparison, which are from CV and are $E_{1/2}$ values except where noted. Cathodic peak potentials are given for the 0/–1 process in Table 5.7 and anodic peak potentials are given for the +1/0 process in Table 5.8.

Table 5.7 Calculated and experimental redox potentials of **7a-e**.

Compound	+1/0 Calculated	+1/0 $E_{1/2}$ / V	0/–1 Calculated	0/–1 E / V
CH_3CN Solution				
7a	7.140	1.007	–2.040	–0.243[2]
7b	7.337	1.035[1]	–2.105	–0.159[2]
7c	7.477	1.104	–2.133	–0.138[2]
7d	7.550	1.146	–2.306	–0.063[2]
7e	7.718	1.192	–2.403	0.017[2]
Δ	0.578	0.185	0.363	0.226
CH_2Cl_2 Solution				
7a	7.140	1.186[1]	–2.040	–0.326[2]
7b	7.337	1.231	–2.105	–0.283[2]
7c	7.477	1.254	–2.133	–0.185[2]
7d	7.550	1.284[1]	–2.306	–0.150[2]
7e	7.718	1.356	–2.403	–0.120[5]
Δ	0.578	0.170	0.363	0.206

1. Irreversible behavior, E_a given.
2. Irreversible behavior, E_c given.

Correlation curves are presented for **7a-e** in Figures 5.13 and 5.14, and for **8a-e** in Figures 5.15 – 5.17. The results are graphed by process type and each graph includes results for both solvents.

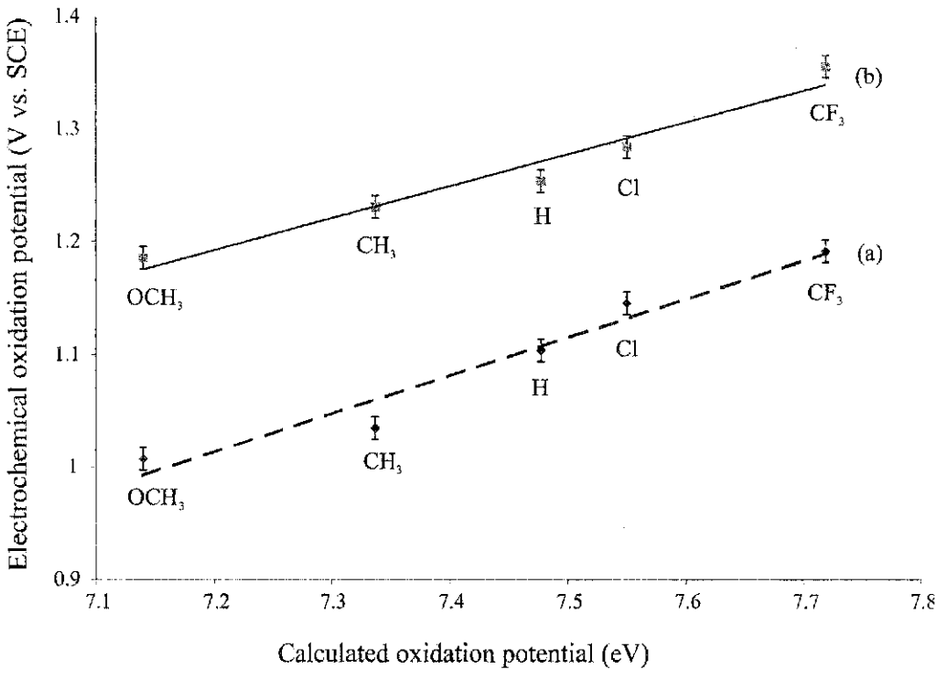

Figure 5.13 Plot of the calculated vs. experimental oxidation potential of **7a-e** as measured by cyclic voltammetry in (a) CH_3CN and (b) CH_2Cl_2 solution.

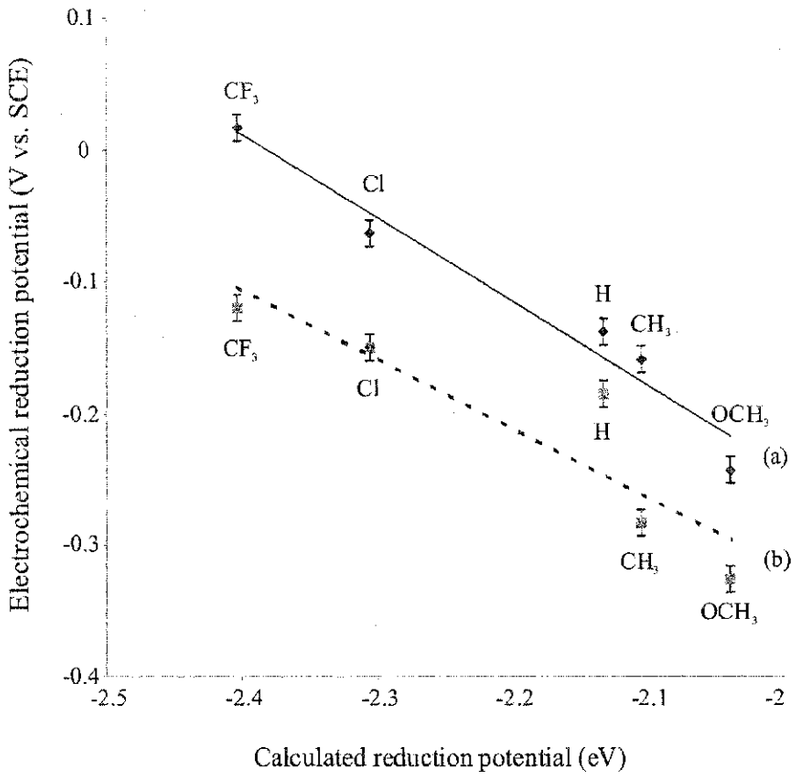

Figure 5.14 Plot of the calculated vs. experimental reduction potential of **7a-e** as measured by cyclic voltammetry in (a) CH_3CN and (b) CH_2Cl_2 solution.

Excellent correlation was obtained between the gas phase oxidation potentials and the solution phase oxidation potentials in both solvent systems for **7a-e**. Correlation between the gas phase and solution phase reduction potentials are not as good as the oxidation potentials, possibly reflecting difficulty in measurements taken from the irreversible electrochemical process. The agreement for **7c** in CH_2Cl_2 is particularly poor, the origin of which could not be determined from careful reconsideration of the data.

Table 5.8 Calculated and experimental redox potentials of **8a-e** for the monomeric radical.

Compound	+1/0 Calculated	+1/0 E / V	0/–1 Calculated	0/–1 $E_{1/2}$ / V
CH_3CN Solution				
8a	7.203	+0.970[1]	–1.917	–0.202
8b	7.419	+1.047[1]	–1.973	–0.172
8c	7.565	+1.113[1]	–2.018	–0.158
8d	7.635	+1.114[1]	–2.197	–0.118
8e	7.812	+1.218[1]	–2.271	–0.078
Δ	0.609	0.248	0.354	0.124
CH_2Cl_2 Solution				
8a	7.203	+1.140[1]	–1.917	–0.135
8b	7.419	+1.191[1]	–1.973	–0.112
8c	7.565	+1.213[1]	–2.018	–0.102
8d	7.635	+1.271[1]	–2.197	–0.072
8e	7.812	+1.308[1]	–2.271	–0.028
Δ	0.609	0.168	0.354	0.107

1. Irreversible behaviour, E_a given.

Correlation of the gas phase redox potentials with the solvent phase redox potentials of the monomeric radicals **8a-e** was also excellent. It seemed appropriate to correlate only data from presumed monomeric radicals of **8a-e** with the calculated results. In fact, equally good correlations were obtained using the dimeric data. Figure 5.15 is noteworthy because for **8a-e** at low concentrations this was an irreversible process. Nevertheless, good correlation between calculated and experimental values is obtained.

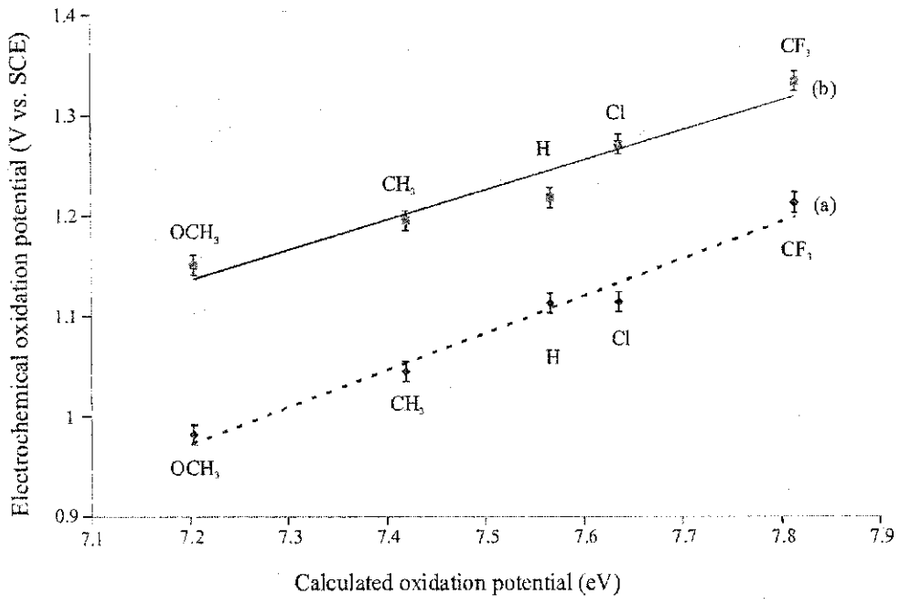

Figure 5.15 Plot of the calculated vs. experimental oxidation potential of **8a-e** as measured by cyclic voltammetry in (a) CH_3CN and (b) CH_2Cl_2 solution.

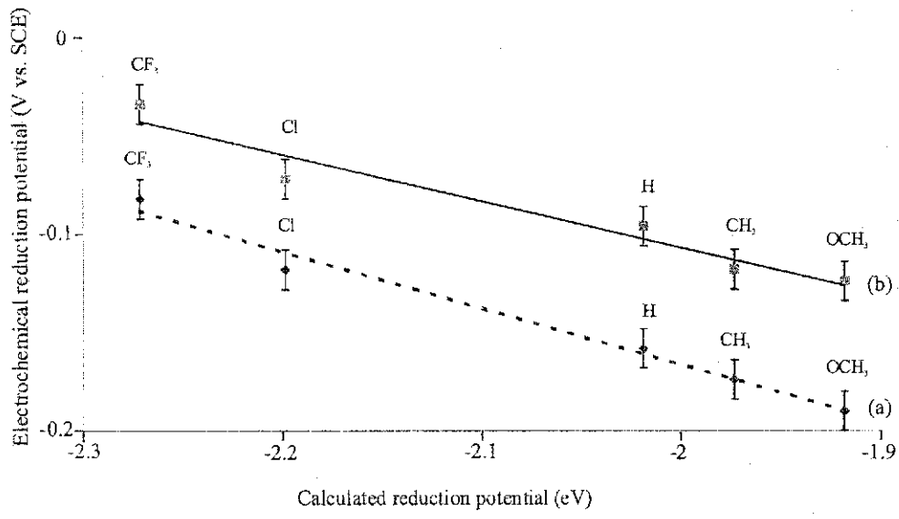

Figure 5.16 Plot of the calculated vs. experimental reduction potential of **8a-e** as measured by cyclic voltammetry in (a) CH_3CN and (b) CH_2Cl_2 solution.

I consider this to be an important confirmation of the reliability of the electrochemical data for this series obtained from CV. It is possible that the free solubility of **8a-e** in both

solvents was a factor in the reliability of these measurements. Good correlation is also obtained for the reduction process in Figure 5.16.

All the redox potentials obtained from Osteryoung squarewave voltammetry were also correlated against the calculated values. I discovered that, in all cases when an irreversible process was present, the correlation of the Osteryoung data was extremely poor. For example, the +1/0 process of **8a-e** is irreversible at low concentration and Figure 5.17 graphs the results for this process. The results are much poorer than from the CV data as graphed in Figure 5.15 (CH_3CN solution: regression coefficient is 0.94 for CV vs. 0.69 for OSWV; CH_2Cl_2 solution: 0.96 for CV vs. 0.79 for OSWV). For fully reversible processes such as 0/–1 of **8a-e**, the Osteryoung data seemed to correlate just as well as the CV data.

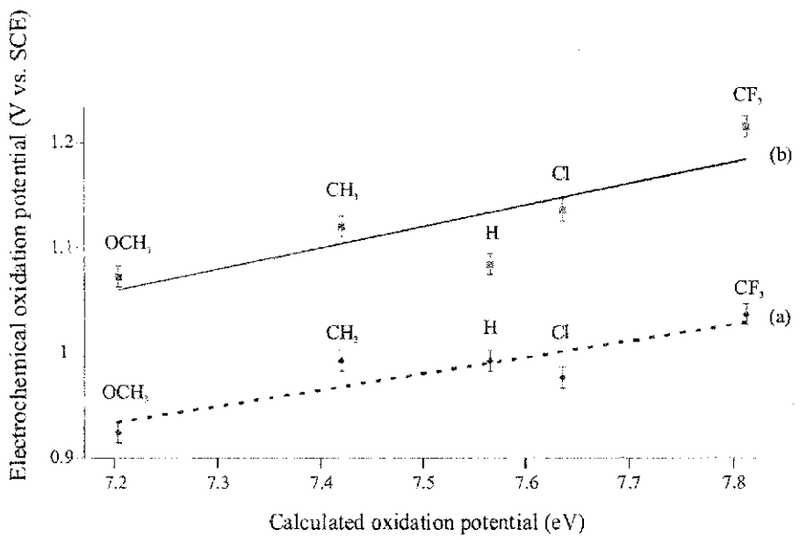

Figure 5.17 Plot of the calculated vs. experimental oxidation potential of **8a-e** as measured by Osteryoung squarewave voltammetry in (a) CH_3CN and (b) CH_2Cl_2 solution.

The statistical results simply confirm the difficulties I experienced in extracting reliable potential data from OSWV experiments whenever an irreversible process was encountered. Therefore the OSWV method is good at following the electrochemical process (especially at very low concentrations), but CV is far superior for the determination of reliable voltammetric data.

5.4.4 Error limits for the voltammetric data.

The BAS software reports potentials to the nearest mV. I have retained this level of precision in the data tables. However, I have also examined the reproducibility of the potential values from many repetitive CV experiments, and from this I am quite certain that the precision of the measurements reported in this thesis are not much better than ± 10 mV, i.e., to the nearest 0.01 V. The error bars in Figures 5.13 – 5.17 are set to ± 0.01 V. Consideration of Figure 5.16, one of the best correlations that I have obtained between experiment and calculation, provides strong support that ± 0.01 V is a judicious choice of the error limit.

5.5 Conclusions

To my knowledge this is the first application of the OSWV method to the study of redox-active heterocycles. While OSWV is useful due to the high signal-to-noise at low analyte concentrations, it is terrible at measuring potentials for all but fully reversible processes in solution. CV is far superior for irreversible processes, as well as giving excellent data for reversible processes.

The cell potentials of thiatriazine radicals are smaller than that of the equally substituted 1,2,3,5-dithiadiazoles, but still considerably larger than more recently

discovered bifunctional radicals. Because of the complexity of the monomer-dimer equilibrium, I cannot be totally certain what the E_{cell} values of truly monomeric thiatriazine rings are. From the low concentration measurements on **8a-e**, values as low as 1.2 V in CH_3CN and 1.3 V in CH_2Cl_2 were determined. The dimers appear to have slightly higher E_{cell} values of 1.3 V in CH_3CN and 1.4 V in CH_2Cl_2. These values are noticeably smaller than those reported previously for 1,2,3,5-dithiadiazoles (1.4 V in CH_3CN and 1.6 V in CH_2Cl_2). Perhaps more importantly, the thiatriazine E_{cell} values are ten times more tunable than an equivalently substituted set of dithiadiazoles.[8] The E_{cell} values become smaller with more strongly electron donating substituents. This comparison is based on thiatriazines bearing only one varying substituent. This was a deliberate choice to allow for comparison with dithiadiazoles, which can only bear a single substituent. It is to be expected, however, that doubly substituting a thiatriazine would lead to an even greater tunability of the E_{cell} values.

5.6 Thesis conclusions and future prospects

1,2,4,6-thiatriazine radicals are considered to be neutral radical conductors in the context of molecular metal design. After initial investigations they were largely ignored in favor of other prospective ring systems. A more general route to 1,2,4,6-thiatriazine radicals has been reported in this thesis.

Two crystal structures were obtained for the radicals 5-phenyl-3-trichloromethyl-1,2,4,6-thiatriazine **7c** and 5-phenyl-3-trifluoromethyl-1,2,4,6-thiatriazine **8c**. **7c** displayed a unique head-to-tail packing arrangement not seen in previous thiatriazine structures. As well, two crystal structures of the precursor phenyl/trichloro imidoylamidine **1c** and phenyl/trifluoromethyl imidoylamidine **2c** have been reported.

These are novel structures and show strong intramolecular hydrogen bonding and relatively weak intermolecular hydrogen bonding.

EPR of the 1,2,4,6-thiatriazine radicals are highly diagnostic and display coupling to three unique nitrogen atoms. The nitrogen coupling shows a definite trend as the remote aryl substituents move from electron donating to electron witdrawing. DFT calculations of the hyperfine coupling constants and the oxidation and reduction potentials corroborated well with experimental data.

Solution electrochemistry measurements assessed the redox tunability of the radicals to remote aryl substituents, which found them to be more tunable than the equally substituted dithiadiazoles. Potentially, if synthetic routes can be found, doubly substituted selenatriazines with electron donating substituents could achieve E_{cell} values of 1 V or less. Similarly, fused thiatriazine rings could also lower E_{cell} values considerably. This would be a significant achievement in the design of redox-active heterocycles as potential molecular metals.

This thesis has also encountered the major potential downside to the use of thiatriazines in molecular metal design, which is the strong tendency to form localized dimers. This may be a major impediment to obtaining an infinite conduction band in a thiatriazine containing solid. Significant efforts will be required to crystal engineer thiatriazines with appropriate substituents in order to maximize inter-stack contacts which play a major role in overcoming Peierls distortion. The inter-dimer contacts observed in the crystal structure of **8c** (Section 3.5) provide hope that this can someday be realized.

References

1. Harris, D. C. *Quantitative Chemical Analysis*; W.H. Freeman and Company: New York, 1995.

2. Boeré, R. T.; Roemmele, T. L. *Coord. Chem. Rev.* **2000**, *210*, 369.

3. Day Jr, M. C.; Selbin, J. *Theoretical Inorganic Chemistry*; Van Nostrand Reinhold: New York, 1969.

4. Pietrzyk, D. J. *Anal. Chem.* **1974**, *46*, R52.

5. Heinze, J. *Angew. Chem. Int. Ed. Engl.* **1984**, *23*, 831.

6. Osteryoung, J. *Acc. Chem. Res.* **1993**, *26*, 77.

7. Skoog, D. A.; West, D. M.; Holler, F. J. *Fundamentals of Analytical Chemistry*; 6th ed.; Saunders College Publishing: Orlando, 1992; p 500.

8. Boeré, R. T.; Moock, K. H. *J. Am. Chem. Soc.* **1995**, *117*, 4755.

9. Boeré, R. T.; Moock, K. H.; Parvez, M. *Z. Anorg. Allg. Chem.* **1994**, *620*, 1589.

10. Barriere, F.; Camire, N.; Geiger, W. E.; Mueller-Westerhoff, U. T.; Sanders, R. *J. Am. Chem. Soc.* **2002**, *124*, 7262.

11. Banister, A. J.; Hauptman, Z. V.; Kendrick, A. G.; Small, R. W. H. *J. Chem. Soc., Dalton Trans.* **1987**, 915.

12. Boeré, R. T.; Cordes, A. W.; Hayes, P. J.; Oakley, R. T.; Reed, R. W.; Pennington, W. T. *Inorg. Chem.* **1986**, *25*, 2445.

Chapter 6

Experimental Details

6.1 Introduction

A review of all synthetic chemical work completed and previously discussed in this thesis, along with all crystallographic data will be presented here in its entirety. The majority of reagents used were obtained from commercial sources (Aldrich, Fisher, EM Science). Trichloroacetonitrile was obtained commercially and kept under refrigeration prior to use. Trifluoroacetonitrile (PCR Inc.) was obtained commercially and used as received. SCl_2 was distilled from PCl_3 with $CaCl_2$ moisture protection. Triphenylantimony and HCl(g) (Praxair) were obtained commercially and used as received. Benzamidine was liberated from benzamidine hydrochloride hydrate by treatment with 1.7M potassium hydroxide and extraction into dichloromethane and was sublimed in vacuo prior to use. *Para*-substituted phenyl amidines were prepared according to literature methods[1].

Unless otherwise indicated, all procedures were performed under an atmosphere of purified N_2 using a drybox, Schlenkware, and vacuum-line techniques. Solvents used were reagent-grade or better. Acetonitrile (HPLC grade) was double-distilled from P_2O_5 and CaH_2. Dichloromethane was distilled from CaH_2. N-heptane was dried by distillation over $LiAlH_4$. Anhydrous ether was dried by distillation from sodium wire.

Infrared spectra were obtained as KBr plates and were recorded on a Bomem MB102 Fourier transform spectrometer. Melting points were determined on an Electrothermal melting point apparatus and are uncorrected. ESR spectra (X band) were recorded on a Bruker EMX10 spectrometer as solutions in dichloromethane in 4mm

Pyrex glass tubes sealed under vacuum. NMR spectra were acquired at 250.13 (^{1}H) and 62.90 (^{13}C) MHz on a Bruker Tecmag AC250 spectrometer using $CDCl_3$ as the solvent and thus as reference. Mass spectra were recorded by the Mass Spectrometry Center, University of Alberta, Edmonton. Microanalyses were performed by M-H-W Laboratories in Phoenix, AZ.

Some of the characterization data has been placed elsewhere in the thesis. NMR coupling constants of compounds **1a-e**, **2a-e**, **5a-e**, and **6a-e** are discussed in Chapter 2, along with elemental analysis and mass spectral data of **1a-e**, **2a-e**, **7a-e**, and **8a-e**.

6.2 Synthesis of the trichloromethyl imidoylamidines **1a-e**

(i) $C_6H_5C_3N_3H_3Cl_3$ **1c** . Trichloroacetonitrile (1.24g, 8.6mmol) was added dropwise at 15-20°C to benzamidine **9c** (1.02g, 8.5mmol) in 7mL dried acetonitrile. The mixture was heated at reflux for 1.5 hours, then cooled and rotary evaporated to leave a faintly purple solid. All remaining liquids were vacuum filtered off to leave 2.15g of solid product (8.1mmol, 96% yield); mp 68-69°C; ^{1}H NMR (δ, $CDCl_3$): 6.6 (s, NH), 7.4-7.6 (m, 3H, phenyl), 7.9-8.0 (m, 2H, phenyl), 9.4 (s, NH), 10.7 (s, NH); ^{13}C NMR (δ, $CDCl_3$): 98.0, 127.6, 129.0, 132.1, 135.5, 164.7, 168.2; IR 3320 (s), 3284 (s), 3135 (m), 1629 (vs), 1589 (s), 1573 (s), 1508 (s), 1482 (s), 1444 (s), 1326 (s), 1298 (sh), 1180 (sh), 1161 (m), 1073 (w), 1038 (m), 1001 (w), 973 (w), 928 (m), 844 (m), 821 (s), 805 (sh), 780 (m), 765 (m), 713 (s), 694 (s), 651 (m), 575 (m), 615 (w), 521 (w), 454 (w), 420 (w) cm^{-1}; mass spectrum (*m/e*) 262 ($PhC_2N_3H_2CCl_3^+$, 58%), 201 ($PhC_2N_2H_2Cl_2^+$, 2%), 146 ($PhC_2N_3H_3^+$, 99%), 129 ($PhC_2N_2^+$, 6%), 104 ($PhCNH^+$, 100%). Analysis calculated (found): 40.86 (40.78) %C, 3.05 (3.10) %H, 15.88 (15.69) %N.

(ii) p-$CH_3C_6H_4C_3N_3H_3Cl_3$ **1b**. Prepared by the same method reported for **1c** using **9b** (2.97g, 22.1mmol) and trichloroacetonitrile (3.23g, 22.4mmol) to give 5.96g of light pink solid (21.4mmol, 97% yield); mp 42-44°C; ^{1}H NMR (δ, $CDCl_3$): 2.4 (s, CH_3), 6.6 (s, NH), 7.2 (d, phenyl), 7.8 (d, phenyl), 9.3 (s, NH), 10.7 (s, NH); ^{13}C NMR (δ, $CDCl_3$): 21.7 (s), 98.1 (s), 127.5 (s), 129.6 (s) 132.6 (s), 142.6 (s), 164.7 (s), 168.2 (s); IR 3451 (m), 3419 (m), 3324 (m), 3121 (w), 1624 (vs), 1615 (vs), 1585 (s), 1563 (s), 1523 (s), 1473 (s), 1398 (m), 1327 (s), 1310 (m), 1259 (w), 1185 (m), 1159 (m), 1131 (m), 1115 (m), 1022 (m), 934 (w), 834 (s), 812 (s), 773 (sh), 756 (s), 739 (sh), 697 (w), 670 (m), 647 (m), 580 (m), 539 (m), 520 (m), 456 (w), 449 (w) cm^{-1}; mass spectrum (*m/e*) 276 ($CH_3PhC_2N_3H_2CCl_3^+$, 94%), 215 ($CH_3PhC_2N_2H_2Cl_2^+$, 2%), 160 ($CH_3PhC_2N_3H_3^+$, 97%), 143 ($CH_3PhC_2N_2^+$, 8%), 118 (CH_3PhCNH^+, 100%). Analysis calculated (found): 43.12 (41.79) %C, 3.62 (3.70) %H, 15.08 (13.13) %N.

(iii) p-$CH_3OC_6H_4C_3N_3H_3Cl_3$ **1a**. Prepared by the same method reported for **1c** using **9a** (4.08g, 27.2mmol) and trichloroacetonitrile (3.93g, 27.2mmol) to give a 7.69g of pink solid (26.1mmol, 96% yield); mp 104-106°C; ^{1}H NMR (δ, $CDCl_3$): 3.9 (s, OCH_3), 6.5 (s, NH), 7.0 (d, phenyl), 7.9 (d, phenyl), 9.3 (s, NH), 10.7 (s, NH); ^{13}C NMR (δ, $CDCl_3$): 55.7 (s), 98.2 (s), 114.3 (s), 127.8 (s), 129.4 (s), 163.0 (s), 164.2 (s), 168.2 (s). IR 3388 (s), 3318 (m), 3136 (w), 3007 (w), 2984 (w), 2938 (w), 2840 (w), 1898 (w), 1618 (sh), 1607 (vs), 1568 (s), 1525 (m), 1492 (vs), 1465 (sh), 1449 (sh), 1439 (m), 1419 (m), 1328 (s), 1312 (m), 1303 (m), 1257 (s), 1184 (m), 1176 (m), 1161 (m), 1142 (s), 1116 (w), 1035 (m), 1023 (sh), 835 (s), 822 (m), 805 (m), 786 (m), 764 (m), 670 (w), 652 (w), 634 (m), 602 (m), 562 (m), 522 (m), 483 (w), 447 (w) cm^{-1}; mass spectrum (*m/e*) 292 ($CH_3OPhC_2N_3H_2CCl_3^+$, 54%), 176 ($CH_3OPhC_2N_3H_3^+$, 91%), 159 ($CH_3OPhC_2N_2^+$,

8%), 134 ($CH_3OPhCNH^+$, 100%) Analysis calculated (found): 40.78 (40.69) %C, 3.42 (3.42) %H, 14.26 (13.02) %N.

(iv) p-$ClC_6H_4C_3N_3H_3Cl_3$ **1d**. Prepared by the same method reported for **1c** using **9d** (4.01g, 25.9mmol) and trichloroacetonitrile (3.80g, 26.3mmol) to give 7.72g of light purple solid (25.8mmol, 99%); mp 111-113°C; ^1H NMR (δ, $CDCl_3$): 6.7 (s, NH), 7.4 (d, phenyl), 7.9 (d, phenyl), 9.4 (s, NH), 10.7 (s, NH); ^{13}C NMR (δ, $CDCl_3$): 97.8 (s), 128.9 (s), 129.2 (s), 133.8 (s), 138.4 (s), 163.6 (s), 167.9 (s). IR 3442 (m), 3314 (m), 3127 (w), 3056 (w), 1628 (s), 1600 (s), 1583 (s), 1561 (s), 1506 (m), 1483 (sh), 1469 (vs), 1401 (w), 1327 (s), 1302 (w), 1258 (w), 1179 (w), 1158 (s), 1126 (w), 1100 (sh), 1085 (m), 1025 (m), 1014 (m), 970 (w), 934 (w), 848 (s), 813 (s), 803 (m), 762 (s), 742 (m), 734 (m), 676 (w), 648 (m), 623 (m), 576 (m), 529 (m), 476 (w), 458 (w) cm^{-1}; mass spectrum (*m/e*) 298 ($ClPhC_2N_3H_2CCl_3^+$, 83%), 180 ($ClPhC_2N_3H_3^+$, 100%), 163 ($ClPhC_2N_2^+$, 7%), 138 ($ClPhCNH^+$, 86%). Analysis calculated (found): 36.16 (36.20) %C, 2.36 (2.47) %H, 14.05 (14.27) %N.

(v) p-$CF_3C_6H_4C_3N_3H_3Cl_3$ **1e**. Prepared by the same method reported for **1c** using **9e** (3.05g, 16.2mmol) and trichloroacetonitrile (2.38g, 16.5mmol) to give 5.29g of light purple solid (15.9mmol, 98%); mp 96-97°C; ^1H NMR (δ, $CDCl_3$): 6.6 (s, NH), 7.7 (d, phenyl), 8.1 (d, phenyl), 9.5 (s, NH), 10.8 (s, NH); ^{13}C NMR (δ, $CDCl_3$): 97.6 (s), 124.0 (q, 273 Hz), 126.0 (q, 4 Hz), 128.0 (s), 133.8 (q, 33 Hz), 138.9 (s), 163.4 (s), 168.0 (s). IR 3469 (s), 3322 (s), 3100 (w), 1619 (s), 1587 (s), 1576 (s), 1522 (s), 1484 (s), 1411 (w), 1326 (vs), 1312 (s), 1299 (sh), 1165 (s), 1154 (s), 1120 (s), 1109 (sh), 1068 (s), 1033 (m), 1016 (s), 981 (w), 932 (w), 859 (s), 834 (m), 814 (s), 799 (s), 761 (s), 749 (s), 709 (s), 679 (m), 647 (w), 601 (m), 589 (w), 510 (m), 493 (s), 458 (m), 420 (m), 406 (w) cm^{-1};

mass spectrum (*m/e*) 330 ($CF_3PhC_2N_3H_2CCl_3^+$, 89%), 214 ($CF_3PhC_2N_3H_3^+$, 100%), 197 ($CF_3PhC_2N_2^+$, 8%), 172 (CF_3PhCNH^+, 95%). Analysis calculated (found): 36.12 (36.03) %C, 2.12 (2.19) %H, 12.64 (12.48) %N.

6.3 Synthesis of the trifluoromethyl imidoylamidines **2a-e**

(vi) $C_6H_5C_3N_3H_3F_3$ **2c**. Trifluoroacetonitrile (2.06g, 21.7mmol) was metered on a vacuum line and added to 2.53g (21.1mmol) of benzamidine **9c** in 20mL of distilled acetonitrile. This was performed in a 300 x 25mm heavy-wall Pyrex tube fitted with a Rotaflow stopcock, containing a magnetic stirring bar. This was weighed frozen under vacuum to ensure an accurate measurement of the gas. The mixture was allowed to warm to room temperature, and then heated to 60°C with stirring for 10 min. to dissolve the remaining precipitate and ensure completion of the reaction. This was then cooled to room temperature and rotary evaporated, leaving a clear oil. All remaining liquids were vacuum filtered off, and the oil was placed in the fridge over the weekend, which solidified and gave 4.37g of white solid (20.3mmol, 96% yield); mp 42–45°C; IR 3330 (m), 3118 (w), 1631 (s), 1600 (s), 1579 (s), 1513 (s), 1481 (s), 1449 (s), 1420 (m), 1320 (w), 1300 (w), 1224 (s), 1164 (s), 1144 (vs), 1076 (w), 1031 (m), 1000 (s), 932 (w), 878 (m), 826 (m), 800 (w), 775 (m), 715 (m), 695 (s), 614 (w), 602 (w), 583 (m), 516 (w), 448 (w), 421 (w) cm^{-1}; ^1H NMR (δ, $CDCl_3$): 6.8 (s, NH), 7.38-7.54 (m, 3H, phenyl), 7.83-7.88 (m, 2H, phenyl), 9.1 (s, NH), 11.0 (s, NH); ^{13}C NMR (δ, $CDCl_3$): 117.8 (q, 281 Hz), 127.4 (s), 129.0 (s), 132.2 (s), 135.2 (s), 163.5 (q, 33 Hz), 165.9 (s); mass spectrum (*m/e*) 214 ($PhC_2N_3H_2CF_3^+$, 100%), 169 ($PhC_2N_2H_2F_2^+$, 4%), 146 ($PhC_2N_3H_3^+$, 12%), 129

($PhC_2N_2^+$, 6%), 104 ($PhCNH^+$, 48%). Analysis calculated (found): 50.24 (50.35) %C, 3.75 (4.01) %H, 19.53 (19.37) %N.

(vii) p-$CH_3C_6H_5C_3N_3H_3F_3$ **2b**. Prepared by the same method reported for **2c** using trifluoroacetonitrile (1.34g, 14.1mmol) and **9b** (1.96g, 14.6mmol) in 15mL of dried acetonitrile. A pink solid remained, which was sublimed in vacuo at 48°C to leave 2.48g of pure white crystals (10.8mmol, 77% yield); mp 54-57°C; IR 3455 (m), 3345 (m), 3330 (m), 1612 (s), 1571 (m), 1524 (m), 1486 (s), 1400 (m), 1289 (w), 1231 (s), 1175 (s), 1154 (vs), 1111 (sh), 1019 (m), 998 (m), 954 (w), 867 (w), 842 (m), 831 (m), 820 (m), 781 (m), 734 (m), 687 (m), 670 (w), 593 (w), 543 (m), 513 (m), 466 (w), 441 (w) cm^{-1}; ^1H NMR (δ, $CDCl_3$): 2.4 (s, CH_3), 6.7 (s, NH), 7.3 (d, 2H, phenyl), 7.8 (d, 2H, phenyl), 9.1 (s, NH), 11.0 (s, NH); ^{13}C NMR (δ, $CDCl_3$): 21.7 (s), 117.8 (q, 281 Hz), 127.6 (s), 129.7 (s), 132.4 (s), 142.8 (s), 163.6 (q, 33 Hz), 165.8 (s); mass spectrum (*m/e*) 228 ($CH_3PhC_2N_3H_2CF_3^+$, 100%), 183 ($CH_3PhC_2N_2H_2F_2^+$, 2%), 160 ($CH_3PhC_2N_3H_3^+$, 7%), 143 ($CH_3PhC_2N_2^+$, 4%), 118 (CH_3PhCNH^+, 30%). Analysis calculated (found): 52.40 (52.34) %C, 4.40 (4.60) %H, 18.33 (18.50) %N.

(viii) p-$CH_3OC_6H_5C_3N_3H_3F_3$ **2a**. Prepared by the same method reported for **2c** using trifluoroacetonitrile (1.09g, 11.5mmol) and **9a** (1.58g, 10.5mmol) in 10mL of dried acetonitrile. A white solid remained, which was sublimed in vacuo at 46°C to leave 1.43g of pure white crystals (5.8mmol, 56% yield); mp 41-45°C; IR 3383 (m), 3325 (m), 3178 (w), 1601 (s), 1572 (s), 1485 (s), 1466 (sh), 1438 (m), 1423 (m), 1399 (m), 1311 (m), 1261 (s), 1233 (s), 1221 (s), 1174 (vs), 1141 (vs), 1113 (sh), 1094 (m), 1029 (m), 998 (m), 837 (s), 815 (w), 786 (m), 758 (w), 745 (w), 729 (w), 708 (w), 689 (w), 642 (w), 614 (w), 588 (w), 563 (m), 514 (w), 479 (w), 433 (w) cm^{-1}; ^1H NMR (δ, $CDCl_3$): 3.9 (s,

OCH_3), 6.7 (s, NH), 6.9 (d, 2H, phenyl), 7.9 (d, 2H, phenyl), 9.0 (s, NH), 11.0 (s, NH); ^{13}C NMR (δ, $CDCl_3$): 55.7 (s), 114.3 (s), 117.9 (q, 281 Hz), 127.3 (s), 129.3 (s), 163.1 (s), 163.4 (q, 33 Hz), 165.3 (s); mass spectrum (*m/e*) 244 ($CH_3OPhC_2N_3H_2CF_3^+$, 42%), 199 ($CH_3OPhC_2N_2H_2F_2^+$, 4%), 176 ($CH_3OPhC_2N_3H_3^+$, 20%), 159 ($CH_3OPhC_2N_2^+$, 13%), 134 ($CH_3OPhCNH^+$, 100%). Analysis calculated (found): 48.98 (48.85) %C, 4.11 (4.22) %H, 17.14 (17.32) %N.

(ix) p-$ClC_6H_5C_3N_3H_3F_3$ **2d**. Prepared by the same method reported for **2c** using trifluoroacetonitrile (2.07g, 21.8mmol) and **9d** (3.25g, 21.0mmol) in 20mL dried acetonitrile. A white solid remained, which was sublimed in vacuo at 49°C to leave 4.72g of pure white crystals (18.9mmol, 90% yield); mp 45-48°C; IR 3333 (s), 3257 (m), 3102 (m), 1644 (s), 1600 (s), 1572 (w), 1515 (m), 1475 (m), 1428 (w), 1395 (w), 1300 (w), 1226 (s), 1194 (s), 1179 (m), 1160 (sh), 1146 (vs), 1089 (m), 1017 (s), 884 (w), 844 (m), 836 (w), 794 (w), 732 (m), 675 (w), 647 (w), 625 (w), 592 (w), 519 (w), 485 (w), 458 (w), 428 (w) cm^{-1}; ^1H NMR (δ, $CDCl_3$): 6.7 (s, NH), 7.4 (d, 2H, phenyl), 7.8 (d, 2H, phenyl), 9.2 (s, NH), 11.0 (s, NH); ^{13}C NMR (δ, $CDCl_3$): 117.7 (q, 281 Hz), 128.8 (s), 129.3 (s), 133.6 (s), 138.6 (s), 163.3 (q, 34 Hz), 164.8 (s); mass spectrum (*m/e*) 248 ($ClPhC_2N_3H_2CF_3^+$, 42%), 180 ($ClPhC_2N_3H_3^+$, 10%), 163 ($ClPhC_2N_2^+$, 13%), 138 ($ClPhCNH^+$, 100%). Analysis calculated (found): 43.31 (43.50) %C, 2.83 (3.00) %H, 16.83 (17.06) %N.

(x) p-$CF_3C_6H_5C_3N_3H_3F_3$ **2e**. Prepared by the same method reported for **2c** using trifluoroacetonitrile (1.02g, 10.7mmol) and **9e** (1.98g, 10.5mmol) in 10mL dried acetonitrile. A white solid remained, which was sublimed in vacuo at 60°C to leave 2.52g of pure white crystals (8.9mmol, 85% yield); mp 80-83°C; IR 3330 (m), 3249 (m), 3083

(m), 1636 (m), 1607 (s), 1582 (m), 1527 (s), 1493 (s), 1436 (w), 1406 (m), 1326 (vs), 1299 (sh), 1229 (s), 1202 (s), 1152 (s), 1130 (s), 1112 (sh), 1067 (s), 1019 (s), 962 (w), 886 (w), 852 (s), 830 (w), 801 (w), 761 (m), 713 (s), 692 (w), 630 (w), 601 (w), 590 (sh), 519 (w), 408 (w) cm^{-1}; ^{1}H NMR (δ, $CDCl_3$): 6.8 (s, NH), 7.7 (d, 2H, phenyl), 8.0 (d, 2H, phenyl), 9.3 (s, NH), 11.1 (s, NH); ^{13}C NMR (δ, $CDCl_3$): 117.7 (q, 281 Hz), 123.9 (q, 273 Hz), 126.0 (q, 4 Hz), 127.9 (s), 133.9 (q, 33 Hz), 138.6 (s), 163.2 (q, 34 Hz), 164.7 (s); mass spectrum (*m/e*) 282 ($CF_3PhC_2N_3H_2CF_3^+$, 100%), 237 ($CF_3PhC_2N_2H_2F_2^+$, 5%), 214 ($CF_3PhC_2N_3H_3^+$, 13%), 197 ($CF_3PhC_2N_2^+$, 3%), 172 (CF_3PhCNH^+, 45%); Analysis calculated (found): 42.42 (42.32) %C, 2.49 (2.39) %H, 14.84 (14.88) %N.

6.4 Synthesis of the trichloromethyl imidoylamidine hydrochlorides **3a-e**

(xi) $C_6H_5C_3N_3H_3Cl_3.HCl$ **3c**. Ether was dried, and approximately 200mL was added to a 250mL round bottom flask containing the imidoylamidine **1c** (6.82g, 25.8mmol). This was stirred and HCl(g) was bubbled through, leaving a white precipitate in solution. This was filtered in air to remove the solvent, and dried to leave 7.26g of crude white powder (24.1mmol, 94% yield); dec.175-176°C; IR 3310 (s), 3127 (s), 3013 (s), 1680 (vs), 1625 (s), 1602 (sh), 1522 (w), 1496 (w), 1448 ms), 1429 (s), 1381 (w), 1185 (w), 1154 (w), 1014 (w), 934 (w), 850 (m), 802 (s), 781 (m), 711 (m), 688 (m), 584 (m), 527 (w), 426 (w) cm^{-1}.

(xii) $p\text{-}CH_3C_6H_4C_3N_3H_3Cl_3.HCl$ **3b**. Prepared by the same method as **3c** using **1b** (5.96g, 21.4mmol) and HCl(g), to leave 6.62g of crude white solid (21.0mmol, 98% yield); dec. 175-177°C; IR 3175 (s), 3103 (s), 3005 (s), 1688 (vs), 1629 (s), 1610 (s), 1560 (m), 1528 (m), 1507 (m), 1435 (s), 1403 (sh), 1379 (sh), 1312 (w), 1263 (w), 1191

(m), 1156 (m), 1120 (w), 1030 (m), 1019 (m), 934 (m), 847 (m), 834 (m), 826 (m), 795 (s), 754 (m), 726 (m), 682 (m), 642 (m), 630 (m), 589 (w), 553 (m), 534 (m), 458 (w), 430 (w) cm^{-1}.

(xiii) p-$CH_3OC_6H_4C_3N_3H_3Cl_3$.HCl **3a**. Prepared by the same method as **3c** using **1a** (5.92g, 20.1mmol) and HCl(g) to leave 6.57g of crude white solid (19.8mmol, 99% yield); dec. 184-186°C; IR 3351 (s), 3281 (s), 3120 (s), 3016 (s), 2845 (w), 1690 (s), 1599 (vs), 1504 (m), 1429 (s), 1409 (s), 1316 (m), 1264 (s), 1184 (s), 1160 (s), 1023 (m), 935 (w), 853 (m), 797 (m), 765 (w), 672 (w), 637 (m), 566 (m), 532 (w), 499 (w) cm^{-1}.

(xiv) p-$ClC_6H_4C_3N_3H_3Cl_3$.HCl **3d**. Prepared by the same method as **3c** using **1d** (7.71g, 25.8mmol) and HCl(g) to leave 8.28g of crude white solid (24.7mmol, 96% yield); dec. 241-243°C; IR 3112 (s), 3012 (s), 1683 (vs), 1627 (s), 1593 (s), 1523 (w), 1491 (w), 1438 (s), 1386 (w), 1337 (w), 1182 (w), 1151 (w), 1089 (m), 1031 (w), 1014 (m), 934 (w), 850 (m), 798 (s), 777 (w), 739 (w), 677 (w), 657 (w), 627 (w), 616 (m), 589 (w), 532 (w), 496 (w), 462 (w) cm^{-1}.

(xv) p-$CF_3C_6H_4C_3N_3H_3Cl_3$.HCl **3e**. Prepared by the same method as **3c** using using **1e** (5.29g, 15.9mmol) and HCl(g) to leave 5.32g of crude white solid (14.4mmol, 91% yield); dec.180-183°C; IR 3310 (m), 3128 (s), 2998 (s), 1701 (vs), 1628 (s), 1513 (m), 1439 (s), 1383 (w), 1324 (vs), 1183 (s), 1133 (s), 1118 (s), 1067 (s), 1017 (s), 932 (w), 857 (s), 803 (s), 760 (w), 744 (m), 699 (m), 630 (w), 607 (m), 589 (m), 524 (w), 463 (w), 405 (w) cm^{-1}.

6.5 Synthesis of the trifluoromethyl imidoylamidine hydrochlorides **4a-e**

(xvi) $C_6H_5C_3N_3H_3F_3$.HCl **4c**. Ether was dried, and approximately 200mL were added to a 250mL round bottom flask containing the imidoylamidine **2c** (2.04g, 9.5mmol). This was stirred and $HCl_{(g)}$ was bubbled through, leaving a white precipitate in solution. This was filtered in air, and dried to leave 2.34g of crude white solid (9.3mmol, 98% yield); dec.174-175°C; IR 3203 (s), 3098 (s), 1694 (vs), 1637 (m), 1602 (w), 1528 (w), 1499 (w), 1450 (m), 1415 (m), 1305 (w), 1212 (s), 1193 (m), 1154 (s), 1028 (w), 1002 (w), 933 (w), 843 (w), 795 (w), 783 (w), 724 (w), 696 (m), 659 (w), 603 (w), 591 (m), 515 (w), 502 (w), 426 (w) cm^{-1}.

(xvii) p-$CH_3C_6H_4C_3N_3H_3F_3$.HCl **4b**. Prepared by the same method as **4c** using **2b** (1.59g, 6.9mmol) and $HCl_{(g)}$, to leave 1.50g of crude white solid (5.7mmol, 82% yield); dec.198-200°C; IR 3185 (m), 3085 (m), 2960 (m), 2925 (m), 2854 (w), 1698 (s), 1637 (m), 1609 (m), 1528 (w), 1515 (w), 1428 (m), 1399 (m), 1316 (w), 1292 (w), 1213 (s), 1193 (sh), 1158 (vs), 1122 (w), 1037 (w), 1019 (w), 998 (w), 848 (w), 827 (m), 731 (m), 674 (w), 652 (w), 637 (w), 594 (w), 567 (w), 516 (w), 498 (w), 468 (w), 420 (w) cm^{-1}.

(xviii) p-$CH_3OC_6H_4C_3N_3H_3F_3$.HCl **4a**. Prepared by the same method as **4c** using **2a** (1.01g, 4.1mmol) and $HCl_{(g)}$, to leave 1.09g of crude white solid (3.9mmol, 94% yield); dec.213-215°C; IR 3199 (s), 3123 (s), 3027 (s), 2846 (w), 1705 (s), 1675 (m), 1641 (w), 1604 (s), 1584 (m), 1509 (m), 1457 (m), 1430 (m), 1408 (s), 1317 (m), 1266 (s), 1210 (vs), 1186 (m), 1158 (s), 1030 (m), 989 (w), 852 (w), 835 (m), 751 (w), 723 (w), 689 (w), 651 (m), 631 (w), 573 (m), 518 (w), 505 (w), 415 (w) cm^{-1}.

(xix) p-$ClC_6H_4C_3N_3H_3F_3$.HCl **4d**. Prepared by the same method as **4c** using **2d** (2.40g, 9.6mmol) and $HCl_{(g)}$, to leave 2.65g of crude white solid (9.3mmol, 97% yield);

dec.>244°C; IR 3199 (s), 3103 (s), 3020 (m), 1697 (s), 1637 (m), 1593 (m), 1523 (w), 1491 (w), 1459 (w), 1421 (m), 1394 (m), 1310 (w), 1282 (w), 1223 (s), 1210 (vs), 1190 (m), 1162 (s), 1091 (m), 1013 (w), 848 (w), 805 (w), 738 (w), 697 (w), 661 (w), 637 (m), 593 (w), 519 (w), 493 (w), 470 (w), 412 (w) cm^{-1}.

(xx) p-$CF_3C_6H_4C_3N_3H_3F_3$.HCl **4e**. Prepared by the same method as **4c** using **2e** (2.37g, 8.4mmol) and $HCl_{(g)}$, to leave 2.65g of crude white solid (8.3mmol, 99% yield); dec.181-183°C; IR 3187 (s), 3105 (s), 3021 (s), 1705 (s), 1643 (m), 1541 (w), 1517 (w), 1429 (m), 1402 (w), 1327 (vs), 1302 (w), 1226 (s), 1212 (s), 1191 (m), 1164 (s), 1131 (s), 1120 (s), 1068 (s), 1016 (m), 858 (m), 812 (w), 761 (w), 699 (m), 668 (w), 624 (m), 595 (w), 514 (w), 463 (w), 415 (w) cm^{-1}.

6.6 Synthesis of the 1-chloro-5-Aryl-3-trichloromethyl-1,2,4,6-thiatriazines **5a-e**

(xxi) $C_6H_5C_2N_3SClCCl_3$ **5c**. Freshly distilled SCl_2 (3mL, 47.2mmol) in 10mL acetonitrile was added dropwise to the imidoylamidine.HCl **3c** (2.36g, 7.8mmol) in 50mL acetonitrile and under N_2 flow. The solution turned a clear yellow color once all of the SCl_2 was added. The temperature of the reaction mixture was gradually raised to 80°C and was allowed to reflux until the release of hydrogen chloride had ceased (approx. 2 hours). The solution was then allowed to cool and placed in the freezer overnight. The solvent was removed in vacuo, and the crude product was crystallized from hot heptane to give dark pink moisture-sensitive plates (2.11g, 6.4mmol, 82% yield); mp 91-95°C; ^1H NMR (δ, $CDCl_3$): 7.53-7.60 (m, 2H, phenyl), 7.68-7.74 (m, H, phenyl), 8.49-8.53 (m, 2H, phenyl); mass spectrum (*m/e*) 327 ($PhC_3N_3S^{35}Cl_4^+$, 0.65%), 292 ($PhC_3N_3S^{35}Cl_3^+$, 100%),

189 ($C_2N_2S^{35}Cl_3^+$, 5%), 149 ($PhCN_2S^+$, 71%), 129 ($PhC_2N_2^+$, 33%), 103 ($PhCN^+$, 39%), 76 ($C_6H_4^+$, 22%).

(xxii) p-$CH_3C_6H_5C_2N_3SClCCl_3$ **5b**. Prepared by the same method as **5c** using **3b** (2.58g, 8.2mmol) in 60mL acetonitrile and distilled SCl_2 (3.1mL, 48.8mmol) in 10mL acetonitrile. The crude product was recrystallized from hot heptane to give yellow moisture-sensitive needles (1.98g, 5.8mmol, 70% yield); mp 97-99°C; ^{1}H NMR (δ, $CDCl_3$): 2.48 (s, CH_3), 7.35 (d, phenyl), 8.40 (d, phenyl); mass spectrum (*m/e*) 341 ($CH_3PhC_3N_3S^{35}Cl_4^+$, 2.2%), 306 ($CH_3PhC_3N_3S^{35}Cl_3^+$, 100%), 271 ($CH_3PhC_3N_3S^{35}Cl_2^+$, 13%), 225 ($CH_3PhC_3N_2{}^{35}Cl_2^+$, 2%), 189 ($C_2N_2S^{35}Cl_3^+$, 4%), 163 ($CH_3PhCN_2S^+$, 78%), 143 ($CH_3PhC_2N_2^+$, 16%), 117 ($CH_3PhCN$, 44%), 89 ($C_7H_5$, 18%).

(xxiii) p-$CH_3OC_6H_5C_2N_3SClCCl_3$ **5a**. Prepared by the same method as **5c** using **3a** (2.50g, 7.6mmol) in 50mL acetonitrile and distilled SCl_2 (3.0mL, 47.2mmol) in 10mL acetonitrile. After placing in the freezer overnight orange yellow crystals appeared in solution (1.86g, 5.2mmol, 69% yield); mp 90-91°C; ^{1}H NMR (δ, $CDCl_3$): 3.94 (s, OCH_3), 7.03 (d, phenyl), 8.49 (d, phenyl); mass spectrum (*m/e*) 357 ($CH_3OPhC_3N_3S^{35}Cl_4^+$, 1.1%), 322 ($CH_3OPhC_3N_3S^{35}Cl_3^+$, 31%), 308 ($CH_3OPhC_3N_2S^{35}Cl_3^+$, 0.3%), 189 ($C_3N_2SCl_3$, 1%), 179 ($CH_3OPhCN_2S^+$, 13%), 133 ($CH_3OPhCN$, 100%), 103 ($C_7H_5N$, 6%), 90 ($C_6H_4N$, 10%).

(xxiv) p-$ClC_6H_5C_2N_3SClCCl_3$ **5d**. Prepared by the same method as **5c** using **3d** (3.16g, 9.4mmol) in 60mL acetonitrile and distilled SCl_2 (3.6mL, 56.7mmol) in 10mL acetonitrile. The crude product was crystallized from hot heptane to give pink crystals (2.37g, 6.5mmol, 69% yield); mp 98-99°C; ^{1}H NMR (δ, $CDCl_3$): 7.53 (d, phenyl), 8.45

(d, phenyl); mass spectrum (*m/e*) 361 ($PhC_3N_3S^{35}Cl_5^+$, 1.1%), 326 ($PhC_3N_3S^{35}Cl_4^+$, 77%), 189 ($C_3N_2SCl_3$, 6%), 163 (PhC_2N_2Cl, 18%), 137 (PhCNCl, 38%), 102 (C_7H_4N, 29%).

(xxv) p-$CF_3C_6H_5C_2N_3SClCCl_3$ **5e**. Prepared by the same method as **5c** using **3e** (2.23g, 6.0mmol) in 45mL dried acetonitrile and distilled SCl_2 (1.9mL, 29.9mmol) in 10mL dried acetonitrile. Attempts at crystallization from hot heptane, acetonitrile, or hexane failed to yield purer crystals for analysis. Instead a reddish oil resulted (1.55g, 3.9mmol, 65% yield); ^{1}H NMR (δ, $CDCl_3$): 7.84 (d, phenyl), 8.62 (d, phenyl).

6.7 Synthesis of the 1-chloro-5-Aryl-3-trifluoromethyl-1,2,4,6-thiatriazines **6a-e**

(xxvi) $C_6H_5C_2N_3SClCF_3$ **6c**. Freshly distilled SCl_2 (2.8mL, 44.1mmol) in 10mL acetonitrile was added dropwise to the imidoylamidine.HCl **4c** (2.24g, 8.9mmol) in 30mL acetonitrile and under $N_{2(g)}$ flow. The solution turned a clear yellow color once all the SCl_2 was added. The mixture was then refluxed for 1.5 hours, which turned from yellow to an orangish red color. A precipitate was found in solution, which was filtered off, and the solvent was removed in vacuo to leave an orange oil. Recrystallization attempts failed to produce purer samples for analysis (2.23g, 8.0mmol, 90% yield); ^{1}H NMR (δ, $CDCl_3$): 7.52-7.58 (m, 2H, phenyl), 7.67-7.74 (m, H, phenyl), 8.45-8.48 (m, 2H, phenyl).

(xxvii) p-$CH_3C_6H_5C_2N_3SClCF_3$ **6b**. Prepared by the same method as **6c** using SCl_2 (1.8mL, 28.3mmol) in 10mL acetonitrile added dropwise to **4b** (1.47g, 5.5mmol) in 25mL acetonitrile. The solvent was removed in vacuo, leaving a dark orangish red solid (1.77g, 97% yield); ^{1}H NMR (δ, $CDCl_3$): 2.49 (s, CH_3), 7.35 (d, 2H, phenyl), 8.37 (d, 2H, phenyl).

(xxviii) p-$CH_3OC_6H_5C_2N_3SClCF_3$ **6a**. Prepared by the same method as **6c** using SCl_2 (1.6mL, 25.1mmol) in 10mL acetonitrile added dropwise to **4a** (1.45g, 5.1mmol) in 25mL acetonitrile. The solvent was removed in vacuo, leaving a dark orange oil. Recrystallization with hot toluene followed by hot acetonitrile left an orange oil (1.29g, 81% yield); ^{1}H NMR (δ, $CDCl_3$): 3.94 (s, CH_3O), 7.02 (d, 2H, phenyl), 8.45 (d, 2H, phenyl).

(xxix) p-$ClC_6H_5C_2N_3SClCF_3$ **6d**. Prepared by the same method as **6c** using SCl_2 (2.2mL, 34.6mmol) in 10mL acetonitrile added dropwise to **4d** (2.54g, 8.9mmol) in 40mL acetonitrile. The solvent was removed in vacuo, leaving a dark orange oil. This was recrystallized with hot heptane to leave an orange solid (2.78g, 99% yield); ^{1}H NMR (δ, $CDCl_3$): 7.53 (d, 2H, phenyl), 8.41 (d, 2H, phenyl).

(xxx) p-$CF_3C_6H_5C_2N_3SClCF_3$ **6e**. Prepared by the same method as **6c** using SCl_2 (2.2mL, 34.6mmol) in 10mL acetonitrile added dropwise to **4e** (2.13g, 6.7mmol) in 40mL acetonitrile. The solvent was removed in vacuo, leaving a dark orange oil. (2.50g, 98% yield); ^{1}H NMR (δ, $CDCl_3$): 7.82 (d, 2H, phenyl), 8.59 (d, 2H, phenyl).

6.8 Synthesis of the 3-trichloromethyl-5-Aryl-1,2,4,6-thiatriazine free radicals **7a-e**

(xxxi) $C_6H_5C_2N_3SCCl_3$ **7c**. To **5c** (1.51g, 4.6mmol) was added 15mL acetonitrile. The solution was freeze thaw degassed three times to remove trace amounts of oxygen. Once at room temperature the triphenylantimony (0.87g, 2.5mmol) was added with stirring. A fine black precipitate was formed, and the purple/green crystals were vacuum filtered to give 0.83g of crude product. (62% yield); dec. 98-101°C; mass spectrum (*m/e*) 292 ($PhC_3N_3S^{35}Cl_3^+$, 72%), 257 ($PhC_3N_3S^{35}Cl_2^+$, 27%), 149 ($PhCN_2S^+$, 100%), 129

($PhC_2N_2^+$, 53%), 103 ($PhCN^+$, 58%), 76 ($C_6H_4^+$, 29%). Analysis calculated (found): 36.82 (36.88) %C, 1.72 (1.69) %H, 14.31 (14.07) %N.

(xxxii) p-$CH_3C_6H_5C_2N_3SCl_3$ **7b**. To **5b** (1.04g, 3.0mmol) was added triphenylantimony (0.59g, 1.7mmol) in 12mL acetonitrile to give 0.49g of dark purple product (1.6mmol, 53% yield); dec. 112-4°C; mass spectrum (*m/e*) 308 ($CH_3PhC_3N_3S^{35}Cl_3^+$, 49%), 163 ($CH_3PhCN_2S^+$, 100%), 143 ($CH_3PhC_2N_2^+$, 21%), 117 (CH_3PhCN^+, 69%). Analysis calculated (found): 39.05 (38.89) %C, 2.29 (1.96) %H, 13.66 (13.36) %N.

(xxxiii) p-$CH_3OC_6H_5C_2N_3SCl_3$ **7a**. To **5a** (0.92g, 2.6mmol) was added triphenylantimony (0.50g, 1.4mmol) in 10mL acetonitrile to give 0.52g of dark purple product (1.6mmol, 63% yield); dec. 98-101°C; mass spectrum (*m/e*) 324 ($CH_3OPhC_3N_3S^{35}Cl_3^+$, 15%), 179 ($CH_3OPhCN_2S^+$, 12%), 159 ($CH_3OPhC_2N_2^+$, 2%), ($CH_3OPhCN^+$, 100%). Analysis calculated (found): 37.12 (36.89) %C, 2.18 (2.35) %H, 12.98 (12.89) %N.

(xxxiv) p-$ClC_6H_5C_2N_3SCl_3$ **7d**. To **5d** (1.07g, 2.9mmol) was added triphenylantimony (0.58g, 1.6mmol) in 10mL acetonitrile to give 0.59g of dark purple product (1.8mmol, 61% yield); dec. 98-100°C; mass spectrum (*m/e*) 328 ($ClPhC_3N_3S^{35}Cl_3^+$, 100%), 165 ($ClPhC_2N_2^+$, 13%), 137 ($ClPhCN^+$, 93%). Analysis calculated (found): 32.95 (33.12) %C, 1.23 (1.56) %H, 12.81 (12.69) %N.

(xxxv) p-$CF_3C_6H_5C_2N_3SCl_3$ **7e**. To **5e** (2.63g, 6.6mmol) was added triphenylantimony (1.28g, 3.6mmol) in 30mL acetonitrile to give 1.28g of dark purple product (3.5mmol, 53% yield); 100-3°C; mass spectrum (*m/e*) 362 ($CF_3PhC_3N_3S^{35}Cl_3^+$,

100%), 217 ($CF_3PhCN_2S^+$, 51%), 197 ($CF_3PhC_2N_2^+$, 80%) 171 (CF_3PhCN^+, 42%). Analysis calculated (found): 50.24 (50.35) %C, 3.75 (4.01) %H, 19.53 (19.37) %N.

6.9 Synthesis of the 3-trifluoromethyl-5-Aryl-1,2,4,6-thiatriazine free radicals **8a-e**

(xxxvi) $C_6H_5C_2N_3SCF_3$ **8c**. To **6c** (2.23g, 8.0mmol) was added 25mL acetonitrile. The solution was freeze thaw degassed three times to remove all trace amounts of oxygen. Once at room temperature the triphenylantimony (1.42g, 4.0mmol) was added with stirring. A fine dark purple precipitate was formed, and the crystals were vacuum filtered to give 1.14g of crude product. (4.7mmol, 59% yield); dec. 110-3°C; mass spectrum (*m/e*) 245 ($PhC_3N_3S^{35}F_3^+$, 43%), 149 ($PhCN_2S^+$, 6%), 129 ($PhC_2N_2^+$, 3%), 104 ($PhCN^+$, 100%). Analysis calculated (found): 44.26 (44.12) %C, 2.06 (2.24) %H, 17.21 (17.13) %N.

(xxxvii) p-$CH_3C_6H_5C_2N_3SCF_3$ **8b**. To **6b** (1.05g, 3.6mmol) was added triphenylantimony (0.64g, 1.8mmol) in 15mL acetonitrile to give 0.46g of dark purple product (1.8mmol, 50% yield); dec. 140-2°C; mass spectrum (*m/e*) 258 ($CH_3PhC_3N_3SF_3^+$, 100%), 239 ($CH_3PhC_3N_3SF_2^+$, 4%), 163 ($CH_3PhCN_2S^+$, 24%), 117 (CH_3PhCN^+, 45%). Analysis calculated (found): 46.51 (46.67) %C, 2.73 (2.96) %H, 16.27 (16.41) %N.

(xxxviii) p-$CH_3OC_6H_5C_2N_3SCF_3$ **8a**. To **6a** (1.25g, 4.0mmol) was added triphenylantimony (0.79g, 2.2mmol) in 20mL acetonitrile to give 0.41g of dark purple product (1.5mmol, 37% yield); dec. 135-140°C; mass spectrum (*m/e*) 274 ($CH_3OPhC_3N_3SF_3^+$, 65%), 255 ($CH_3OPhC_3N_3SF_2^+$, 4%), 179 ($CH_3OPhCN_2S^+$, 3%), 117 (CH_3OPhCN^+, 100%). Analysis calculated (found): 43.80 (43.90) %C, 2.57 (2.71) %H, 15.32 (15.18) %N.

(xxxix) p-$ClC_6H_5C_2N_3SCF_3$ **8d**. To **6d** (2.78g, 8.9mmol) was added triphenylantimony (1.71g, 4.8mmol) in 30mL acetonitrile to give 1.36g of dark purple product (4.9mmol, 55% yield); dec. 131-4°C; mass spectrum (*m/e*) 278 ($ClPhC_3N_3SF_3^+$, 100%), 259 ($ClPhC_3N_3SF_2^+$, 5%), 183 ($ClPhCN_2S^+$, 18%), 137 ($ClPhCN^+$, 47%). Analysis calculated (found): 38.79 (38.72) %C, 1.45 (1.41) %H, 15.08 (15.08) %N.

(xxxx) p-$CF_3C_6H_5C_2N_3SCF_3$ **8e**. To **6e** (2.32g, 6.7mmol) was added triphenylantimony (1.31g, 3.7mmol) in 25mL acetonitrile to give 0.45g of dark purple product (1.4mmol, 20% yield); dec. 101-5°C; mass spectrum (*m/e*) 312 ($CF_3PhC_3N_3SF_3^+$, 100%), 197 ($CH_3PhC_2N_2^+$, 24%), 171 (CF_3PhCN^+, 30%). Analysis calculated (found): 38.47 (38.52) %C, 1.29 (1.53) %H, 13.46 (13.34) %N.

6.10 Crystallography data tables

Table 6.1 Crystal data and structure refinement for **1c**.

	1c	
Empirical formula	$C_9H_8Cl_3N_3$	
Formula weight	264.53	
Temperature	173(2) K	
Wavelength	0.71073 Å	
Crystal system	Triclinic	
Space group	$P\bar{1}$	
Unit cell dimensions	a = 10.2999(3) Å	α = 85.5518(12)°
	b = 10.9423(3) Å	β = 86.5092(12)°
	c = 15.6902(4) Å	γ = 81.5436(11)°
Volume	1741.67(8) $Å^3$	
Z	6	
Density (calculated)	1.513 Mg/m^3	
Absorption coefficient	0.758 mm^{-1}	
F(000)	804	
Crystal size	0.18 x 0.15 x 0.10 mm^3	
θ range for data collection	1.3 to 27.7°.	
Index ranges	-13<=h<=13, -14<=k<=14, -20<=l<=20	
Reflections collected	14588	
Independent reflections	7908 [R(int) = 0.076]	
Observed data [I>2σ(I)]	4900	
Completeness to θ = 27.7°	96.8 %	
Absorption correction	Multi-scan method	
Max. and min. transmission	0.928 and 0.876	
Refinement method	Full-matrix least-squares on F^2	
Data / restraints / parameters	7908 / 0 / 443	
Goodness-of-fit on F^2	0.97	
Final R indices [I>2σ(I)]	R_1 = 0.055, wR_2 = 0.126	
R indices (all data)	R_1 = 0.107, wR_2 = 0.151	
Weighting scheme	$w = 1/[\sigma^2(Fo^2) + (0.0777P)^2]$ where $P = (Fo^2 + 2Fc^2)/3$	
(Δ/θ)max	0.001	
Extinction coefficient	0.0229(19)	
Largest diff. peak and hole	0.46 and -0.49 $e.Å^{-3}$	

Table 6.2 Atomic coordinates ($x\ 10^4$) and equivalent isotropic displacement parameters ($Å^2 x\ 10^3$) for **1c**. U(eq) is defined as one third of the trace of the orthogonalized U^{ij} tensor.

Atom	x	y	z	U(eq)
Cl(1A)	-3962(1)	-3130(1)	598(1)	38(1)
Cl(2A)	-2507(1)	-5570(1)	549(1)	48(1)
Cl(3A)	-1415(1)	-3503(1)	-295(1)	51(1)
N(1A)	-1604(2)	-2527(2)	1460(2)	27(1)
N(2A)	-289(3)	-2860(3)	2662(2)	34(1)
N(3A)	-1365(3)	-4625(3)	2018(2)	46(1)
C(1A)	-798(3)	-810(3)	2003(2)	26(1)
C(2A)	-767(3)	-136(3)	1211(2)	30(1)
C(3A)	-648(3)	1110(3)	1164(2)	40(1)
C(4A)	-571(3)	1704(3)	1911(2)	41(1)
C(5A)	-611(3)	1043(3)	2696(2)	40(1)
C(6A)	-729(3)	-211(3)	2751(2)	31(1)
C(7A)	-900(3)	-2147(3)	2047(2)	26(1)
C(8A)	-1709(3)	-3756(3)	1448(2)	31(1)
C(9A)	-2361(3)	-3989(3)	615(2)	30(1)
Cl(1B)	1562(1)	-4465(1)	4258(1)	41(1)
Cl(2B)	-623(1)	-2698(1)	4852(1)	43(1)
Cl(3B)	1410(1)	-3775(1)	5983(1)	39(1)
N(1B)	1782(2)	-1916(2)	3731(2)	25(1)
N(2B)	2826(3)	-137(3)	3687(2)	29(1)
N(3B)	2278(3)	-1444(3)	5115(2)	39(1)
C(1B)	2535(3)	-1056(3)	2369(2)	24(1)
C(2B)	2669(3)	-2204(3)	2017(2)	29(1)
C(3B)	2843(3)	-2272(3)	1141(2)	35(1)
C(4B)	2902(3)	-1211(3)	611(2)	37(1)
C(5B)	2776(3)	-67(3)	957(2)	35(1)
C(6B)	2589(3)	3(3)	1836(2)	27(1)
C(7B)	2372(3)	-1026(3)	3322(2)	23(1)
C(8B)	1797(3)	-2100(3)	4606(2)	25(1)
C(9B)	1096(3)	-3214(3)	4912(2)	28(1)

Cl(1C)	2793(1)	3019(1)	3061(1)	45(1)
Cl(2C)	5431(1)	3375(1)	3385(1)	54(1)
Cl(3C)	4205(1)	4547(1)	1886(1)	55(1)
N(1C)	5067(2)	1002(2)	2686(2)	23(1)
N(2C)	6094(3)	-327(3)	1651(2)	27(1)
N(3C)	5213(3)	2040(3)	1304(2)	38(1)
C(1C)	5870(3)	-1102(3)	3132(2)	24(1)
C(2C)	6019(3)	-824(3)	3969(2)	29(1)
C(3C)	6153(3)	-1774(3)	4614(2)	35(1)
C(4C)	6123(4)	-2979(3)	4429(2)	39(1)
C(5C)	5980(4)	-3256(3)	3600(2)	39(1)
C(6C)	5848(3)	-2323(3)	2950(2)	29(1)
C(7C)	5677(3)	-82(3)	2445(2)	23(1)
C(8C)	4927(3)	2012(3)	2112(2)	25(1)
C(9C)	4360(3)	3185(3)	2578(2)	31(1)

Table 6.3 Bond lengths [Å], angles [°] and H-bonds [Å and °] for **1c**.

Cl(1A)-C(9A)	1.775(3)
Cl(2A)-C(9A)	1.770(3)
Cl(3A)-C(9A)	1.771(3)
N(1A)-C(7A)	1.332(4)
N(1A)-C(8A)	1.366(4)
N(2A)-C(7A)	1.323(4)
N(3A)-C(8A)	1.280(4)
C(1A)-C(2A)	1.396(4)
C(1A)-C(6A)	1.398(4)
C(1A)-C(7A)	1.479(4)
C(2A)-C(3A)	1.382(4)
C(3A)-C(4A)	1.396(5)
C(4A)-C(5A)	1.379(5)
C(5A)-C(6A)	1.391(5)
C(8A)-C(9A)	1.559(4)
Cl(1B)-C(9B)	1.767(3)
Cl(2B)-C(9B)	1.783(3)
Cl(3B)-C(9B)	1.775(3)
N(1B)-C(7B)	1.327(4)
N(1B)-C(8B)	1.373(4)
N(2B)-C(7B)	1.322(4)
N(3B)-C(8B)	1.280(4)
C(1B)-C(6B)	1.382(4)
C(1B)-C(2B)	1.397(4)
C(1B)-C(7B)	1.496(4)
C(2B)-C(3B)	1.381(4)
C(3B)-C(4B)	1.381(5)
C(4B)-C(5B)	1.387(5)
C(5B)-C(6B)	1.388(4)
C(8B)-C(9B)	1.538(4)
Cl(1C)-C(9C)	1.769(3)
Cl(2C)-C(9C)	1.772(3)
Cl(3C)-C(9C)	1.768(3)
N(1C)-C(7C)	1.328(4)

N(1C)-C(8C)	1.367(4)
N(2C)-C(7C)	1.327(4)
N(3C)-C(8C)	1.282(4)
C(1C)-C(6C)	1.392(4)
C(1C)-C(2C)	1.393(4)
C(1C)-C(7C)	1.490(4)
C(2C)-C(3C)	1.391(4)
C(3C)-C(4C)	1.376(5)
C(4C)-C(5C)	1.380(5)
C(5C)-C(6C)	1.385(5)
C(8C)-C(9C)	1.549(4)

C(7A)-N(1A)-C(8A)	119.9(3)
C(2A)-C(1A)-C(6A)	119.5(3)
C(2A)-C(1A)-C(7A)	120.0(3)
C(6A)-C(1A)-C(7A)	120.4(3)
C(3A)-C(2A)-C(1A)	120.3(3)
C(2A)-C(3A)-C(4A)	120.0(3)
C(5A)-C(4A)-C(3A)	119.8(3)
C(4A)-C(5A)-C(6A)	120.7(3)
C(5A)-C(6A)-C(1A)	119.6(3)
N(2A)-C(7A)-N(1A)	125.8(3)
N(2A)-C(7A)-C(1A)	117.4(3)
N(1A)-C(7A)-C(1A)	116.8(3)
N(3A)-C(8A)-N(1A)	127.7(3)
N(3A)-C(8A)-C(9A)	122.4(3)
N(1A)-C(8A)-C(9A)	109.9(3)
C(8A)-C(9A)-Cl(2A)	112.3(2)
C(8A)-C(9A)-Cl(3A)	110.0(2)
Cl(2A)-C(9A)-Cl(3A)	108.30(16)
C(8A)-C(9A)-Cl(1A)	109.2(2)
Cl(2A)-C(9A)-Cl(1A)	107.95(17)
Cl(3A)-C(9A)-Cl(1A)	109.07(18)
C(7B)-N(1B)-C(8B)	120.3(2)
C(6B)-C(1B)-C(2B)	119.5(3)
C(6B)-C(1B)-C(7B)	122.3(3)

C(2B)-C(1B)-C(7B)	118.2(3)
C(3B)-C(2B)-C(1B)	119.9(3)
C(2B)-C(3B)-C(4B)	120.4(3)
C(3B)-C(4B)-C(5B)	120.1(3)
C(4B)-C(5B)-C(6B)	119.6(3)
C(1B)-C(6B)-C(5B)	120.5(3)
N(2B)-C(7B)-N(1B)	125.4(3)
N(2B)-C(7B)-C(1B)	118.3(3)
N(1B)-C(7B)-C(1B)	116.3(2)
N(3B)-C(8B)-N(1B)	126.9(3)
N(3B)-C(8B)-C(9B)	123.4(3)
N(1B)-C(8B)-C(9B)	109.8(2)
C(8B)-C(9B)-Cl(1B)	111.5(2)
C(8B)-C(9B)-Cl(3B)	113.4(2)
Cl(1B)-C(9B)-Cl(3B)	107.40(17)
C(8B)-C(9B)-Cl(2B)	106.6(2)
Cl(1B)-C(9B)-Cl(2B)	109.58(16)
Cl(3B)-C(9B)-Cl(2B)	108.35(17)
C(7C)-N(1C)-C(8C)	120.2(2)
C(6C)-C(1C)-C(2C)	119.8(3)
C(6C)-C(1C)-C(7C)	120.5(3)
C(2C)-C(1C)-C(7C)	119.7(3)
C(3C)-C(2C)-C(1C)	119.5(3)
C(4C)-C(3C)-C(2C)	120.3(3)
C(3C)-C(4C)-C(5C)	120.2(3)
C(4C)-C(5C)-C(6C)	120.2(3)
C(5C)-C(6C)-C(1C)	119.9(3)
N(2C)-C(7C)-N(1C)	125.5(3)
N(2C)-C(7C)-C(1C)	118.3(3)
N(1C)-C(7C)-C(1C)	116.2(2)
N(3C)-C(8C)-N(1C)	127.4(3)
N(3C)-C(8C)-C(9C)	122.7(3)
N(1C)-C(8C)-C(9C)	109.9(2)
C(8C)-C(9C)-Cl(3C)	112.8(2)
C(8C)-C(9C)-Cl(1C)	110.1(2)
Cl(3C)-C(9C)-Cl(1C)	108.30(18)

C(8C)-C(9C)-Cl(2C)	108.8(2)
Cl(3C)-C(9C)-Cl(2C)	107.92(16)
Cl(1C)-C(9C)-Cl(2C)	108.93(17)

D-H...A	d(D-H)	d(H...A)	d(D...A)	<(DHA)
N(2A)-H(2A2)...N(3A)	0.91(4)	1.97(3)	2.656(4)	130(3)
N(2B)-H(2B2)...N(3B)	0.97(4)	1.85(4)	2.641(4)	137(3)
N(2C)-H(2C2)...N(3C)	0.96(4)	1.88(4)	2.642(4)	134(3)
N(2A)-H(2A1)...N(1B)	0.86(4)	2.27(4)	3.127(4)	172(3)
N(2B)-H(2B1)...N(1C)	0.84(4)	2.27(4)	3.074(4)	160(3)
N(2C)-H(2C1)...N(1A)#1	0.81(4)	2.33(4)	3.139(4)	171(3)
N(3A)-H(3A1)...Cl(2A)	0.88(4)	2.37(3)	2.969(3)	125(3)
N(3B)-H(3B1)...Cl(3B)	0.85(4)	2.49(4)	3.024(3)	122(3)
N(3C)-H(3C1)...Cl(3C)	0.88(4)	2.41(3)	2.978(3)	122(3)

Symmetry transformations used to generate equivalent atoms:

#1 x+1,y,z

Table 6.4 Anisotropic displacement parameters ($Å^2$ x 10^3) for **1c**. The anisotropic displacement factor exponent takes the form: $-2\pi^2[h^2 a^{*2} U^{11} + ... + 2 h k a^* b^* U^{12}]$.

Atom	U^{11}	U^{22}	U^{33}	U^{23}	U^{13}	U^{12}
Cl(1A)	35(1)	44(1)	36(1)	-9(1)	-13(1)	1(1)
Cl(2A)	61(1)	32(1)	53(1)	-15(1)	-17(1)	-8(1)
Cl(3A)	55(1)	67(1)	35(1)	-12(1)	9(1)	-20(1)
N(1A)	29(1)	25(1)	28(1)	-3(1)	-7(1)	-3(1)
N(2A)	41(2)	28(2)	34(2)	1(1)	-14(1)-10	(1)
N(3A)	69(2)	24(2)	46(2)	2(1)	-27(2)	-8(2)
C(1A)	20(2)	29(2)	30(2)	-2(1)	-3(1)	-4(1)
C(2A)	28(2)	32(2)	30(2)	-1(1)	-2(1)	-5(1)
C(3A)	33(2)	33(2)	53(2)	7(2)	-5(2)	-3(2)
C(4A)	37(2)	26(2)	60(2)	-5(2)	-3(2)	-3(2)
C(5A)	39(2)	34(2)	48(2)	-18(2)	5(2)	-2(2)
C(6A)	30(2)	33(2)	32(2)	-7(1)	0(1)	-3(1)
C(7A)	25(2)	27(2)	26(2)	0(1)	-2(1)	-4(1)
C(8A)	30(2)	31(2)	31(2)	-9(1)	-5(1)	0(1)
C(9A)	34(2)	30(2)	29(2)	-6(1)	-6(1)	-5(1)
Cl(1B)	67(1)	23(1)	33(1)	-3(1)	-9(1)	-8(1)
Cl(2B)	32(1)	48(1)	48(1)	13(1)	-1(1)	-13(1)
Cl(3B)	56(1)	36(1)	26(1)	4(1)	-8(1)	-13(1)
N(1B)	29(1)	26(1)	21(1)	-3(1)	-2(1)	-9(1)
N(2B)	35(2)	31(2)	25(2)	-6(1)	3(1)	-15(1)
N(3B)	56(2)	46(2)	20(2)	-6(1)	0(1)	-27(2)
C(1B)	20(2)	28(2)	25(2)	-3(1)	-2(1)	-5(1)
C(2B)	33(2)	28(2)	27(2)	-2(1)	-4(1)	-2(1)
C(3B)	37(2)	38(2)	28(2)	-11(2)	-5(1)	3(2)
C(4B)	34(2)	56(2)	21(2)	-7(2)	1(1)	-2(2)
C(5B)	29(2)	46(2)	29(2)	7(2)	-4(1)	-8(2)
C(6B)	23(2)	32(2)	28(2)	-1(1)	-3(1)	-5(1)
C(7B)	22(2)	25(2)	22(2)	-2(1)	-1(1)	-4(1)
C(8B)	29(2)	26(2)	22(2)	-3(1)	0(1)	-6(1)
C(9B)	34(2)	27(2)	25(2)	-2(1)	-4(1)	-10(1)
Cl(1C)	46(1)	32(1)	55(1)	-10(1)	15(1)	-1(1)

Cl(2C)	75(1)	36(1)	57(1)	-13(1)	-25(1)	-13(1)
Cl(3C)	90(1)	24(1)	46(1)	10(1)	9(1)	3(1)
N(1C)	28(1)	21(1)	22(1)	0(1)	-2(1)	-5(1)
N(2C)	27(2)	28(2)	25(1)	-5(1)	0(1)	4(1)
N(3C)	55(2)	31(2)	24(2)	4(1)	2(1)	1(1)
C(1C)	22(2)	21(2)	30(2)	-1(1)	-3(1)	-1(1)
C(2C)	35(2)	26(2)	28(2)	-2(1)	-6(1)	-7(1)
C(3C)	45(2)	34(2)	27(2)	2(1)	-9(2)	-6(2)
C(4C)	48(2)	32(2)	35(2)	8(2)	-7(2)	-1(2)
C(5C)	52(2)	20(2)	44(2)	-1(1)	-2(2)	-4(2)
C(6C)	34(2)	27(2)	27(2)	-5(1)	-1(1)	-3(1)
C(7C)	22(2)	24(2)	24(2)	-1(1)	-2(1)	-7(1)
C(8C)	26(2)	24(2)	24(2)	1(1)	-2(1)	-3(1)
C(9C)	43(2)	22(2)	27(2)	2(1)	0(1)	-6(1)

Table 6.5 Hydrogen coordinates ($x\ 10^4$) and isotropic displacement parameters ($Å^2 x\ 10^3$) for **1c**.

Atom	x	y	z	U(eq)
H(2A1)	220(30)	-2540(30)	2970(20)	33(9)
H(2A2)	-390(30)	-3670(30)	2710(20)	32(9)
H(3A1)	-1570(30)	-5330(30)	1860(20)	39(10)
H(2A)	-832	-535	694	36
H(3A)	-618	1560	615	48
H(4A)	-481	2567	1881	49
H(5A)	-570	1452	3211	48
H(6A)	-752	-677	3295	38
H(2B1)	3290(40)	330(30)	3390(20)	41(11)
H(2B2)	2810(40)	-280(40)	4310(30)	54(11)
H(3B1)	2210(40)	-1750(40)	5630(30)	50(12)
H(2B)	2646	-2943	2386	35
H(3B)	2919	-3061	901	42
H(4B)	3025	-1262	3	44
H(5B)	2818	668	586	41
H(6B)	2509	791	2080	33
H(2C1)	6630(30)	-940(30)	1580(20)	26(9)
H(2C2)	5950(30)	370(30)	1240(20)	41(10)
H(3C1)	5100(30)	2810(30)	1070(20)	31(9)
H(2C)	6024	19	4096	35
H(3C)	6271	-1588	5189	42
H(4C)	6198	-3626	4880	47
H(5C)	5985	-4102	3475	47
H(6C)	5730	-2510	2374	35

Table 6.6 Torsion angles [°] for **1c**.

C(6A)-C(1A)-C(2A)-C(3A)	1.0(5)
C(7A)-C(1A)-C(2A)-C(3A)	-178.8(3)
C(1A)-C(2A)-C(3A)-C(4A)	-0.6(5)
C(2A)-C(3A)-C(4A)-C(5A)	0.2(5)
C(3A)-C(4A)-C(5A)-C(6A)	-0.1(5)
C(4A)-C(5A)-C(6A)-C(1A)	0.5(5)
C(2A)-C(1A)-C(6A)-C(5A)	-0.9(5)
C(7A)-C(1A)-C(6A)-C(5A)	178.9(3)
C(8A)-N(1A)-C(7A)-N(2A)	-1.9(5)
C(8A)-N(1A)-C(7A)-C(1A)	178.2(3)
C(2A)-C(1A)-C(7A)-N(2A)	146.2(3)
C(6A)-C(1A)-C(7A)-N(2A)	-33.6(4)
C(2A)-C(1A)-C(7A)-N(1A)	-33.8(4)
C(6A)-C(1A)-C(7A)-N(1A)	146.4(3)
C(7A)-N(1A)-C(8A)-N(3A)	11.2(5)
C(7A)-N(1A)-C(8A)-C(9A)	-169.9(3)
N(3A)-C(8A)-C(9A)-Cl(2A)	-1.9(4)
N(1A)-C(8A)-C(9A)-Cl(2A)	179.1(2)
N(3A)-C(8A)-C(9A)-Cl(3A)	-122.5(3)
N(1A)-C(8A)-C(9A)-Cl(3A)	58.5(3)
N(3A)-C(8A)-C(9A)-Cl(1A)	117.8(3)
N(1A)-C(8A)-C(9A)-Cl(1A)	-61.2(3)
C(6B)-C(1B)-C(2B)-C(3B)	-0.5(5)
C(7B)-C(1B)-C(2B)-C(3B)	-179.0(3)
C(1B)-C(2B)-C(3B)-C(4B)	0.9(5)
C(2B)-C(3B)-C(4B)-C(5B)	-0.6(5)
C(3B)-C(4B)-C(5B)-C(6B)	0.0(5)
C(2B)-C(1B)-C(6B)-C(5B)	0.0(4)
C(7B)-C(1B)-C(6B)-C(5B)	178.3(3)
C(4B)-C(5B)-C(6B)-C(1B)	0.3(5)
C(8B)-N(1B)-C(7B)-N(2B)	-11.3(5)
C(8B)-N(1B)-C(7B)-C(1B)	168.3(3)
C(6B)-C(1B)-C(7B)-N(2B)	-28.7(4)
C(2B)-C(1B)-C(7B)-N(2B)	149.7(3)

C(6B)-C(1B)-C(7B)-N(1B)	151.7(3)
C(2B)-C(1B)-C(7B)-N(1B)	-29.9(4)
C(7B)-N(1B)-C(8B)-N(3B)	4.1(5)
C(7B)-N(1B)-C(8B)-C(9B)	-177.7(3)
N(3B)-C(8B)-C(9B)-Cl(1B)	-138.1(3)
N(1B)-C(8B)-C(9B)-Cl(1B)	43.7(3)
N(3B)-C(8B)-C(9B)-Cl(3B)	-16.7(4)
N(1B)-C(8B)-C(9B)-Cl(3B)	165.1(2)
N(3B)-C(8B)-C(9B)-Cl(2B)	102.4(3)
N(1B)-C(8B)-C(9B)-Cl(2B)	-75.8(3)
C(6C)-C(1C)-C(2C)-C(3C)	0.3(5)
C(7C)-C(1C)-C(2C)-C(3C)	177.7(3)
C(1C)-C(2C)-C(3C)-C(4C)	-0.7(5)
C(2C)-C(3C)-C(4C)-C(5C)	0.9(5)
C(3C)-C(4C)-C(5C)-C(6C)	-0.8(5)
C(4C)-C(5C)-C(6C)-C(1C)	0.5(5)
C(2C)-C(1C)-C(6C)-C(5C)	-0.2(5)
C(7C)-C(1C)-C(6C)-C(5C)	-177.6(3)
C(8C)-N(1C)-C(7C)-N(2C)	-5.9(4)
C(8C)-N(1C)-C(7C)-C(1C)	175.5(2)
C(6C)-C(1C)-C(7C)-N(2C)	-31.5(4)
C(2C)-C(1C)-C(7C)-N(2C)	151.1(3)
C(6C)-C(1C)-C(7C)-N(1C)	147.1(3)
C(2C)-C(1C)-C(7C)-N(1C)	-30.3(4)
C(7C)-N(1C)-C(8C)-N(3C)	7.3(5)
C(7C)-N(1C)-C(8C)-C(9C)	-172.3(2)
N(3C)-C(8C)-C(9C)-Cl(3C)	-1.8(4)
N(1C)-C(8C)-C(9C)-Cl(3C)	177.8(2)
N(3C)-C(8C)-C(9C)-Cl(1C)	119.3(3)
N(1C)-C(8C)-C(9C)-Cl(1C)	-61.1(3)
N(3C)-C(8C)-C(9C)-Cl(2C)	-121.4(3)
N(1C)-C(8C)-C(9C)-Cl(2C)	58.1(3)

Table 6.7 Crystal data and structure refinement for **2c**

	2c
Empirical formula	$C_9H_8F_3N_3$
Formula weight	215.18
Temperature	293(2) K
Wavelength	0.71073 Å
Crystal system	Monoclinic
Space group	$P2_1/n$
Unit cell dimensions	a = 8.9727(10) Å
	b = 16.4707(12) Å β= 101.974(12)°
	c = 14.0827(14) Å
Volume	2036.0(3) $Å^3$
Z	8
Density (calculated)	1.404 Mg/m^3
Absorption coefficient	0.126 mm^{-1}
F(000)	880
θ range for data collection	2.47 to 25.94°.
Index ranges	-11<=h<=11, -20<=k<=20, -17<=l<=17
Reflections collected	28380
Independent reflections	3795 [R(int) = 0.1143]
Structure solution	direct
Solution program	SHELXS-97 (Sheldrick, 1997)
Refinement method	Full-matrix least-squares on F^2
Refinement program	SHELXL-97 (Sheldrick, 1997)
Completeness to θ = 25.94°	95.7 %
Absorption correction	None
Data / restraints / parameters	3795 / 0 / 296
GooF (all data)	0.846
Final R indices [I>2σ(I)]	R_1 = 0.0653, wR_2 = 0.1724
R indices (all data)	R_1 = 0.1360, wR_2 = 0.2047
Extinction coefficient	0.002(3)
Largest diff. peak and hole	0.404 and -0.275 $e.Å^{-3}$

Table 6.8 Atomic coordinates ($x\ 10^4$) and equivalent isotropic displacement parameters ($Å^2 \times 10^3$) for **2c**. U(eq) is defined as one third of the trace of the orthogonalized U^{ij} tensor.

	x	y	z	U(eq)
F(1)	12078(4)	919(2)	3453(3)	158(2)
F(2)	9849(6)	738(3)	2751(5)	219(3)
F(3)	10576(7)	304(2)	4084(5)	255(4)
N(1)	8830(3)	1588(2)	4261(2)	66(1)
N(2)	8965(4)	2878(2)	4962(3)	70(1)
N(3)	10965(5)	2335(2)	3993(4)	105(1)
C(1)	6886(4)	1994(2)	5088(3)	65(1)
C(2)	6550(5)	1204(2)	5287(3)	81(1)
C(3)	5270(6)	1042(3)	5652(4)	102(2)
C(4)	4323(6)	1656(3)	5807(4)	112(2)
C(5)	4643(6)	2437(3)	5591(4)	103(2)
C(6)	5912(5)	2613(2)	5236(3)	81(1)
C(7)	8307(4)	2165(2)	4747(2)	61(1)
C(8)	10190(5)	1685(2)	3989(3)	74(1)
C(9)	10720(7)	914(3)	3621(5)	109(2)
F(11)	1375(4)	77(3)	791(3)	170(2)
F(12)	2512(5)	-896(2)	319(3)	188(2)
F(13)	2633(4)	282(2)	-238(2)	141(1)
N(11)	4132(3)	846(2)	1512(2)	65(1)
N(12)	6340(4)	710(2)	2730(3)	79(1)
N(13)	4855(4)	-529(2)	1762(3)	86(1)
C(11)	5224(4)	2024(2)	2366(2)	64(1)
C(12)	3871(6)	2407(2)	2397(3)	82(1)
C(13)	3840(7)	3227(3)	2584(3)	102(2)
C(14)	5141(9)	3665(3)	2720(4)	113(2)
C(15)	6489(7)	3309(3)	2670(3)	105(2)
C(16)	6544(5)	2479(2)	2495(3)	87(1)
C(17)	5233(4)	1138(2)	2196(3)	61(1)
C(18)	4013(4)	34(2)	1340(3)	68(1)
C(19)	2679(6)	-145(2)	538(4)	94(1)

Table 6.9 Bond lengths [Å] and angles [°] for **2c**

F(1)-C(9)	1.289(5)
F(2)-C(9)	1.341(7)
F(3)-C(9)	1.220(6)
N(1)-C(7)	1.313(4)
N(1)-C(8)	1.362(5)
N(2)-C(7)	1.320(4)
N(3)-C(8)	1.276(5)
C(1)-C(2)	1.377(5)
C(1)-C(6)	1.386(5)
C(1)-C(7)	1.480(5)
C(2)-C(3)	1.379(6)
C(3)-C(4)	1.367(6)
C(4)-C(5)	1.366(7)
C(5)-C(6)	1.366(6)
C(8)-C(9)	1.487(6)
F(11)-C(19)	1.342(6)
F(12)-C(19)	1.277(5)
F(13)-C(19)	1.293(5)
N(11)-C(17)	1.318(4)
N(11)-C(18)	1.360(4)
N(12)-C(17)	1.319(5)
N(13)-C(18)	1.263(5)
C(11)-C(12)	1.376(5)
C(11)-C(16)	1.381(5)
C(11)-C(17)	1.480(5)
C(12)-C(13)	1.378(6)
C(13)-C(14)	1.352(8)
C(14)-C(15)	1.359(8)
C(15)-C(16)	1.392(6)
C(18)-C(19)	1.494(6)
C(7)-N(1)-C(8)	120.0(3)
C(2)-C(1)-C(6)	119.5(4)
C(2)-C(1)-C(7)	119.0(3)

C(6)-C(1)-C(7)	121.4(3)
C(1)-C(2)-C(3)	119.6(4)
C(4)-C(3)-C(2)	120.6(4)
C(5)-C(4)-C(3)	119.7(5)
C(4)-C(5)-C(6)	120.7(4)
C(5)-C(6)-C(1)	119.9(4)
N(1)-C(7)-N(2)	124.9(4)
N(1)-C(7)-C(1)	117.2(3)
N(2)-C(7)-C(1)	118.0(3)
N(3)-C(8)-N(1)	128.1(4)
N(3)-C(8)-C(9)	120.3(4)
N(1)-C(8)-C(9)	111.6(4)
F(3)-C(9)-F(1)	108.2(5)
F(3)-C(9)-F(2)	101.8(6)
F(1)-C(9)-F(2)	103.1(5)
F(3)-C(9)-C(8)	116.2(5)
F(1)-C(9)-C(8)	116.2(4)
F(2)-C(9)-C(8)	109.6(5)
C(17)-N(11)-C(18)	120.5(3)
C(12)-C(11)-C(16)	119.0(4)
C(12)-C(11)-C(17)	119.4(3)
C(16)-C(11)-C(17)	121.5(4)
C(11)-C(12)-C(13)	120.5(5)
C(14)-C(13)-C(12)	120.0(5)
C(13)-C(14)-C(15)	120.9(5)
C(14)-C(15)-C(16)	119.8(5)
C(11)-C(16)-C(15)	119.7(5)
N(11)-C(17)-N(12)	125.7(3)
N(11)-C(17)-C(11)	116.7(3)
N(12)-C(17)-C(11)	117.6(3)
N(13)-C(18)-N(11)	128.3(4)
N(13)-C(18)-C(19)	121.2(3)
N(11)-C(18)-C(19)	110.5(3)
F(12)-C(19)-F(13)	109.9(5)
F(12)-C(19)-F(11)	105.2(5)
F(13)-C(19)-F(11)	101.5(4)

F(12)-C(19)-C(18)	114.2(4)
F(13)-C(19)-C(18)	114.3(4)
F(11)-C(19)-C(18)	110.6(4)

Symmetry transformations used to generate equivalent atoms:

Table 6.10 Anisotropic displacement parameters ($Å^2 \times 10^3$) for **2c**. The anisotropic displacement factor exponent takes the form: $-2\pi^2[h^2 a^{*2} U^{11} + ... + 2 h k a^* b^* U^{12}]$.

	U^{11}	U^{22}	U^{33}	U^{23}	U^{13}	U^{12}
F(1)	123(3)	130(3)	240(5)	-34(2)	83(3)	22(2)
F(2)	192(4)	182(4)	273(6)	-144(5)	23(4)	34(3)
F(3)	359(7)	95(2)	398(8)	93(4)	282(7)	106(3)
N(1)	69(2)	53(2)	72(2)	-4(1)	6(2)	5(1)
N(2)	86(2)	57(2)	66(2)	-11(2)	12(2)	-5(2)
N(3)	99(3)	86(3)	141(4)	-28(2)	50(3)	-15(2)
C(1)	68(2)	62(2)	58(2)	0(2)	0(2)	6(2)
C(2)	89(3)	65(2)	89(3)	3(2)	18(3)	0(2)
C(3)	109(4)	88(3)	111(4)	6(3)	26(3)	-11(3)
C(4)	99(4)	121(4)	122(4)	4(3)	40(3)	1(3)
C(5)	86(3)	110(4)	113(4)	2(3)	20(3)	25(3)
C(6)	81(3)	77(2)	79(3)	2(2)	6(2)	14(2)
C(7)	71(2)	49(2)	57(2)	-1(2)	0(2)	6(2)
C(8)	77(3)	63(2)	79(3)	-6(2)	9(2)	6(2)
C(9)	109(4)	78(3)	147(5)	-19(3)	43(4)	3(3)
F(11)	91(2)	212(4)	188(4)	-6(3)	-14(3)	-35(2)
F(12)	237(4)	68(2)	195(4)	-11(2)	-105(3)	-35(2)
F(13)	198(3)	109(2)	87(2)	15(2)	-38(2)-46	(2)
N(11)	74(2)	50(2)	65(2)	2(1)	4(2)	-6(1)
N(12)	87(2)	59(2)	78(2)	1(2)	-11(2)	0(2)
N(13)	103(3)	51(2)	96(3)	-1(2)	1(2)	4(2)
C(11)	86(3)	56(2)	48(2)	2(2)	5(2)	-7(2)
C(12)	106(3)	67(2)	69(3)	-6(2)	11(2)	8(2)
C(13)	145(5)	77(3)	78(3)	-6(2)	9(3)	23(3)
C(14)	182(6)	62(3)	82(3)	4(2)	-1(4)	-12(3)
C(15)	142(5)	79(3)	80(3)	11(2)	-10(3)-37	(3)
C(16)	101(3)	72(2)	76(3)	16(2)	-6(3)	-20(2)
C(17)	70(2)	58(2)	53(2)	6(2)	7(2)	-3(2)
C(18)	77(3)	55(2)	69(2)	4(2)	5(2)	-8(2)
C(19)	105(4)	60(2)	103(4)	5(2)	-12(3)-20	(2)

Table 6.11 Hydrogen coordinates (x 10^4) and isotropic displacement parameters ($Å^2$ x 10^3) for **2c**.

	x	y	z	U(eq)
H(2)	7183	783	5175	121
H(3)	5049	509	5796	153
H(4)	3465	1542	6057	167
H(5)	3991	2853	5687	155
H(6)	6122	3147	5093	121
H(12)	2971	2110	2290	122
H(13)	2925	3479	2618	153
H(14)	5113	4218	2849	169
H(15)	7372	3620	2752	158
H(16)	7465	2232	2465	130
H(2A)	8560(40)	3190(20)	5330(30)	75(12)
H(10A)	6400(50)	160(30)	2650(30)	100(14)
H(12A)	7080(60)	930(30)	3220(40)	118(18)
H(1A)	9780(50)	3000(20)	4700(30)	82(13)
H(13A)	4610(50)	-980(30)	1560(30)	93(14)
H(3A)	11740(50)	2250(30)	3800(30)	97(17)

Table 6.12 Crystal data and structure refinement for **7c**.

	7c	
Empirical formula	$C_9H_5Cl_3N_3S$	
Formula weight	293.57	
Temperature	293(2) K	
Wavelength	0.71073 Å	
Crystal system	Triclinic	
Space group	$P\bar{1}$	
Unit cell dimensions	a = 6.3713(9) Å	α = 108.525(19)°
	b = 9.5741(16) Å	β = 100.568(18)°
	c = 10.0030(17) Å	γ = 97.717(19)°
Volume	556.48(15) $Å^3$	
Z	2	
Density (calculated)	1.752 Mg/m^3	
Absorption coefficient	0.982 mm^{-1}	
F(000)	294	
Crystal size	0.40 x 0.24 x 0.16 mm^3	
θ range for data collection	2.21 to 25.81°.	
Index ranges	-7<=h<=7, -11<=k<=11, -12<=l<=12	
Reflections collected	7683	
Independent reflections	1986 [R(int) = 0.0513]	
Completeness to θ = 25.81°	92.8 %	
Absorption correction	None	
Refinement method	Full-matrix least-squares on F^2	
Data / restraints / parameters	1986 / 0 / 145	
Goodness-of-fit on F^2	1.032	
Final R indices [I>2σ(I)]	R_1 = 0.0352, wR_2 = 0.0932	
R indices (all data)	R_1 = 0.0476, wR_2 = 0.1034	
Largest diff. peak and hole	0.340 and -0.387 $e.Å^{-3}$	

Table 6.13 Atomic coordinates ($x\ 10^4$) and equivalent isotropic displacement parameters ($Å^2 \times 10^3$) for **7c**. U(eq) is defined as one third of the trace of the orthogonalized U^{ij} tensor.

	x	y	z	U(eq)
S(1)	1937(1)	-90(1)	8799(1)	36(1)
Cl(3)	7389(1)	3639(1)	13488(1)	50(1)
Cl(2)	3869(2)	4865(1)	12356(1)	56(1)
Cl(1)	3014(2)	2544(1)	13559(1)	62(1)
N(4)	5853(4)	2307(2)	10341(2)	36(1)
C(5)	5577(4)	1495(3)	8920(3)	32(1)
N(6)	3920(4)	368(2)	8099(2)	37(1)
N(2)	2432(4)	1050(2)	10489(2)	35(1)
C(12)	9202(5)	2945(3)	9036(3)	37(1)
C(11)	7300(5)	1888(3)	8216(3)	34(1)
C(3)	4250(5)	2054(3)	10988(3)	34(1)
C(13)	10792(5)	3301(3)	8353(3)	45(1)
C(14)	10521(6)	2614(3)	6888(3)	48(1)
C(10)	4623(5)	3200(3)	12543(3)	37(1)
C(15)	8648(6)	1571(4)	6063(3)	55(1)
C(16)	7034(5)	1207(3)	6727(3)	45(1)

Table 6.14 Bond lengths [Å] and angles [°] for **7c**.

S(1)-N(6)	1.628(2)
S(1)-N(2)	1.640(2)
Cl(3)-C(10)	1.764(3)
Cl(2)-C(10)	1.780(3)
Cl(1)-C(10)	1.759(3)
N(4)-C(3)	1.340(3)
N(4)-C(5)	1.350(3)
C(5)-N(6)	1.329(3)
C(5)-C(11)	1.478(4)
N(2)-C(3)	1.303(4)
C(12)-C(13)	1.385(4)
C(12)-C(11)	1.394(4)
C(11)-C(16)	1.390(4)
C(3)-C(10)	1.545(3)
C(13)-C(14)	1.369(4)
C(14)-C(15)	1.378(5)
C(15)-C(16)	1.386(4)
N(6)-S(1)-N(2)	108.64(12)
C(3)-N(4)-C(5)	118.4(2)
N(6)-C(5)-N(4)	126.3(2)
N(6)-C(5)-C(11)	116.9(2)
N(4)-C(5)-C(11)	116.8(2)
C(5)-N(6)-S(1)	119.27(18)
C(3)-N(2)-S(1)	117.02(19)
C(13)-C(12)-C(11)	119.4(3)
C(16)-C(11)-C(12)	119.4(2)
C(16)-C(11)-C(5)	120.2(3)
C(12)-C(11)-C(5)	120.4(2)
N(2)-C(3)-N(4)	130.1(2)
N(2)-C(3)-C(10)	116.6(2)
N(4)-C(3)-C(10)	113.1(2)
C(14)-C(13)-C(12)	120.6(3)
C(13)-C(14)-C(15)	120.6(3)

C(3)-C(10)-Cl(1)	112.12(18)
C(3)-C(10)-Cl(3)	111.42(19)
Cl(1)-C(10)-Cl(3)	108.85(14)
C(3)-C(10)-Cl(2)	106.60(17)
Cl(1)-C(10)-Cl(2)	108.95(15)
Cl(3)-C(10)-Cl(2)	108.81(14)
C(14)-C(15)-C(16)	119.5(3)
C(15)-C(16)-C(11)	120.4(3)

Symmetry transformations used to generate equivalent atoms:

Table 6.15 Anisotropic displacement parameters ($Å^2 \times 10^3$) for **7c**. The anisotropic displacement factor exponent takes the form: $-2\pi^2[h^2 a^{*2} U^{11} + ... + 2 h k a^* b^* U^{12}]$.

	U^{11}	U^{22}	U^{33}	U^{23}	U^{13}	U^{12}
S(1)	30(1)	35(1)	37(1)	9(1)	8(1)	1(1)
Cl(3)	44(1)	49(1)	43(1)	8(1)	-1(1)	7(1)
Cl(2)	65(1)	39(1)	58(1)	10(1)	7(1)	21(1)
Cl(1)	71(1)	63(1)	45(1)	10(1)	28(1)	-8(1)
N(4)	37(2)	36(1)	33(1)	10(1)	11(1)	0(1)
C(5)	33(2)	29(1)	36(1)	14(1)	6(1)	5(1)
N(6)	36(2)	38(1)	36(1)	14(1)	10(1)	3(1)
N(2)	36(2)	33(1)	38(1)	12(1)	12(1)	7(1)
C(12)	40(2)	32(1)	40(1)	14(1)	10(1)	4(1)
C(11)	40(2)	31(1)	36(1)	18(1)	12(1)	10(1)
C(3)	38(2)	30(1)	37(1)	14(1)	10(1)	9(1)
C(13)	43(2)	40(1)	55(2)	18(1)	17(1)	3(1)
C(14)	49(2)	52(2)	54(2)	27(1)	26(2)	7(1)
C(10)	37(2)	34(1)	37(1)	11(1)	9(1)	3(1)
C(15)	63(3)	64(2)	40(2)	22(1)	21(2)	4(2)
C(16)	42(2)	52(2)	36(1)	15(1)	5(1)	-5(1)

Table 6.16 Hydrogen coordinates (x 10^4) and isotropic displacement parameters ($Å^2$ x 10^3) for **7c**.

	x	y	z	U(eq)
H(12)	9400	3407	10033	44
H(13)	12056	4013	8895	54
H(14)	11611	2854	6446	58
H(15)	8467	1113	5066	66
H(16)	5767	504	6174	54

Table 6.17 Crystal data and structure refinement for **8c**.

	8c	
Empirical formula	$C_9H_5F_3N_3S$	
Formula weight	244.22	
Temperature	293(2) K	
Wavelength	0.71073 Å	
Crystal system	Triclinic	
Space group	$P\bar{1}$	
Unit cell dimensions	a = 9.2220(9) Å	α= 84.054(11)°
	b = 10.8943(11) Å	β= 69.041(11)°
	c = 11.1064(10) Å	γ = 68.239(11)°
Volume	967.21(16) $Å^3$	
Z	4	
Density (calculated)	1.677 Mg/m^3	
Absorption coefficient	0.352 mm^{-1}	
F(000)	492	
Crystal size	0.50 x 0.40 x 0.33 mm^3	
θ range for data collection	2.62 to 28.11°.	
Index ranges	-12<=h<=12, -14<=k<=14, -14<=l<=14	
Reflections collected	13901	
Independent reflections	4269 [R(int) = 0.0399]	
Completeness to θ = 28.11°	90.5 %	
Absorption correction	None	
Refinement method	Full-matrix least-squares on F^2	
Data / restraints / parameters	4269 / 60 / 309	
Goodness-of-fit on F^2	1.048	
Final R indices [I>2σ(I)]	R_1 = 0.0412, wR_2 = 0.1309	
R indices (all data)	R_1 = 0.0500, wR_2 = 0.1381	
Largest diff. peak and hole	0.501 and -0.305 $e.Å^{-3}$	

Table 6.18 Atomic coordinates (x 10^4) and equivalent isotropic displacement parameters ($Å^2$ x 10^3) for **8c**. U(eq) is defined as one third of the trace of the orthogonalized U^{ij} tensor.

	x	y	z	U(eq)
F(1)	-4128(2)	12790(2)	8321(2)	87(1)
F(2)	-4070(2)	10852(2)	8905(3)	103(1)
F(3)	-3779(2)	12066(3)	10063(2)	89(1)
F(1A)	-3750(20)	12970(10)	8814(17)	87(1)
F(2A)	-4007(19)	11431(17)	8030(16)	103(1)
F(3A)	-3889(19)	11287(17)	9885(12)	89(1)
F(4)	-2938(2)	14731(2)	9101(2)	93(1)
F(5)	-1801(2)	15538(2)	9964(2)	86(1)
F(6)	-2683(3)	14006(2)	10870(2)	125(1)
F(4A)	-2460(30)	15380(20)	9048(19)	93(1)
F(5A)	-1880(30)	14950(20)	10750(20)	86(1)
F(6A)	-3090(30)	13910(30)	10230(30)	125(1)
S(1)	1307(1)	9626(1)	8167(1)	40(1)
S(2)	2186(1)	11337(1)	8991(1)	43(1)
N(2)	-710(2)	10347(2)	8874(2)	41(1)
N(5)	457(2)	13742(2)	7860(2)	44(1)
N(3)	1828(2)	10023(2)	6665(2)	43(1)
C(12)	2068(2)	12992(2)	7201(2)	38(1)
C(3)	680(2)	10901(2)	6246(2)	38(1)
N(1)	-963(2)	11484(2)	6938(2)	44(1)
N(6)	2985(2)	11892(2)	7602(2)	45(1)
N(4)	309(2)	12389(2)	9733(2)	46(1)
C(4)	1237(2)	11277(2)	4896(2)	40(1)
C(2)	-1498(2)	11141(2)	8144(2)	38(1)
C(11)	-227(2)	13402(2)	9043(2)	41(1)
C(5)	82(3)	11939(2)	4294(2)	52(1)
C(9)	2924(3)	11005(2)	4211(2)	52(1)
C(18)	4595(2)	12922(2)	5325(2)	51(1)
C(14)	1919(2)	14485(2)	5377(2)	51(1)
C(13)	2870(2)	13474(2)	5954(2)	39(1)
C(17)	5323(3)	13388(2)	4156(3)	61(1)
C(1)	-3384(2)	11730(2)	8828(2)	48(1)
C(16)	4365(3)	14390(2)	3589(3)	64(1)
C(6)	616(3)	12319(2)	3033(2)	63(1)
C(15)	2661(3)	14930(2)	4200(2)	65(1)
C(10)	-1934(3)	14416(2)	9770(2)	54(1)
C(8)	3429(3)	11416(3)	2969(3)	65(1)
C(7)	2276(4)	12075(2)	2377(2)	66(1)

Table 6.19 Bond lengths [Å] and angles [°] for **8c**.

F(1)-C(1)	1.295(2)
F(2)-C(1)	1.309(3)
F(3)-C(1)	1.341(3)
F(1A)-C(1)	1.265(10)
F(2A)-C(1)	1.336(11)
F(3A)-C(1)	1.219(11)
F(4)-C(10)	1.315(3)
F(5)-C(10)	1.320(3)
F(6)-C(10)	1.297(3)
F(4A)-C(10)	1.304(13)
F(5A)-C(10)	1.307(12)
F(6A)-C(10)	1.302(13)
S(1)-S(2)	2.6402(7)
S(1)-N(3)	1.6221(17)
S(1)-N(2)	1.6411(15)
S(2)-N(6)	1.6165(17)
S(2)-N(4)	1.6409(18)
N(2)-C(2)	1.320(2)
N(5)-C(11)	1.320(3)
N(5)-C(12)	1.362(2)
N(3)-C(3)	1.327(2)
C(12)-N(6)	1.327(2)
C(12)-C(13)	1.465(3)
C(3)-N(1)	1.358(2)
C(3)-C(4)	1.469(3)
N(1)-C(2)	1.318(2)
N(4)-C(11)	1.319(2)
C(4)-C(5)	1.393(2)
C(4)-C(9)	1.395(3)
C(2)-C(1)	1.530(2)
C(11)-C(10)	1.529(3)
C(5)-C(6)	1.384(3)
C(9)-C(8)	1.374(3)
C(18)-C(17)	1.373(3)
C(18)-C(13)	1.401(2)
C(14)-C(15)	1.373(3)
C(14)-C(13)	1.390(2)
C(17)-C(16)	1.382(3)
C(16)-C(15)	1.382(3)
C(6)-C(7)	1.373(4)
C(8)-C(7)	1.384(4)

N(3)-S(1)-N(2)	109.26(8)
N(6)-S(2)-N(4)	109.55(8)
C(2)-N(2)-S(1)	115.32(14)
C(11)-N(5)-C(12)	117.47(15)
C(3)-N(3)-S(1)	119.10(14)
N(6)-C(12)-N(5)	125.97(17)
N(6)-C(12)-C(13)	117.27(15)
N(5)-C(12)-C(13)	116.73(15)
N(3)-C(3)-N(1)	126.55(17)
N(3)-C(3)-C(4)	116.88(16)
N(1)-C(3)-C(4)	116.57(15)
C(2)-N(1)-C(3)	117.66(14)
C(12)-N(6)-S(2)	119.54(14)
C(11)-N(4)-S(2)	114.66(14)
C(5)-C(4)-C(9)	119.22(19)
C(5)-C(4)-C(3)	120.34(18)
C(9)-C(4)-C(3)	120.42(17)
N(2)-C(2)-N(1)	131.85(16)
N(2)-C(2)-C(1)	113.15(16)
N(1)-C(2)-C(1)	114.97(14)
N(5)-C(11)-N(4)	132.40(17)
N(5)-C(11)-C(10)	113.31(16)
N(4)-C(11)-C(10)	114.21(18)
C(6)-C(5)-C(4)	119.9(2)
C(8)-C(9)-C(4)	120.1(2)
C(17)-C(18)-C(13)	119.79(19)
C(15)-C(14)-C(13)	120.36(19)
C(14)-C(13)-C(18)	119.21(18)
C(14)-C(13)-C(12)	120.07(16)
C(18)-C(13)-C(12)	120.71(16)
C(18)-C(17)-C(16)	120.5(2)
F(3A)-C(1)-F(1A)	115.3(10)
F(3A)-C(1)-F(1)	129.4(8)
F(1A)-C(1)-F(1)	37.2(7)
F(3A)-C(1)-F(2)	62.6(9)
F(1A)-C(1)-F(2)	140.0(7)
F(1)-C(1)-F(2)	109.8(2)
F(3A)-C(1)-F(3)	42.7(9)
F(1A)-C(1)-F(3)	76.5(8)
F(1)-C(1)-F(3)	105.7(2)
F(2)-C(1)-F(3)	103.6(2)
F(3A)-C(1)-F(2A)	109.6(9)
F(1A)-C(1)-F(2A)	106.9(9)
F(1)-C(1)-F(2A)	69.7(8)
F(2)-C(1)-F(2A)	49.1(8)
F(3)-C(1)-F(2A)	141.7(7)

F(3A)-C(1)-C(2)	114.6(8)
F(1A)-C(1)-C(2)	105.4(8)
F(1)-C(1)-C(2)	114.35(18)
F(2)-C(1)-C(2)	111.16(17)
F(3)-C(1)-C(2)	111.59(16)
F(2A)-C(1)-C(2)	104.2(7)
C(15)-C(16)-C(17)	119.9(2)
C(7)-C(6)-C(5)	120.5(2)
C(14)-C(15)-C(16)	120.2(2)
F(6A)-C(10)-F(4A)	105.8(12)
F(6A)-C(10)-F(6)	42.6(13)
F(4A)-C(10)-F(6)	132.5(10)
F(6A)-C(10)-F(4)	67.8(13)
F(4A)-C(10)-F(4)	42.3(11)
F(6)-C(10)-F(4)	107.0(2)
F(6A)-C(10)-F(5)	134.8(14)
F(4A)-C(10)-F(5)	65.2(11)
F(6)-C(10)-F(5)	109.0(2)
F(4)-C(10)-F(5)	105.0(2)
F(6A)-C(10)-F(5A)	106.9(12)
F(4A)-C(10)-F(5A)	107.3(11)
F(6)-C(10)-F(5A)	67.5(12)
F(4)-C(10)-F(5A)	135.6(10)
F(5)-C(10)-F(5A)	45.9(11)
F(6A)-C(10)-C(11)	113.3(14)
F(4A)-C(10)-C(11)	112.8(10)
F(6)-C(10)-C(11)	112.92(19)
F(4)-C(10)-C(11)	112.00(19)
F(5)-C(10)-C(11)	110.59(18)
F(5A)-C(10)-C(11)	110.2(11)
C(9)-C(8)-C(7)	120.5(2)
C(6)-C(7)-C(8)	119.8(2)

Symmetry transformations used to generate equivalent atoms:

Table 6.20 Anisotropic displacement parameters ($Å^2 \times 10^3$) for **8c**. The anisotropic displacement factor exponent takes the form: $-2\pi^2[h^2 a^{*2} U^{11} + ... + 2 h k a^* b^* U^{12}]$.

	U^{11}	U^{22}	U^{33}	U^{23}	U^{13}	U^{12}
F(1)	47(1)	88(1)	85(2)	37(1)	-16(1)	6(1)
F(2)	47(1)	81(1)	184(3)	-10(1)	-28(1)	-33(1)
F(3)	46(1)	141(2)	52(1)	-12(1)	-7(1)	-9(1)
F(1A)	47(1)	88(1)	85(2)	37(1)	-16(1)	6(1)
F(2A)	47(1)	81(1)	184(3)	-10(1)	-28(1)	-33(1)
F(3A)	46(1)	141(2)	52(1)	-12(1)	-7(1)	-9(1)
F(4)	41(1)	128(2)	95(2)	-31(1)	-20(1)	-7(1)
F(5)	74(1)	58(1)	118(2)	-31(1)	-26(1)	-12(1)
F(6)	101(2)	95(1)	75(2)	22(1)	45(1)	2(1)
F(4A)	41(1)	128(2)	95(2)	-31(1)	-20(1)	-7(1)
F(5A)	74(1)	58(1)	118(2)	-31(1)	-26(1)	-12(1)
F(6A)	101(2)	95(1)	75(2)	22(1)	45(1)	2(1)
S(1)	36(1)	40(1)	41(1)	12(1)	-16(1)-10	(1)
S(2)	41(1)	54(1)	41(1)	17(1)	-21(1)-21	(1)
N(2)	36(1)	48(1)	39(1)	14(1)	-16(1)-16	(1)
N(5)	38(1)	49(1)	36(1)	9(1)	-7(1)	-12(1)
N(3)	40(1)	44(1)	37(1)	6(1)	-13(1)	-7(1)
C(12)	35(1)	43(1)	36(1)	7(1)	-12(1)-17	(1)
C(3)	43(1)	37(1)	36(1)	4(1)	-17(1)-13	(1)
N(1)	39(1)	50(1)	38(1)	11(1)	-15(1)-11	(1)
N(6)	34(1)	52(1)	46(1)	17(1)	-13(1)-17	(1)
N(4)	50(1)	53(1)	33(1)	7(1)	-11(1)-23	(1)
C(4)	47(1)	39(1)	32(1)	2(1)	-15(1)-14	(1)
C(2)	36(1)	41(1)	41(1)	8(1)	-17(1)-15	(1)
C(11)	42(1)	45(1)	35(1)	3(1)	-9(1)	-20(1)
C(5)	56(1)	58(1)	42(1)	10(1)	-23(1)-18	(1)
C(9)	49(1)	58(1)	40(1)	2(1)	-13(1)-13	(1)
C(18)	37(1)	54(1)	50(1)	9(1)	-7(1)	-14(1)
C(14)	43(1)	54(1)	40(1)	12(1)	-7(1)	-9(1)
C(13)	37(1)	41(1)	35(1)	5(1)	-8(1)	-16(1)
C(17)	44(1)	65(1)	52(2)	5(1)	5(1)	-17(1)
C(1)	36(1)	56(1)	50(1)	11(1)	-16(1)-16	(1)
C(16)	63(1)	65(1)	41(1)	12(1)	4(1)	-21(1)
C(6)	76(2)	68(1)	44(1)	13(1)	-31(1)-18	(1)
C(15)	60(1)	63(1)	44(1)	20(1)	-7(1)	-8(1)
C(10)	50(1)	53(1)	44(1)	-1(1)	-2(1)	-18(1)
C(8)	61(1)	74(1)	42(1)	2(1)	-4(1)	-19(1)
C(7)	85(2)	67(1)	34(1)	8(1)	-14(1)-24	(1)

Table 6.21 Hydrogen coordinates (x 10^4) and isotropic displacement parameters ($Å^2$ x 10^3) for **8c**.

	x	y	z	U(eq)
H(5)	-1047	12125	4740	62
H(9)	3708	10545	4596	62
H(18)	5245	12241	5698	61
H(14)	774	14863	5790	62
H(17)	6469	13026	3744	73
H(16)	4867	14702	2797	77
H(6)	-155	12742	2626	75
H(15)	2014	15595	3812	78
H(8)	4553	11249	2523	78
H(7)	2625	12353	1536	79

References

1. Boeré, R. T.; Oakley, R. T.; Reed, R. W. *Journal of Organometallic Chemistry* **1987**, *331*, 161.